PL-TR-94-2275

ZODIACAL LIGHT DATA INVESTIGATION

S. V. Burdick
J. Chalupa
W. K. Cobb
C. L. Hamilton
T. L. Murdock

GRC International, Inc.
5 Cherry Hill Drive, Suite 220
Danvers, MA 01923

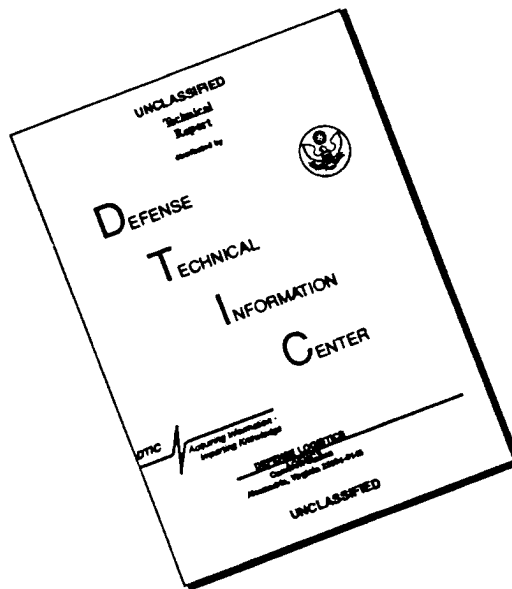21 October 1994

Final Report
12 JULY 1991 THROUGH 31 OCTOBER 1994

PHILLIPS LABORATORY
Directorate of Geophysics
AIR FORCE MATERIEL COMMAND
HANSCOM AFB, MA 01731-3010

19960613 058

DISCLAIMER NOTICE

UNCLASSIFIED
Technical
Report

DEFENSE

TECHNICAL

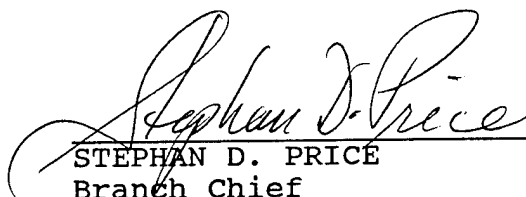INFORMATION

CENTER

DTIC

UNCLASSIFIED

THIS DOCUMENT IS BEST
QUALITY AVAILABLE. THE COPY
FURNISHED TO DTIC CONTAINED
A SIGNIFICANT NUMBER OF
PAGES WHICH DO NOT
REPRODUCE LEGIBLY.

"This technical report has been reviewed and is approved for publication"

FRANK CLARK
Contract Manager

STEPHAN D. PRICE
Branch Chief

ROGER A. VAN TASSEL
Division Director

REPORT DOCUMENTATION PAGE

Public reporting burden for this collection of information is estimated to average 1 hour per response, including the time for reviewing instructions, searching existing data sources, gathering and maintaining the data needed, and completing and reviewing the collection of information. Send comments regarding this burden estimate or any other aspect of this collection of information, including suggestions for reducing this burden, to Washington Headquarters Services, Directorate for Information Operations and Reports, 1215 Jefferson Davis Highway, Suite 1204, Arlington, VA 22202-4302, and to the Office of Management and Budget, Paperwork Reduction Project (0704-0188), Washington, DC 20503.

1. AGENCY USE ONLY *(Leave blank)*	2. REPORT DATE 21 October 1994	3. REPORT TYPE AND DATES COVERED Final 12 July 1991–31 October 1994

4. TITLE AND SUBTITLE

Zodiacal Light Data Investigation

5. FUNDING NUMBERS

F19628-91-C-0104
PE62101F
PR3054
TA 01 WU AR

6. AUTHOR(S)

S.V. Burdick, J. Chalupa, W.K. Cobb, C.L. Hamilton, T.L. Murdock

7. PERFORMING ORGANIZATION NAME(S) AND ADDRESS(ES)

General Research Corporation
5 Cherry Hill Drive, Suite 220
Danvers, MA   01923

8. PERFORMING ORGANIZATION REPORT NUMBER

9. SPONSORING/MONITORING AGENCY NAME(S) AND ADDRESS(ES)

Phillips Laboratory
29 Randolph Road
Hanscom AFB, MA 01731-3010

Contract Manager: Frank Clark/GPOB

10. SPONSORING/MONITORING AGENCY REPORT NUMBER

PL-TR-94-2275

11. SUPPLEMENTARY NOTES

12a. DISTRIBUTION/AVAILABILITY STATEMENT

Approved for Public Release
Distribution unlimited

12b. DISTRIBUTION CODE

13. ABSTRACT *(Maximum 200 words)*

A three year study to support Air Force characterization of the zodiacal background is summarized. The study utilized sounding-rocket data from the Zodiacal Infrared Program (ZIP) and the Earthlimb Clutter (ELC) Experiment; this data provides finer spectral coverage and information closer to the sun than the subsequent Infrared Astronomical Survey (IRAS) and Cosmic Background Explorer (COBE). Work was performed in three main areas: the reduction of the data was upgraded; the reduced data was organized into a readily accessible database; and the zodiacal dust structure was investigated by use of the database. The data reduction was implemented with a pipeline process which took instrumental and environmental effects into account; the data was placed in a common calibration format with COBE and an error analysis was performed. The data archive is readily accessible with a graphical user interface (GUI); it allows the user to work directly with the final data product or to recompute details of the pipeline process. Analysis work has uncovered features of scientific interest in the database.

14. SUBJECT TERMS

Zodiacal Light, Zodiacal Dustbands, Zodiacal Dust Spectrum, IRAS, COBE, ELC

15. NUMBER OF PAGES

104

16. PRICE CODE

17. SECURITY CLASSIFICATION OF REPORT	18. SECURITY CLASSIFICATION OF THIS PAGE	19. SECURITY CLASSIFICATION OF ABSTRACT	20. LIMITATION OF ABSTRACT
Unclassified	Unclassified	Unclassified	SAR

THIS PAGE INTENTIONALLY LEFT BLANK

CONTENTS

LIST OF FIGURES

LIST OF FIGURES

LIST OF TABLES

THIS PAGE INTENTIONALLY LEFT BLANK

ACRONYM LIST

ACS	Attitude Control System
CIB	Cosmic Infrared Background
COBE	Cosmic Background Explorer
DC	Direct Current
DEC	Declination
DIRBE	Diffuse Infrared Background Experiment
ELC	Earthlimb Clutter Experiment
GRCI	GRC International, Inc.
GUI	Graphical User Interfaces
IFOV	Instantaneous Field of View
IR	Infrared
IRAS	Infrared Astronomical Survey
IRDSP	Infrared Data Signal Processing
LOS	Line-of-Sight
LOWTRAN	Low Resolution Transmittance Code
MSX	Midcourse Space Experiment
NASA	National Aeronautics and Space Administration
OAR	Off-Axis Rejection
PSRR	Point Source Rejection Ratio
RA	Right Ascension
SNR	Signal-to-Noise Ratio
TALO	Time-After-Liftoff
ZIP	Zodiacal Infrared Program

THIS PAGE INTENTIONALLY LEFT BLANK

ACKNOWLEDGMENTS

THIS PAGE INTENTIONALLY LEFT BLANK

1   INTRODUCTION

As space-based optical sensors become more accurate and their performance requirements become more exacting, a robust characterization of celestial background effects is needed to properly operate them. The zodiacal light constitutes a key part of this background. In the direction of the zodiacal plane at ~90° solar elongation, the infrared (IR) spectral flux density of zodiacal dust at 12μ is 1×10^{-9} W/μ/cm^2/sr and the flux density of reflected sunlight at 3μ is 5×10^{-11} W/μ/cm^2/sr. In the direction of the zodiacal poles, these quantities are respectively smaller than 2×10^{-10} W/μ/cm^2/sr and 1×10^{-11} W/μ/cm^2/sr. Clearly, a high-performance sensor must accommodate for this range of background flux densities, and an understanding of the zodiacal background is essential to understand the performance of systems using such sensors.

Zodiacal dust consists of minute particles which span a range of sizes. Their IR spectrum is consistent with that of silicates, and typical diameters are in the micron range. The dynamics of zodiacal dust particles are complex. They experience collisions with each other, are influenced by the gravitational fields of the sun, planets and asteroids, and are acted on by solar radiation pressure and by Poynting-Robertson drag. Thus, in addition to its importance for the performance of space-based optical sensors, the zodiacal dust has features of intrinsic scientific interest. Because of the complex dynamics, a database spanning a wide range of observing parameters must be the basis for reliable modelling and characterization of the zodiacal background.

To support Air Force characterization of the zodiacal background, GRC International, Inc. (GRCI) has completed a three-year study under contract to Phillips Laboratory. The effort focused on a database of measurements from Air Force Geophysics Laboratory sounding rockets under the Zodiacal Infrared Program (ZIP) and Earthlimb Clutter Experiment (ELC). The three main activities which comprised the study are:

- A data reduction procedure more sophisticated than that provided when the database was developed and implemented.
- The reduced data were organized into a readily accessible database.
- The structure of the zodiacal dust was investigated by use of the database.

Also, under a subcontract to the University of Florida, numerical simulations were performed to integrate the equations of motion and determine the spatial distribution of zodiacal granules of a given size.

This Final Report is the third in a series of technical reports which GRCI has issued during the contract; in addition, a paper for the open scientific literature is in preparation. The

1

Final Report documents the study and summarizes GRCI's achievements in the above three areas. The report is organized into six sections of which this Introduction is the first. In order to set the subsequent analysis in context, Section 2 provides a brief description of the ZIP and ELC experiments and summarizes the other main available sources of zodiacal data. Section 3 describes the data reduction process; it describes the pipeline process through which the data is run to correct for extrinsic effects, discusses the recalibration which is necessary to normalize the data to a common standard with other measurement programs, and summarizes the error analysis which was performed as part of data reduction. Section 4 presents the data archive; the archive format is laid out and guidelines for the archive user are presented. Section 5 synopsizes the analysis activity, and Section 6 summarizes the report and recapitulates the main results. Detailed results from the data reduction pipeline are recorded in the Appendix.

2   OVERVIEW OF EXPERIMENTS

The ZIP and the ELC experiments flown by the Air Force Geophysics Laboratory provided valuable scientific information about the zodiacal celestial background. ZIP was a dedicated activity focusing on zodiacal issues; the main ELC objective was measurements of the spatial structure in the quiescent atmosphere, limited zodiacal data were obtained. After the ZIP Program was complete, the (IRAS) Infrared Astronomical Survey and (COBE) Cosmic Background Explorer programs obtained extensive IR zodiacal radiance data from orbiting sensors. The ZIP/ELC sensors gave more detailed spectral coverage, and their lines-of-sight passed closer to the Sun, than the COBE/IRAS sensors.

2.1   ZIP

The ZIP Program consisted of two flights on Aries sounding rockets flown from the White Sands Missile Range. The first, ZIP1, was launched at 0350 MDT on 18 August 1980; the second, ZIP2, flew at 0450 MDT on 31 July 1981. The payload was in the earth's shadow during the entire ZIP1 mission, but the ZIP2 rocket transited from the earth's shadow into sunlight. The apogee for each mission was 400 km, which provided about 8 minutes of data acquisition time. Figure 1 shows the configuration of the sensor and spacecraft. Details concerning the payload and telemetry may be found in References 1 and 2.
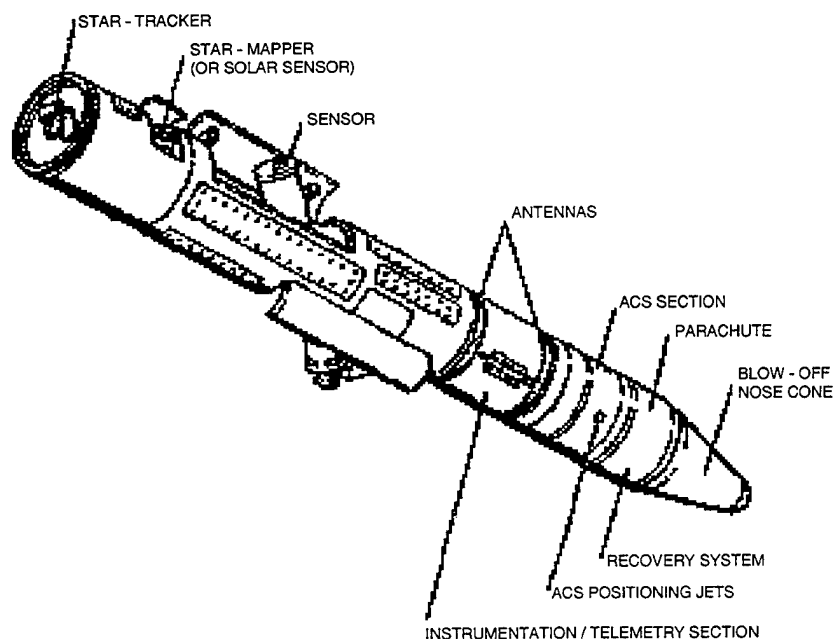
Figure 1   ZIP Sensor/Spacecraft Configuration

3

For each ZIP flight the payload executed a series of rolls about a spin axis aligned by a star tracker towards the star Delta Andromedae. The launch times were chosen so that Delta Andromedae was near transit. The geometry of the ZIP flights is indicated in Figure 2, which should be useful to the reader in visualizing the ZIP1 and ZIP2 roll geometries discussed below.
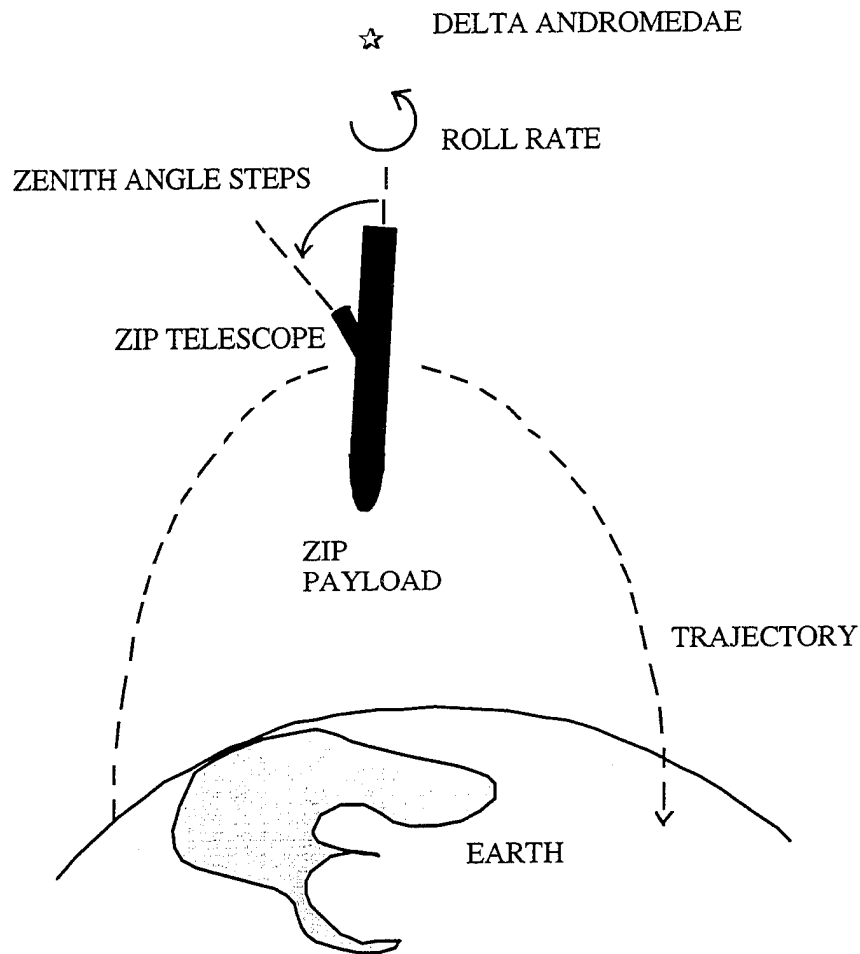
Figure 2   ZIP Flight Geometry

During the first flight, the ZIP telescope's deployment angle from Delta Andromedae was stepped from 40° to 80° in increments of 4°. A 365° roll was executed at each ZIP1 deployment angle for a total of eleven rolls. A constant scan rate of 7.5°/s was maintained for each roll. Before reentry, a final, twelfth roll was executed after backing up one 4° increment to a deployment angle of 76°. The 10th and 12th rolls swept out similar zenith angles, and the mean altitude during Roll 10 was ~350 km and the mean altitude during Roll 12 was ~200 km; this allows the effects of the atmospheric radiance to be quantified. The ecliptic longitude of the sun was 128° for ZIP1. An Aitoff projection of the ZIP1 spatial coverage in Epoch 2000 ecliptic coordinates is shown in Figure 3a. The solar position is marked on the projection.

4

ZIP1 coverage, solar elongation coordinates, 2000 epoch, aitoff projection
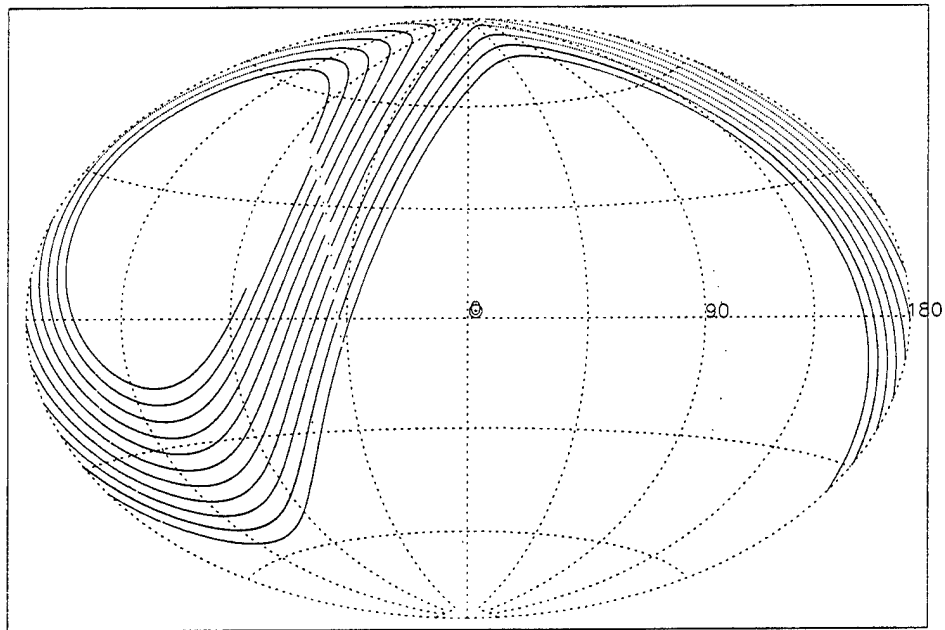
(a)

ZIP2 coverage, solar elongation coordinates, 2000 epoch, aitoff projection
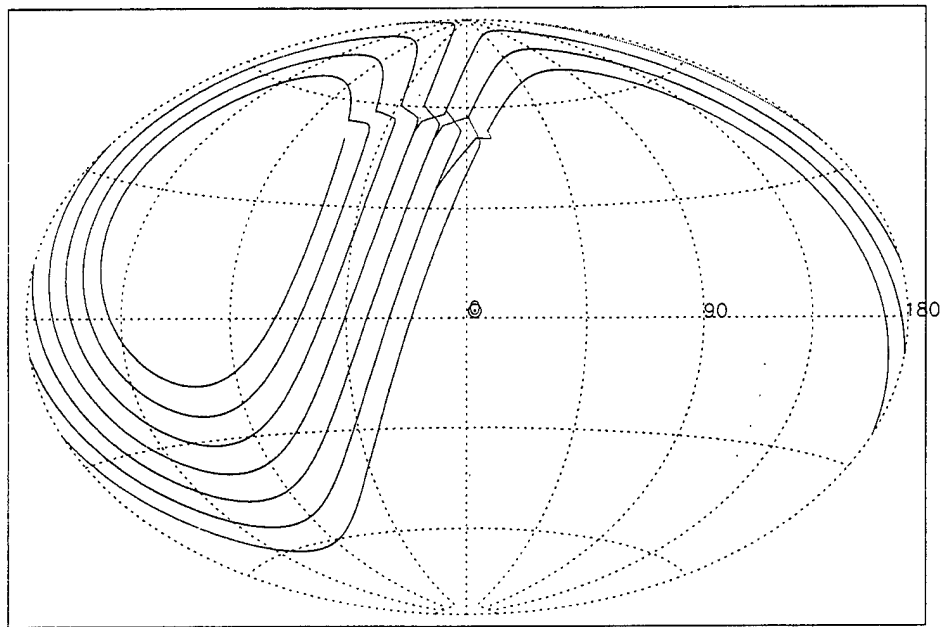
(b)

Figure 3   Aitoff Projection of ZIP Spatial Coverage

(a) ZIP1

(b) ZIP2

During the ZIP2 flight, a 360° roll was executed during each 7.5° deployment increment. The ecliptic longitude of the sun was 145° for ZIP2. The initial zenith angle with respect to Delta Andromedae was approximately 40°. The zenith angle was stepped down to 85° on Roll 7; the direction of the zenith increments was then reversed, and on the final three rolls the zenith angle was stepped back up to 62.5°. The zenith angle reversal provided redundant data which could be utilized to gain information about environmental radiance effects. Although the ZIP2 roll rate was designed to be held steady at 6°/s, the roll jet developed a leak and the roll rate increased steadily during the later rolls. An additional feature of the ZIP2 flight was the presence of a bright glint in the signal after crossing the earth shadow into sunlight on Roll 2. An Aitoff projection of the ZIP2 spatial coverage in Epoch 2000 ecliptic coordinates is shown in Figure 3b. The solar position is marked on the projection.

The ZIP sensor consisted of an off-axis, folded, doubly re-imaging optical system. The focal plane array contained 32 silicon-doped detectors, including two which were covered with metal rather than spectral filters. During the flight, the temperature of the optical bench was ~20K and that of the focal plane was ~7K. The ZIP focal plane layout is shown in Figure 4. The detector array spanned the infrared domain from 2-30 microns in 15 spectral bands which are tabulated in Table 1.

FPA DETECTOR DESIGNATION

SCAN DIRECTION ⟶
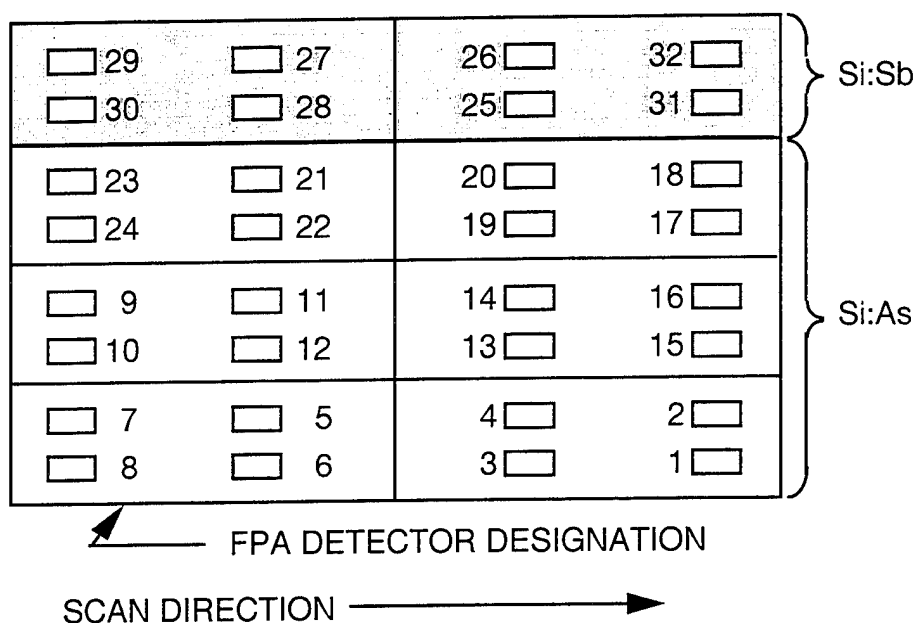
Figure 4   ZIP & ELC Focal Plane Layout

2.2 ELC

The ELC experiment was flown on an Aries sounding rocket launched from the White Sands Missile Range at on 26 October 1983. The ELC sensor was a modified ZIP2 instrument. It used the same optics and calibration plate as the ZIP sensor, but the focal plane was modified with new detectors and filters. The ELC focal plane, shown in Figure 4, had 32 detectors spread over 11 spectral bands which spanned the IR domain from 4-30 microns; the ELC bands are given in Table 2. As for ZIP, the focal plane temperature was ~7K and the optics temperature was 20K.

During data collection, the payload followed a northward trajectory with an apogee of 300km. The sensor opened approximately 96s into the flight at an altitude of 115 km, and took data for some 500s. The sensor completed an initial "long roll" through 430° in azimuth at the local horizontal plane. A series of vertical and horizontal sweeps in and out of the earthlimb measured atmospheric profiles. While the primary purpose of the ELC Experiment was to gather detailed information about earthlimb clutter, the approximately 60s of data during the initial "long roll" did observe the zodiacal background. This zodiacal data was gathered with the spacecraft oriented northward; the northward geometry was chosen to avoid potential contamination effects associated with the rocket booster trailing south behind the sensor.

Despite its brevity, the ELC zodiacal data is unique because of its spatial coverage: during the long roll, the sensor line of sight (LOS) scanned across the zodiacal plane at nearly right angles and only 19° away from the sun--far closer to the sun than the Infrared Astronomical Satellite (IRAS) and COBE were able to observe. Figure 5 shows an Aitoff projection of the ELC long roll in Epoch 2000 ecliptic coordinates. The solar ecliptic longitude was 211°, and is indicated on the plot.
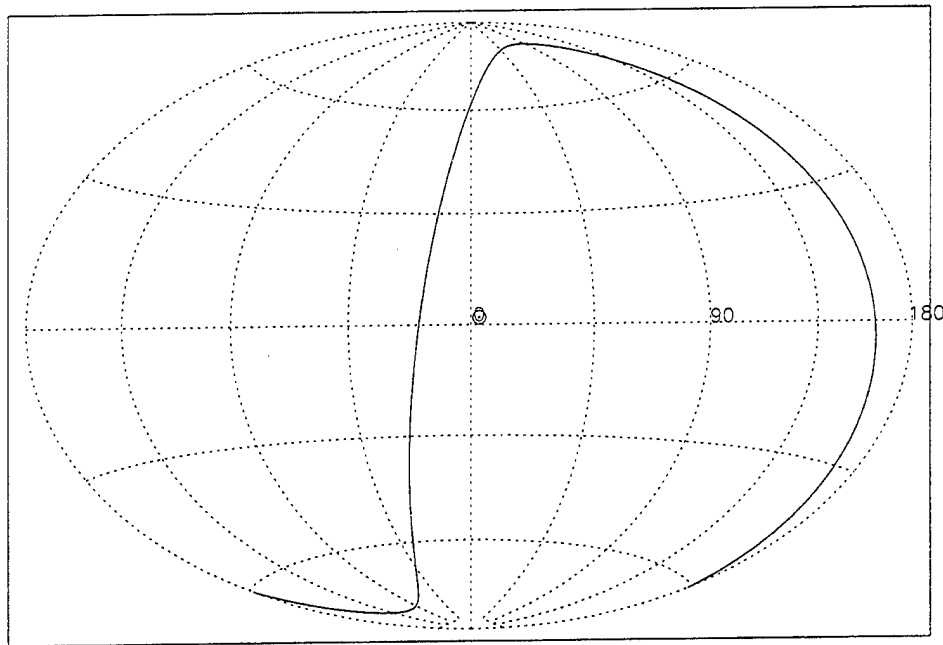
Figure 5   **Aitoff Projection of the ELC Long Roll**

The ELC observations were contemporaneous with the IRAS mission, and two of the ELC bands were similar to the IRAS/COBE 12μ and 25μ bands. Thus, an obvious strategy for tying the ELC calibration to that of IRAS is to find locations in the sky which were observed by the two spacecraft at nearly the same time, and to force consistency between the ELC radiances to the IRAS values. Some differences between the spectral locations of the ELC and IRAS/COBE bands require that color corrections be made during the renormalization.

Similarly, the ZIP and ELC sensors have identical optics and were calibrated in the same fashion. Thus, calibration crossties between the corresponding data sets can be derived. Finally, the rationalization between IRAS and COBE measurements can be utilized to place the zodiacal data from ZIP, ELC, IRAS and COBE in a common calibration framework.

2.3   IRAS AND COBE

In 1983, National Aeronautics and Space Administration (NASA) launched the joint US-European IRAS. IRAS was launched into a 900km sun-synchronous circular polar orbit that allowed it to sample the entire sky nearly twice, primarily at 90° solar elongation, in four infrared bands (12, 25, 60 and 100μ). The IRAS field of view was about 5×10^{-7} steradians. The instrument was cryogenically cooled by liquid helium for 10 months. Although a point-source sky survey was the primary goal of the IRAS mission, Direct Current (DC) sky brightness was also measured. The 12μ and 25μ sky was found to be dominated by the diffuse zodiacal light

8

within our solar system. The band structure due to dust debris from collisions in the major asteroid families was first discovered in the IRAS data. The IRAS calibration has been pegged to COBE.

The COBE was launched in November, 1989 from Vandenberg AFB on a McDonnell-Douglas Delta launch vehicle into an 900 km sun-synchronous circular polar orbit. COBE carried three scientific instruments designed to 1) make precise measurements of the spectrum and anisotropy of the cosmic microwave background radiation on angular scales greater than 7°, and 2) to conduct a search for a diffuse cosmic infrared background radiation with 0.7° angular resolution. The mission goal was to make these measurements to the limit imposed by the local astrophysical foregrounds, which include zodiacal dust. The COBE instruments covered the wavelength range from 1.2μ to 1 cm and were calibrated periodically in orbit by use of internal calibrators and celestial standards. The observing strategy was designed to minimize and allow determination of systematic errors that could result from spacecraft operations, the local environment of the spacecraft, and emissions from foreground astrophysical sources such as the Galaxy and the solar system (including zodiacal dust). The satellite orbit and the instrument field-of-view scanning techniques provide full sky coverage, while simultaneously minimizing solar and terrestrial radiation on the instruments and reducing thermal and radiative perturbations of the measurements. The flight performance generally met or exceeded the design goals.

The Diffuse Infrared Background Experiment (DIRBE) was one of three primary instruments on the COBE spacecraft. DIRBE was cryogenically cooled by liquid helium for a 10 month mission. The main DIRBE objective was to search for a Cosmic Infrared Background (CIB) by making absolute brightness measurements of the diffuse infrared radiation in a 0.7° beam, in 10 photometric bands from 1μ to 350μ and polarimetric measurements from 1.0μ to 3.5μ. In order to carry out this mission, it was necessary to subtract the local foreground signal due primarily to the galaxy and the Zodiacal Light. To this end, DIRBE took definitive measured Zodiacal Light data from 64° to 124° solar elongation. In the present contract, GRCI has pegged the absolute normalization of the ZIP and ELC calibrations to this COBE/DIRBE data.

3   DATA REDUCTION

The data reduction was performed in three stages for both ZIP and ELC. First, instrumental and environmental effects were removed from the signal so that the signal emerging from this pipeline process described only the emission from the zodiacal dust. Next, this signal was recalibrated to the radiance from COBE. Finally, an error analysis of the pipeline procedure was performed to assign a measurement uncertainty to the zodiacal signature. These three stages will be described in the following subsections.

3.1   PIPELINES

3.1.1   The ZIP Pipeline

The ZIP pipeline[3] has three main sections as shown in Figure 6: a preprocessing stage, an instrumental correction stage, and an environmental correction stage. These will be described in turn below. The Appendix records the results for each ZIP channel as the data move through the stages of the pipeline.
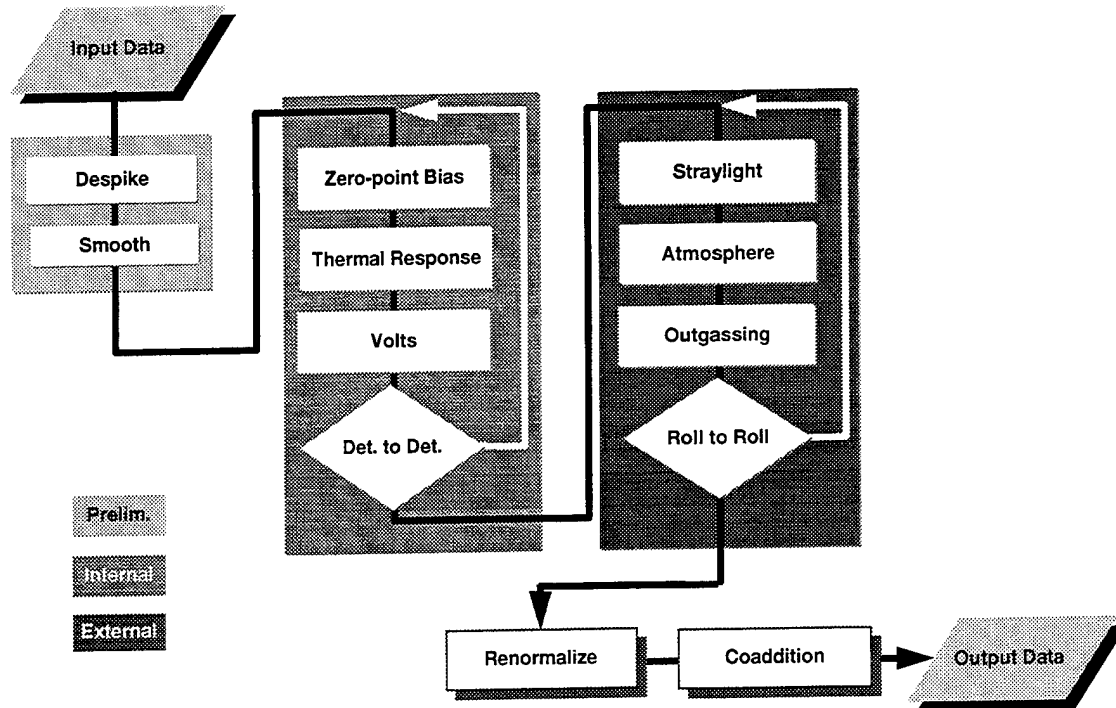

Figure 6   The ZIP Processing Pipeline

3.1.1.1 ZIP Preprocessing

The starting point of the preprocessing was the ZIP data supplied by Phillips Laboratory. We received data which had been quadrature demodulated with the Infrared Data Signal Processing (IRDSP) software package. The ZIP telemetry was not available to us.

The raw high-gain data provided by Philips Laboratory were preprocessed to assure manageability. First, the data set was decimated to a third of its size by averaging every three successive data points, and gaps in the data set were interpolated by use of spline functions; the averaging can be justified by noting that the time scale of variations in the signal features is small compared to the duration associated with three data points.

Next, impulsive "spikes" induced by cosmic rays were removed from the data. The basic procedure has been described in previous GRCI reports. Two running averages of different widths are used to filter the raw data. The resulting averaged data streams are highly correlated except in the vicinity of a spike. In this case the narrow-band average deviates significantly from the wide-band average. Fluctuations of at least three standard deviations (3σ) in the differences between the two averages are used to define the presence of a spike. Once a spike is identified, the algorithm removes it by replacing the excised region with a linear interpolation between the edges of the unperturbed region. The application of linear interpolation implies that if the spike is removed from a region with a gradient in the baseline data, the interpolation technique incorporates the background slope. The effect of despiking (and smoothing) on the ZIP data is shown in Figure 7.
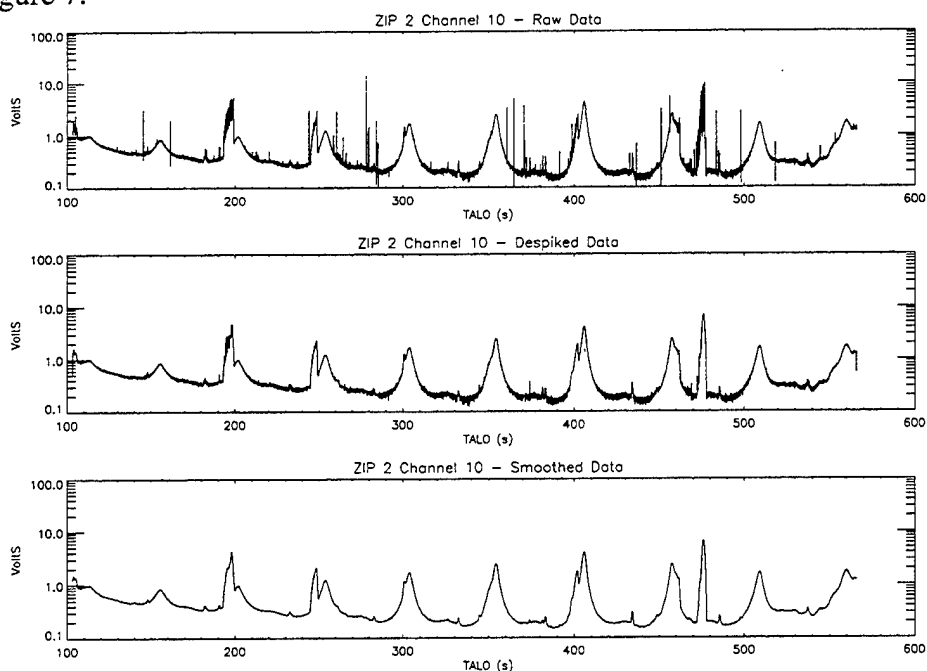

Figure 7   Representative Raw ZIP Data with Subsequent Despiking and Smoothing

11

A nonlinear iterative parabolic filter was applied to the data in order to reduce noise. The filter design was a modified form of the parabolic least squares algorithm described by G.G. Rempel[4]. The basic algorithm is an iterative process in which each iteration consists of a point-by-point smoothing of the entire data array. Every point is smoothed by fitting a parabola centered on a sliding window; the severity of the smoothing can be adjusted by adjusting the width of the sliding window. The center of a window is adjusted by a unique parabola. Therefore, the process can be iterated. In successive iterations, the data are weighted by a function of the deviation from previous iterations. The process continues until the data are stable within a user-defined criterion. For our criterion, we required that the worst-case deviation between iterations be less than one part in 10^4. Figure 7 shows raw ZIP data together with the results of subsequent despiking and smoothing.

3.1.1.2 Corrections for ZIP Instrument Effects

The averaged, despiked and smoothed data were adjusted for instrumental anomalies in the next stage of the pipeline. First, zero-point bias was removed; then corrections were made for the thermal response of the detectors; finally, the telemetry values were converted to irradiances.

The zero-point bias was estimated from the data from the two blind channels (31 and 32) on each ZIP flight. These channels had solid metal in place of spectral filters. Because the onboard and IRDSP processing of these channels was identical to that of the detectors with spectral filters, the signals in the blind channels can provide data needed to determine the zero-point bias associated with the signal processing. Channel 31 of ZIP2 was utilized for the bias correction because this channel had the largest range of variations in the induced signal. We found empirically that the despiked smoothed Channel 31 signal, which is the bias in this dark channel, is related to the amplitude of the noise residuals by the power law

$$y = ax^b \tag{1}$$

y = despiked smoothed dark channel data output in volts
x = |data into pipeline - smoothed, despiked data| (in volts)
a,b are fitting parameters (a = 4.29, b=1.12)

Because the data provided to us had already been passed through IRDSP and were not the original ZIP data, we applied this equation heuristically and did not seek a first-principles derivation. Channel 31 is a dark channel, and accordingly the dark-channel data y represent a

bias (which is known directly *only* for the dark channels). However, the right-hand side of the equation can be determined for all channels from the noise residuals after smoothing. Because the equation holds in Channel 31 over a variety of signal strengths, it is utilized (with the values of a and b determined from Channel 31) to model all channels and infer the zero-point bias from the noise residuals. We assume that the equation describes the functional relationship between noise and bias in *all* channels; this assumption allows us to characterize the bias of channels in which the noise residual differs from the Channel 31 noise. For the same channels which were despiked and smoothed in Figure 7, the effect of zero-point bias removal is shown in Figure 8. Figure 8 and subsequent pipeline figures are formatted as follows. The solid curve, whose scale corresponds to the left vertical axis of the graph, shows the signal after being passed through the appropriate stage of the pipeline, and the dashed curve, which is associated with the right vertical axis, shows the magnitude of the change from the previous stage. When dotted curves appear in a window, they have the scale of the lefthand axis and depict the correction from the previous stage or the signal before the correction was applied (the signal is more structured than the correction).
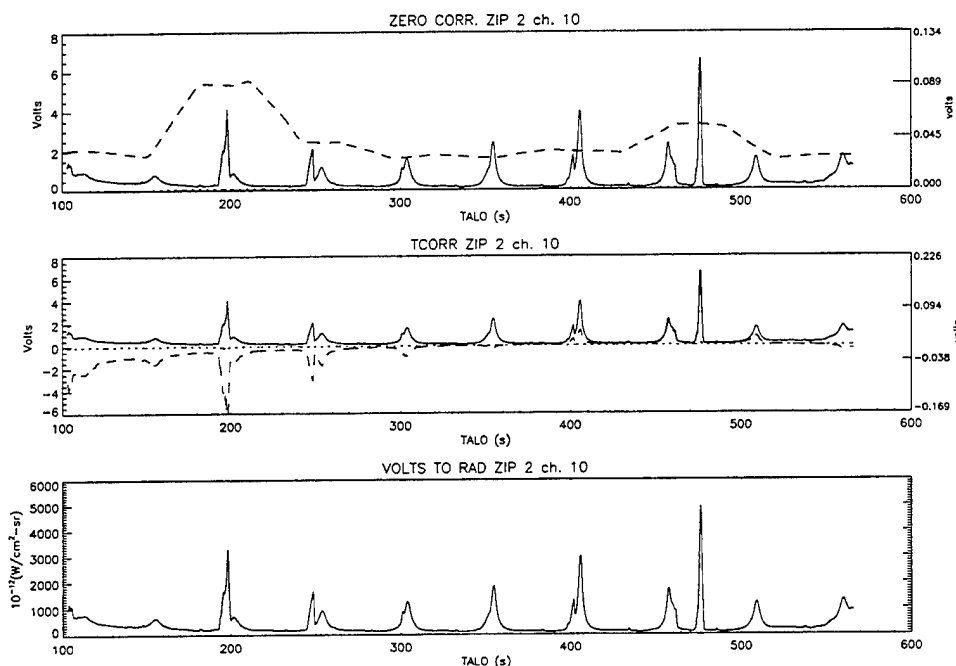

Figure 8   Representative ZIP Data after Zero-Point Bias Removal, Focal-Plane Temperature Correction, and Volts-to-Radiance Conversion

After zero-point bias removal, the irradiance data were corrected for changes of detector responsivity with focal-plane temperature; prior to the GRCI investigation, such a correction had

not been made on the ZIP/ELC data. As was illustrated in Figure 4, the ZIP detectors consist of Si:As and Si:Sb materials. The temperature dependence of the Si:Sb detector responsivity was taken to be the same as that of the Si:Sb ELC detectors[5], and Midcourse Space Experiment (MSX) values were adopted for the Si:As responsivities[6]. The responsivity curves were combined with the data on the temporal behavior of focal plane temperature to determine the time dependence of responsivity for both flights and both detector types. To perform the actual correction, the data (in volts) were divided by the time-dependent normalized responsivity to give the results of Figure 8.

Next, the volts-to-radiance conversion was made based on laboratory calibration with a temperature-controlled plate mounted with the sensor. The black coated metal plate had an emissivity was estimated to be .95±.02. The plate temperature was measured, and the inband irradiance was determined assuming that the plate emitted as a black body and that the detector filter had the response measured at the Naval Oceanographic Science Center. Figure 8 displays this conversion.

Each ZIP spectral band had at least two detectors. The two detector outputs for each given channel were compared and were found to be consistent. The channel-to-channel comparison will be treated more fully in the section on error analysis.

3.1.1.3 Corrections for ZIP Environmental Effects

After instrumental effects are compensated, the resulting signal is not necessarily that from the zodiacal region toward which the sensor is pointing for two reasons: there may be off-axis sources which contaminate the signal, and an atmospheric and outgassing foreground may be present. These effects are taken into account in the pipeline.

The off-axis response (OAR) of the sensor-to-earth thermal flux was determined by the Low Resolution Transmittance (LOWTRAN) code . The off-axis signal determined from the OAR computations was fit to the empirical form

$$OAR_{earth} = C_o exp[-C_1(altitude[km]-200)+(angle\ from\ horizontal)/C_2] \qquad (2)$$

The above equation determines the OAR due to earth and earthlimb contributions, where C_0, C_1 and C_2 are adjustable constants that vary with band. In ZIP 2 the OAR contribution is increased by also including the OAR due to the sun determined by

$$OAR_{sun} = PSRR(\theta)cos\theta\ I\ F/IFOV \qquad (3)$$

where θ is the angle between the sun and the sensor line of sight, I is the total exitance from the sun, F is a distance factor, PSRR is the Point Source Rejection Ratio, and IFOV is the

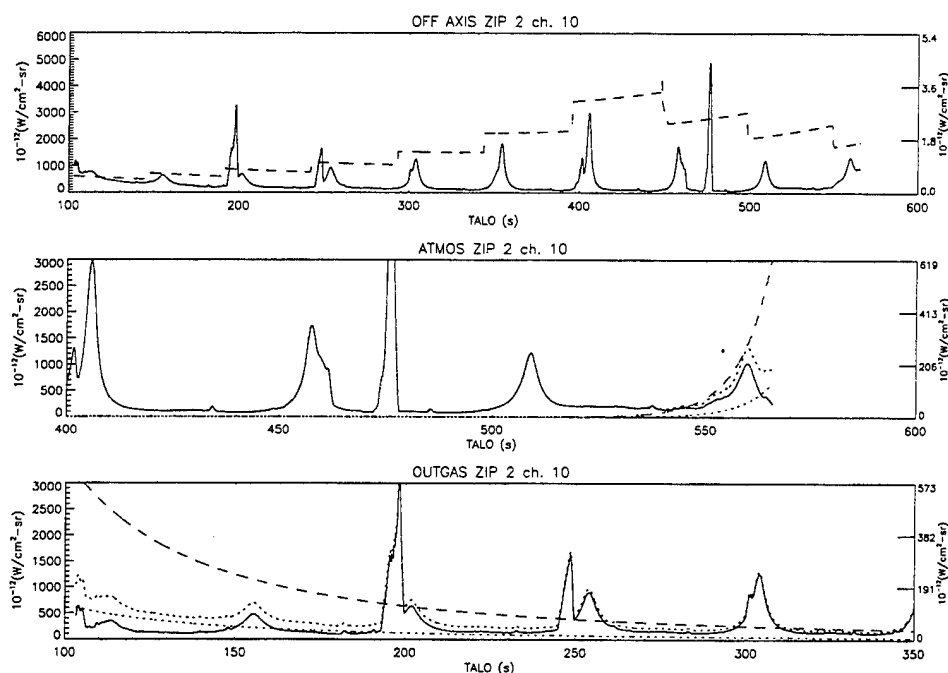Instantaneous Field-of-View in steradians. Figure 9 shows results of the (small) off-axis correction.

Figure 9   Representative ZIP Data after Off-Axis Radiance Correction and Atmosphere/Outgassing Correction

Other sources are evident in the data; we surmise that these are the atmosphere or outgassing material streaming from the spacecraft. We initially attempted to account for these effects by use of first-principles codes, including the data reduction software which was provided with the data. These attempts were inconclusive. We, therefore, formulated the heuristic "ZIP-knows-best" method of determining the combined atmospheric and outgassing correction using roll-to-roll comparisons for the latter half of the flight and radiance trending for the first.

This approach took advantage of the redundant spatial coverage in the latter half of each flight. Rolls with common zenith angle grouped into pairs which survey the same inertial background. The data for the two rolls were compared at the same azimuth positions. The signal difference was obtained over the common range of azimuth shared by the rolls; some spline interpolation was necessary because the slew rate was not constant. The difference between the higher-altitude signal and the one from the lower-altitude roll is believed to be primarily due to the atmosphere. The atmospheric-radiance result was smoothed and fit with the low-altitude roll's time sequence. This atmospheric correction was then subtracted from the data stream. This

effectively corrected for environmental effects in the latter half of the flight. The "ZIP-knows-best" roll-correction is depicted in Figure 9.

There is no redundant roll coverage in the beginning of the ZIP flights, though there is a very clear extraneous signal present. This signal falls off gradually as a power law or exponential variation for the first few hundred seconds of data. Our approach was to once again rely upon the "ZIP knows-best" philosophy, in the sense of using the data to map the appropriate decay of radiance with time. The typical model for outgassing radiance is one in which the radiance decays as a power of time $R(t) \sim \alpha + \beta/t^n$ where α and β are constants and n is a number close to 1 (the α term, which formally represents a constant bias, is close to zero). We used the minima of the data to obtain a "best" solution by performing an iterative least squares fit to the above stated form. Figure 9 shows results of the outgassing correction.

3.1.2   The ELC Pipeline

Because the zodiacal part of the ELC mission consisted of a single 430° roll, much less data were produced than for the ZIP missions. As was the case for ZIP, we received data which had been run through IRDSP. As can be seen from Figure 10, the ELC pipeline[7], which was constructed first, is more compact than the ZIP pipeline. The pipeline stages are initialization, despiking, lowpass-filtering, atmospheric compensation and smoothing. Reference 7 presents the results for each ELC channel as the data are passed through successive stages of the pipeline.
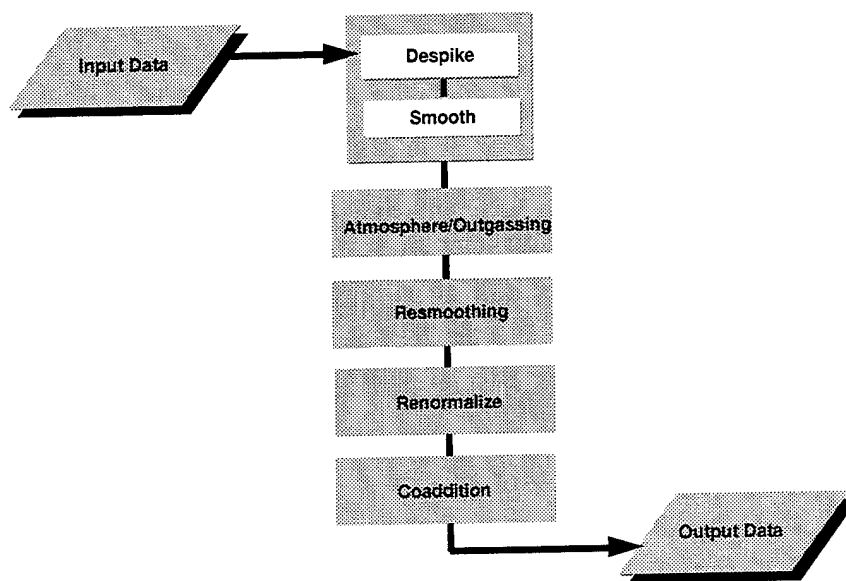

Figure 10   The ELC Processing Pipeline

16

The full ELC data sets consist of nearly 200,000 data points spanning the period from roughly 100s to 500s after launch. After receiving machine-readable files from Anthony D'Agati of Phillips Laboratory, we separated out the 120-180s subset which contained zodiacal information. We also culled the data streams of those detectors which showed no evidence of zodiacal light. Figure 11a shows sample data which emerged from the initialization phase of the ELC pipeline.
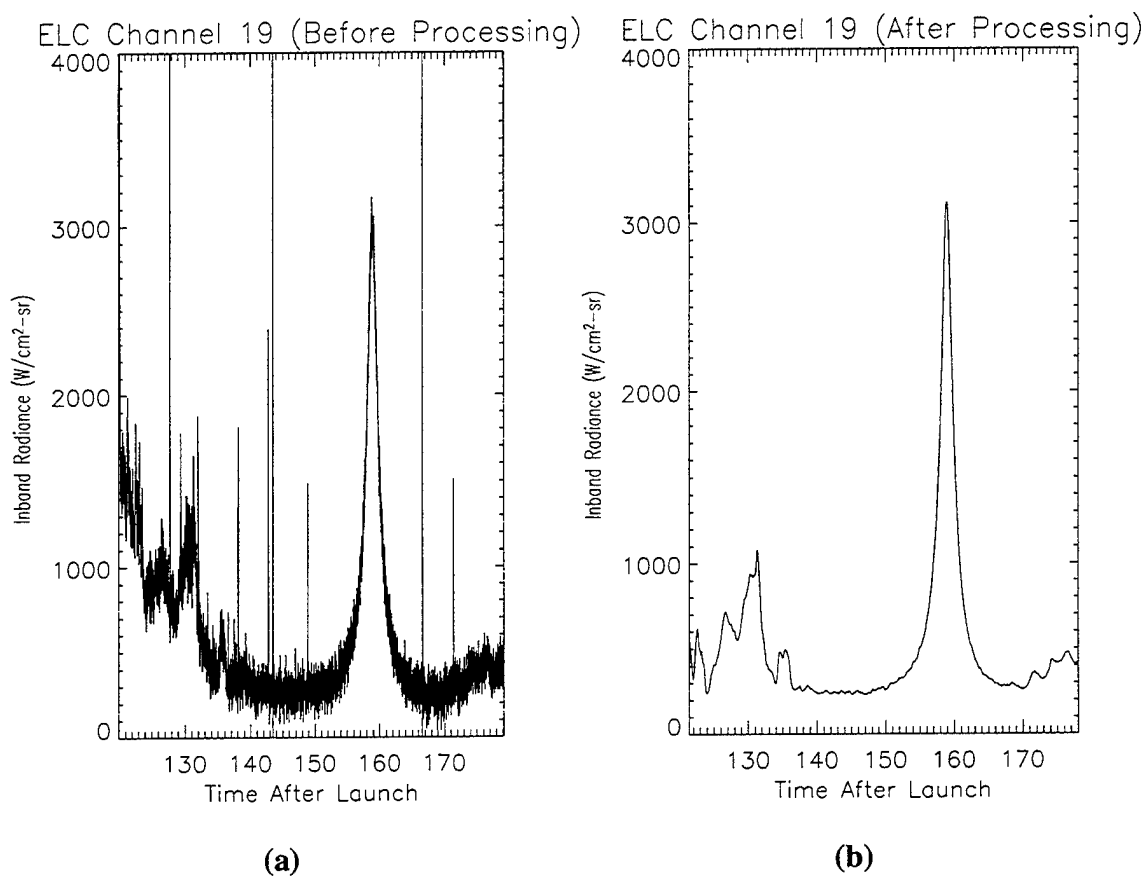

Figure 11   Representative ELC Data
a) Before Processing
b) After Processing

The data were despiked in the next phase of the pipeline. The cosmic-ray-induced spikes were identified by a procedure similar to the ZIP despiker: the data streams were scanned with wide and narrow boxcar averages, regions with 5σ discrepancies were removed, and the data gaps were filled by interpolation. (In fact, the ELC despiker chronologically preceded the ZIP despiker.)

17

Next, the despiked data were smoothed by application of a lowpass Butterworth filter. At Dr. S. Price's suggestion, the data were also smoothed using the parabolicRempel filter which was discussed in connection with the ZIP pipeline. No significant difference was found between the results of the Butterworth and Rempel filters.

To first order, the ELC OAR should be a factor of ~6.5 better than ZIP because the ELC detectors are smaller. Therefore, the issue of off-axis irradiance was not considered relevant for ELC and a stage of the pipeline was not devoted to this issue.

Because of the limited amount of ELC data relative to ZIP, less information is available for phenomenological atmospheric and outgassing modelling. Thus, the correction for atmospheric radiance and outgassing was performed by a roll-to-roll comparison using an "ELC-knows-best" approach. Such a comparison was possible because the Long Roll occupied an angular extent of 430°.

The data resulting after the roll-to-roll comparison remained noisy, and it was again smoothed with a boxcar average to yield Figure 11b. One smoothing was performed on the ZIP data and two on ELC, as the ELC data are significantly noisier than the ZIP data.

3.2   RECALIBRATION

The next task is to make the ZIP and ELC rocket probe data consistent with the larger COBE/DIRBE database. To do this, a color correction arising from the difference between ZIP/ELC and COBE/DIRBE bandpasses must be applied, and the ZIP/ELC data must be normalized to the COBE/DIRBE calibrations; a caveat is that we have used a preliminary DIRBE archive (good to ±10%) which was made available to us by courtesy of the DIRBE Science Working Group. The renormalization can be comprised of both a gain and an offset. If F is the power measured in a given ZIP/ELC spectral band (as determined by the pipeline process up to the renormalization stage) and F_{DIRBE} is the power in the corresponding DIRBE band, the relationship

$$F_{renormalized} = k_{gain}F + k_{offset} = k_{color}F_{DIRBE} \tag{4}$$

is adopted for the recalibration; the k's are recalibration parameters and the F's are inband fluxes. For a given ZIP/ELC band, the color correction factor k_{color} is computed by considering the nearest band of the DIRBE instrument and rescaling for a blackbody bandwidth and responsivity:

$$k_{color} = \frac{\int_{flight} d\lambda\, B(\lambda,T)R_{ZIP}(\lambda)}{\int_{DIRBE} d\lambda\, B(\lambda,T)R_{DIRBE}(\lambda)}, \tag{5}$$

18

where $R(\lambda)$ is the generalized spectral responsivity and $B(\lambda,T)$ is the Planck function. The temperature of the Planck function is chosen to be the temperature of that component of the zodiacal light which the sensor is observing (thermal radiation at long wavelengths and reflected sunlight at short wavelengths); in a given waveband, the renormalization factor is relatively insensitive to a reasonable choice of T. When the color correction could plausibly be applied to match a ZIP/ELC band with two different DIRBE bands, we adopted the choice which ultimately led to the best overall fit with the DIRBE data. Table 1 presents k_{color} for the DIRBE to ZIP photometric transformations, and Table 2 presents k_{color} for the DIRBE to ELC transformations. In these tables, λ_{cg} is the center of gravity of the band and $\Delta\lambda$ is the effective bandwidth at the given blackbody temperature.

Table 1   ZIP/DIRBE Color Correction Factors

ZIP Band	ZIP Channels	Squareband		Corresponding DIRBE Band	Squareband		BB Temperature	k_{color}
		λ_{cg}	$\Delta\lambda$		λ_{cg}	$\Delta\lambda$	(K)	
1	1,2	3.06	1.02	4	4.8	.57	5000	9.45
2	3,4	3.84	1.95	4	4.8	.57	5000	7.67
3	5,6	5.85	1.54	4	4.8	.57	5000	1.32
4	7,8	8.22	1.81	5	11.5	7.5	200	.143
5	9,10	11.01	4.22	5	11.5	7.5	200	.720
6	11,12	10.6	2.31	5	11.5	7.5	200	.362
7	13,14	10.78	1.10	5	11.5	7.5	200	.165
8	15,16	13.19	1.80	5	11.5	7.5	200	.352
9	17,18	15.31	1.67	5	11.5	7.5	200	.350
10	19,20	16.78	3.23	6	22.5	15	200	.601
11	21,22	18.79	1.91	6	22.5	15	200	.311
12	23,24	20.93	2.15	6	22.5	15	200	.301
13	25,26	22.69	2.15	6	22.5	15	200	.346
14	27,28	25.40	3.97	6	22.5	15	200	.427
15	29,30	27.12	4.23	6	22.5	15	200	.367

Table 2   ELC/DIRBE Color Correction Factors

ELC Band	Squareband		Corresponding DIRBE Band	BB Temperature	k_{color}
	λ_{cg}	$\Delta\lambda$		(K)	
1	5.06	.71	4	280	2.64
2	9.64	.63	5	280	0.091
3	10.61	.91	5	280	0.133
4	11.51	.99	5	280	0.141
5	12.00	7.01	5	280	0.932
6	12.51	1.17	5	280	0.158
7	13.76	1.93	5	280	0.237
8	15.19	1.14	5	280	0.124
9	26.46	7.98	6	280	0.322

Because the ELC flight took place on 25 October (day of year 298) and the DIRBE cryogen was exhausted on 20 September (day of year 261) there is no DIRBE data for the similar day-of-year as the ELC flight. Therefore, we use the last available DIRBE dataset, corrected by the extrapolated sinusoidal annual variation of the zodiacal light seen in the IRAS and DIRBE data.

Next, the recalibration factors can be determined in terms of COBE/DIRBE and ZIP/ELC observations of the same patch of sky. The first step is to generate a DIRBE-based synthetic "scan" corresponding to the appropriate rocket LOS. These synthetic scans were created from weekly-averaged DIRBE data in the appropriate DIRBE bands for the 1990 equivalent calendar dates of the ZIP and ELC flights. These data were then multiplied by k_{color} to generate predicted ZIP and ELC inband fluxes.

The measured ZIP and ELC pipeline fluxes were fit to these predicted fluxes using both gain and offset corrections k_{gain} and k_{offset}. (In practice, the ZIP2 and ELC flights did not require offset corrections). The fit minimized the parameter Ξ, which is defined as the mean-square difference

$$\Xi = \frac{1}{n}\sum_{time}\left[k_{color}F_{DIRBE} - \left(k_{gain}F + k_{offset}\right)\right]^2 , \qquad (6)$$

where the sum is over all n contributing elements of the time series. We considered the option of weighting the above sum by the signal-to-noise ratio (SNR), but concluded that the high-SNR zodiacal plane occupies such a small fraction of the time series that the proposed new degree of

freedom for weighting lacks utility. Prior to the fit, times containing contamination data (due e.g. to the booster) were removed from the ZIP and ELC time series.

Table 3 presents the recalibration parameters for the ZIP channels, and Table 4 presents the ELC recalibration parameters.

Table 3a   ZIP1 Renormalization Factors

ZIP CHANNEL	k_{gain}	k_{offset}	Ξ w/(cm^2·sr-μ)
1	0.283	0.0	9.273e-12
2	0.273	5.0e-12	9.521e-12
3	0.616	5.0e-12	4.199e-12
4	0.534	5.0e-12	4.751e-12
5	0.109	1.0e-12	1.052e-12
6	0.108	0.0	8.229e-13
7	1.304	2.0e-11	1.792e-11
8	1.199	1.0e-11	1.687e-11
9	1.242	7.0e-11	4.854e-11
10	1.091	7.0e-11	5.312e-11
11	1.269	7.0e-11	1.991e-11
12	1.059	4.0e-11	2.124e-11
13	0.955	2.5e-11	1.007e-11
14	0.920	2.0e-11	1.047e-11
15	1.537	1.0e-11	2.250e-11
16	1.788	3.0e-11	2.565e-11
17	2.873	5.0e-11	1.469e-11
18	2.577	5.0e-11	2.131e-11
19	2.078	5.0e-11	2.959e-11
20	2.552	5.0e-11	2.809e-11
21	3.141	3.0e-11	2.195e-11
22	3.819	3.0e-11	1.939e-11
23	4.306	3.0e-11	2.201e-11
24	3.632	3.0e-11	2.305e-11
25	2.941	1.0e-12	4.498e-11
26	6.200	1.0e-11	4.640e-11
27	5.432	1.0e-11	3.093e-11
28	3.935	3.0e-11	3.153e-11
29	3.921	4.0e-11	3.755e-11
30	3.892	1.0e-11	3.612e-11

Table 3b   ZIP2 Renormalization Factors

ZIP CHANNEL	k_{gain}	Ξ w/(cm^2·sr-μ)
1	0.235	1.015e-11
2	0.135	7.756e-12
3	0.056	4.602e-12
4	0.111	5.642e-12
5	0.061	1.282e-12
6 *	0.866	9.977e-13
7	1.597	3.271e-11
8	0.430	1.886e-11
9	2.103	7.033e-11
10	1.614	5.656e-11
11	2.142	3.752e-11
12	1.421	2.485e-11
13	1.820	2.468e-11
14	0.930	8.710e-12
15	2.112	2.938e-11
16	1.709	2.737e-11
17	4.556	4.237e-11
18	3.480	2.473e-11
19	3.419	6.395e-11
20	3.502	5.180e-11
21	3.691	5.755e-11
22	3.419	3.325e-11
23	4.643	4.115e-11
24	3.422	3.061e-11
25	2.706	7.124e-11
26	1.728	8.068e-11
27	2.967	7.946e-11
28	2.404	7.782e-11
29	1.508	8.361e-11
30	1.846	7.998e-11

* "Dead" Channel

Table 4   ELC Renormalization Factors

ELC CHANNEL	k_{gain}	Ξ w/(cm^2·sr-μ)
1	0.247	1.850e-12
2	0.618	5.659e-12
3	0.863	7.792e-12
4	1.206	1.119e-11
5	0.749	7.048e-11
6	1.126	1.082e-11
7	1.620	1.246e-11
8	1.153	8.871e-12
9	1.214	2.513e-11

3.3   ANALYSIS OF UNCERTAINTY

There are two kinds of uncertainty in the ZIP and ELC data: an uncertainty in the absolute bias of the data, and an uncertainty in the repeatability. The uncertainty in the absolute bias depends on details of the ground calibration which are no longer available. However, because the ZIP and ELC data are recalibrated to the COBE/DIRBE data (and the COBE/DIRBE calibration is regarded as correct), the uncertainty in absolute bias is not crucial to this investigation.

The uncertainty in repeatability can be determined by taking advantage of the fact that each ZIP and ELC band has at least two detectors, i.e., each band has a minimum of two channels. If the inband energies F1 and F2 recorded in the channels of a two-channel band are treated as independent random variables with identical mean values and standard deviations, by linearizing in the deviations from the mean, the standard deviation can be determined from the quantity

$$X \equiv \frac{F_1 - F_2}{F_1 + F_2} \cong \frac{\delta F_1 - \delta F_2}{2\overline{F}} \quad . \tag{7}$$

Taking the mean square yields

$$\overline{X^2} = \frac{\sigma^2}{2\overline{F}^2} \quad . \tag{8}$$

23

The relative standard deviation $\sigma / \overline{F}$ can therefore be determined from the channel-to-channel comparison. The above procedure is readily generalized to bands with an arbitrary number of channels. Results for the ZIP and ELC bands are shown in Tables 5 and 6.

Table 5   ZIP Fractional Uncertainty

Band #	ZIP1	ZIP2
1	*	*
2	0.193	0.086
3	0.208	*
4	0.213	0.276
5	0.019	0.017
6	0.155	0.180
7	0.107	0.093
8	0.043	0.070
9	0.063	0.048
10	0.015	0.025
11	0.077	0.053
12	0.056	0.026
13	0.168	0.179
14	0.063	0.098
15	0.116	0.138

*Only One Channel Available

Table 6   ELC Fractional Uncertainty

Band #	ELC
1	0.569
2	0.336
3	0.199
4	0.299
5	0.168
6	0.165
7	0.134
8	0.311
9	0.160

4 DESCRIPTION OF DATA ARCHIVE

4.1 DESCRIPTION OF ARCHIVE

The zodiacal archive generated by our contract activity consists of the renormalized and reprocessed ZIP and ELC data. The ZIP and ELC archives are time ordered with a right ascension/declination (RA/DEC) coordinate and time-after-liftoff (TALO) field followed by a radiance value for each respective channel. All of the flight data has been reduced to a 0.1° angular resolution. The unit of inband intensity is W/cm^2/sr. The squareband effective wavelengths and bandwidths are also included. Because of the three-point averages taken in the preprocessing phase of the ZIP pipeline, the ZIP time history has 1/3 of the entries in the original ZIP data stream. To maintain identical time steps in the ELC and ZIP archives, after pipeline processing was complete, the ELC data was averaged over an appropriate time increment. This step completed the pipeline processing. The number of entries in the resulting ELC archive is approximately one-tenth of the number in the original ELC data stream.

The archive is provided in both ASCII and IDL XDR formats. The analysis pipeline and display tools are written in IDL. The pipeline stages are coded in modular form so that a user can modify the processing. For the user's convenience, the XDR-formatted data is included to enable the quick restoration of data without the necessity of a lengthy ASCII ingestion procedure.

4.1.1 The ZIP Archives

The pipeline results for the ZIP1 and ZIP2 flights are recorded in separate archives. The first entry in each ZIP archive is an enumeration of the radiometric bands for the corresponding ZIP flight. Subsequently, both archives will present time histories of the sensor orientation and the inband radiances. Each of the 30843 entries in the time history will present the TALO, the sensor right ascension and declination, and the radiance values in every channel.

4.1.2 The ELC Archives

The structure of the ELC archive is similar to that of the ZIP archive: an enumeration of the radiometric bands is followed by time histories of the sensor orientation and inband radiances. The time history consists of 3113 entries.

4.2 DISPLAY TOOLS AND GRAPHICAL USER INTERFACES

4.2.1 Display Tools

We have developed a number of IDL tools for the access, display and manipulation of the ZODI archive. These tools are listed below.

read_arc.pro: IDL routine to ingest the *.xdr archive into dynamic IDL structures

z1_clip.pro: IDL routine to remove anomalous first two rolls from ZIP1 timeseries

z_contam.pro: IDL routine to remove contaminated data from any flight

arc_view.pro: IDL procedure to make top-level shaded surface display of an entire flight archive: radiance vs wavelength & time

z_time.pro: IDL procedure to plot time-ordered archive radiance by channel and by band

z_cvrg.pro: IDL procedure to display the coverage in given astronomical coordinates, epoch, and map projection

zsp_time.pro: IDL procedure to plot spectra at given TALO

zsp_cord.pro: IDL procedure to plot spectra at given coordinate location

z_scan.pro: IDL procedure to plot synthetic orthogonal scans at constant longitude or latitude in given coordinate system

z_skymap.pro: IDL procedure to make falsecolor skymap

The above tools are unsupported and have only limited documentation.

4.2.2   Graphical User Interfaces (GUIs)

GUIs have been written to access the archive and to demonstrate the actual pipeline used to create the ZIP archives. These GUIs are provided with the caveat that PC-based IDL is required to utilize them. The GUIs themselves were developed with Microsoft Visual Basic and can be freely distributed in .exe form for PC platforms.

There are two separate GUIs. The first, denoted "ZIP Pipeline", allows the user to load a preliminary processed mission (smoothed and despiked ZIP1 or ZIP2) and to step a user-selected band through various stages of the pipeline processing. The corrections are made in real time and at any point a user can choose a diagnostic step such as roll-to-roll comparisons or detector radiance vs cohabitant detector radiance. The latter diagnostic step also gives a value for the gain

26

and offset difference between same band channels. The readme file included with this GUI gives brief installation and operational instructions.

The second GUI, dubbed "Archive Tools," acts as an integrated interface to a subset of the display tools listed prior. It eliminates some computational redundancy concerning map projections and coordinate transformations. "Archive Tools" also presents the user with graphical representations of the tools available to him. An instructional readme file is included.

The first visible window in both GUIs is a prompt for the user's IDL license and site; necessary to allow the GUI to control IDL. Refer to the desktop Figure 12 to view the layout of the GUIs. The top window, beside the IDL prompt, is "ZIP Pipeline." The bottom window is "Archive Tools."
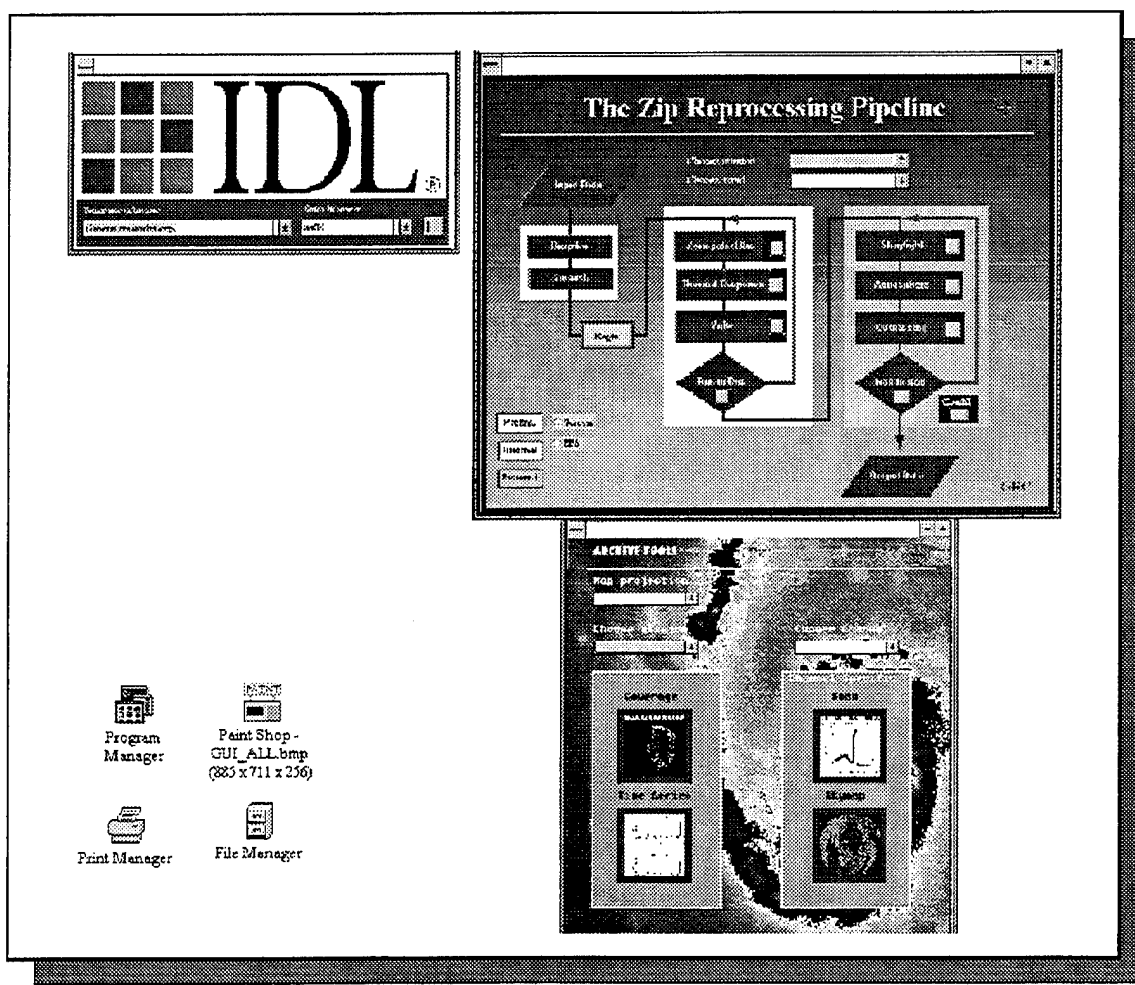
Figure 12   Layout of Provided GUIs

5   ANALYSIS OF ZODIACAL STRUCTURE

We have identified interesting spatial and temporal features in the ZIP and ELC data. The ZIP and ELC bands near 12μm and 25μm which match closely with IRAS and COBE are best suited for this investigation: they are the broadest ZIP and ELC bands and have some of the best signal-to-noise ratios. The multiple plane crossings by the ZIP scans allow a three-dimensional picture of the zodiacal cloud to be constructed and compared with existing zodiacal models. In addition, ELC may give some indications of dustbands at large elongation angles.

The temporal structure has also been studied. Although the ZIP and ELC flights flew within a four-year period, there appears to be considerable temporal variability in the polar-region spectra. This variability appears at the polar region which has very little asteroidal dust in the line-of-sight. In view of the conjecture that dust from the cometary belt falls in toward the Sun, one of the possibilities for interpreting this variability might be to hypothesize a cold (~ 100K) component to the background.

The results and details of the analysis activity will be recorded in the format of a scientific paper for the open astronomical literature.

6   SUMMARY AND CONCLUSIONS

This report has described a three-year study which GRCI has performed under contract to Phillips Laboratory to support Air Force characterization of the zodiacal background; such characterization is required to reliably operate high-performance space-based optical sensors. The GRCI effort was focused on the ZIP and ELC databases. Work was performed in three main areas:

- The reduction of the experimental data was upgraded.
- The reduced data was organized into a readily accessible database.
- The structure of the zodiacal dust was investigated by use of the database.

This Final Report completes a series of three technical reports which have been issued during the contract; in addition, a paper for the open scientific literature is in preparation.

The data reduction upgrade was implemented by means of a pipeline process which allowed for instrumental and environmental effects; the pipeline was followed by recalibration and error analysis. Development of the instrument part of the pipeline revealed the utility of the ZIP dark channels for removing dark noise from the data; also, we took into account the temperature dependence of the sensor responsivity, which was not considered in the reduction software supplied to GRCI with the data. During work on the environmental pipeline, our efforts to account for atmospheric/outgassing effects with predictive first-principles codes, including those in the data reduction package provided with the data, were inconclusive; instead, we developed a roll-to-roll comparison technique for extracting this correction by a self-consistent method based on the data. After the data had been run through the pipeline, the data were recalibrated. Because the reduction software which was provided to GRCI with the data did not have a recalibration capability, we proceeded by adjusting the gain and bias to achieve optimal consistency with COBE; after the gain and bias were adjusted, the ZIP/ELC archive and the COBE results were in good agreement. Notwithstanding the fact that the gain and bias had been adjusted to achieve consistency with COBE, a method to perform an error analysis was developed: channel-to-channel comparisons within a band quantified the repeatability of the measurements.

A data archive was designed to be a convenient resource for optical sensor mission planning and for zodiacal light studies, and the archive was constructed. It is being provided to Phillips Laboratory separately from this report. The archive puts the ZIP and ELC data on a common basis with COBE. The archive is readily accessed with a GUI. It gives the user options to work directly with the final data product or to recompute details of the pipeline process.

Analysis work has identified features of scientific interest in the ZIP/ELC data. These features will be discussed in a paper in preparation for the open scientific literature.

In summary, the ZIP/ELC data have been reduced and rationalized with COBE. A user-friendly, accessible data archive has been constructed for the ZIP/ELC measurements. Features of interest for solar system structure have been identified in the data. GRCI's work has provided a capability to Phillips Laboratory whereby the ZIP/ELC results can be readily utilized to provide celestial background information to support the missions of space-based optical sensors.

REFERENCES

1   S.D. Price, T.L. Murdock, L.P. Marcotte, "Infrared Observation of the Zodiacal Dust Cloud", Astronomical Journal, Vol. 85, No. 6, p. 765, June 1980.

2   T.L. Murdock and S.D. Price, "Infrared Measurements of Zodiacal Light", Astronomical Journal, Vol. 90, No.2, p. 375, February 1985.

3   W.K. Cobb, C.L. Hamilton, J.G. Eoll, T.L. Murdock, "Zodiacal Light Data Investigation -- Interim Results for the Zodiacal Infrared Project (ZIP) Experiments", GRCI Technical Report 1949-02-93-TR, (30 September 1993).

4   G.G. Rempel, "Nonlinear (Parabolic) Smoothing of Experimental Data", Izvestia Earth Physics, No. 3, 1974, pp.101-105.

5   "Earthlimb Clutter Focal Plane Assembly Final Test Data Report and Users Manual", Naval Research Laboratories Technical Report 83-1187, 19 January 1983.

6   "SPIRIT III/EDX Focal Plane Array Subsystem Critical Design Review Package", Aerojet   ElectroSystems, November 1989.

7   W.K. Cobb, S.V. Burdick, and T.L. Murdock, "Zodiacal Light Data Investigation -- Interim Results for the Earthlimb Clutter Experiment", Air Force Phillips Laboratory Technical Report PL-TR-93-2179, (GRCI Technical Report 1949-01-93-TR), (15 July 1993). ADA274461

THIS PAGE INTENTIONALLY LEFT BLANK

APPENDIX

The figures in this Appendix record the stages of the pipeline process for all channels in the ZIP1 and ZIP2 flights; the corresponding results for ELC are given in Reference 7. The pipeline runs smoothly for the great majority of the ZIP channels, but there is a small number of difficult cases. Although the data quality in ZIP1 Channels 1 and 2 and in ZIP2 Channel 1 is well below the norm, results for these channels are presented. However, the ZIP2 Channel 6 data is so poor that this channel is considered dead and pipeline results are not provided.

Each figure tracks the major intermediate stages of the data in a given ZIP channel as the data traverses the processing pipeline. Each figure is subdivided into six windows with the common horizontal axis of TALO in seconds. The top three windows show instrument effect corrections, and have units of volts. The bottom three windows show environmental corrections and have units of inband radiance.

The main trace in each window shows the data after it has passed through the pipeline stage corresponding to the window. This main trace is plotted using a dot per time series point (in time intervals in which the data are relatively constant, the points coalesce to mimic a solid line); the dot-per-data-point format was adopted because it faithfully represents the discrete character of the time series and because a continuous interpolating line would create spurious spike-like structures and visually exaggerate the importance of outliers from the main data trend. The Zero-Point/Temperature, Outgas/OAR and Atmosphere windows use a short-dashed line (----) to represent the data before the pipeline correction was applied; a long-dashed line (– – – –) is used to represent the correction itself; in the Zero-Point/Temperature window, this correction is typically so small that a separate righthand axis is introduced to set the scale for the long-dashed line. As a guide to the eye, the bottom three windows use a horizontal dotted line (·····) to indicate the zero of the vertical axis.
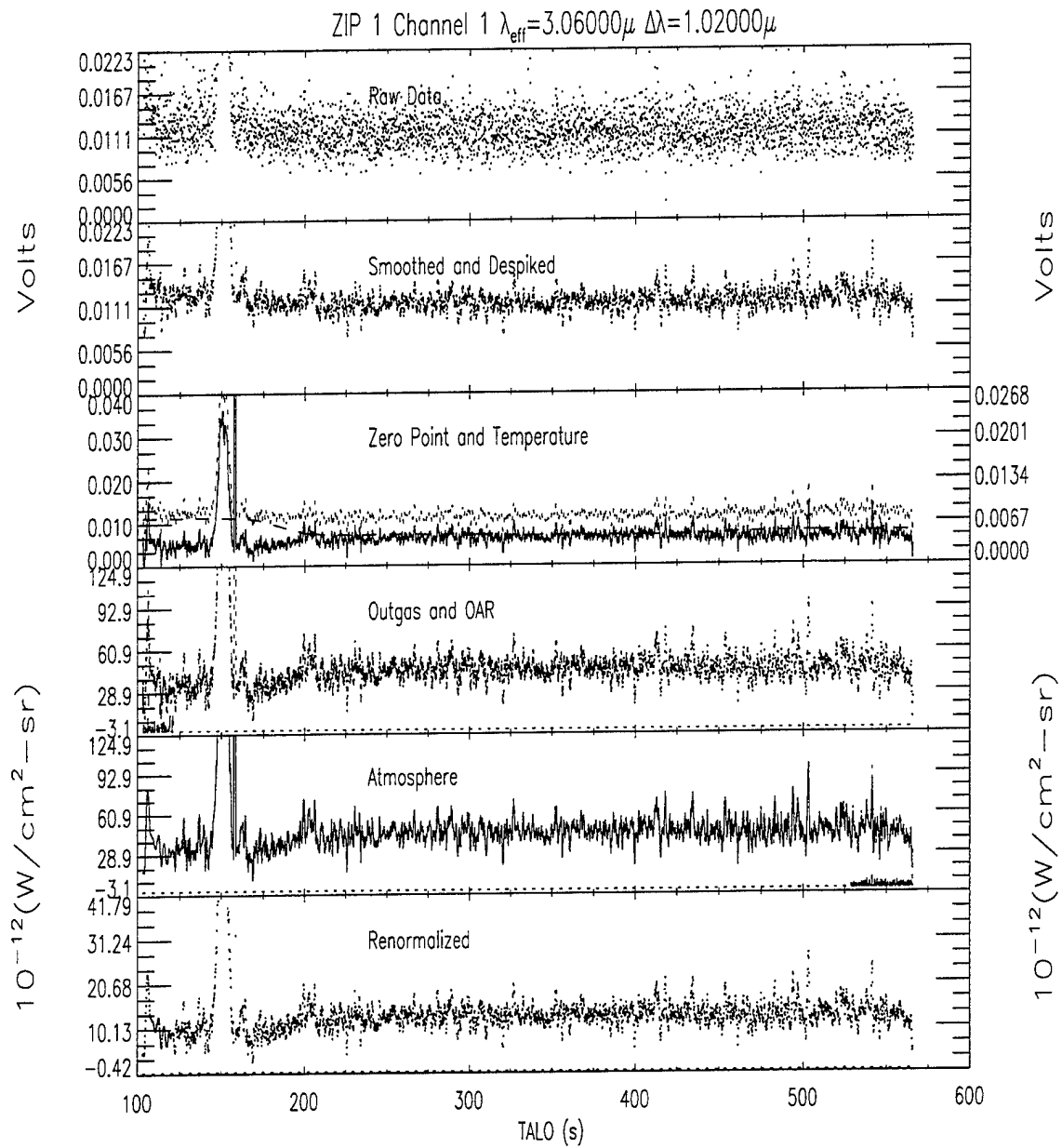
Figure A.1   Pipeline Flow for ZIP1 Channel 1
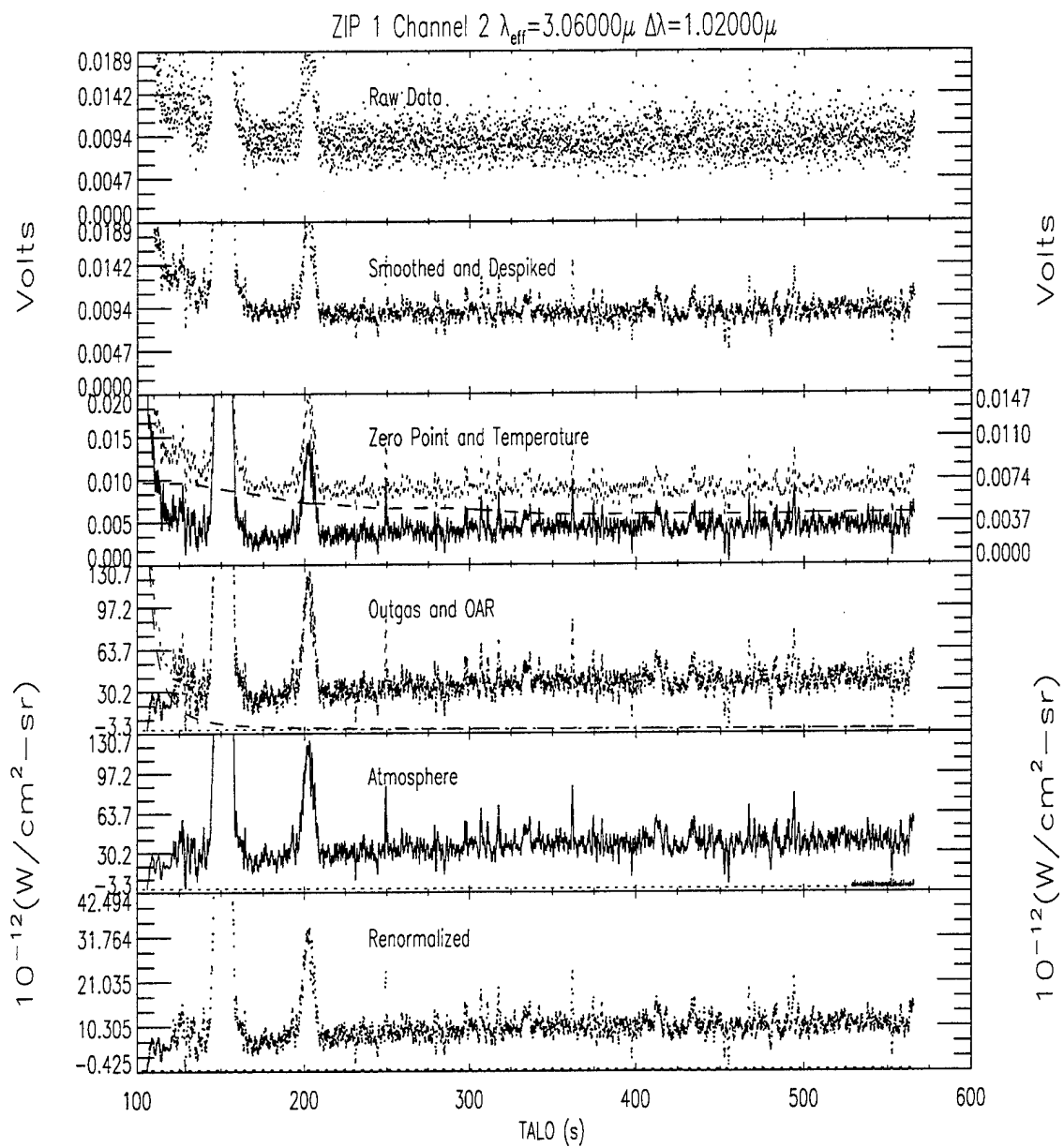
Figure A.2   Pipeline Flow for ZIP1 Channel 2
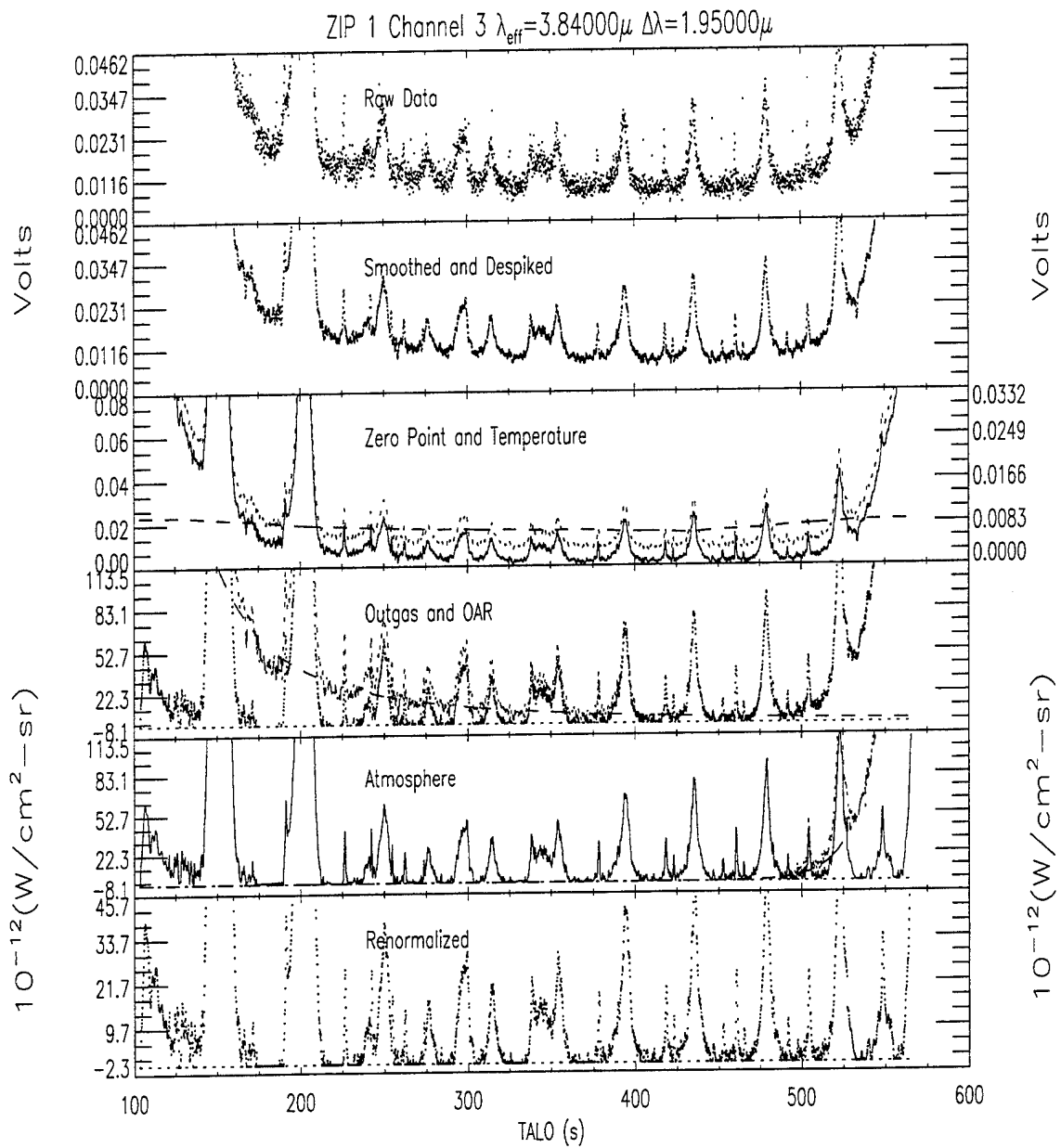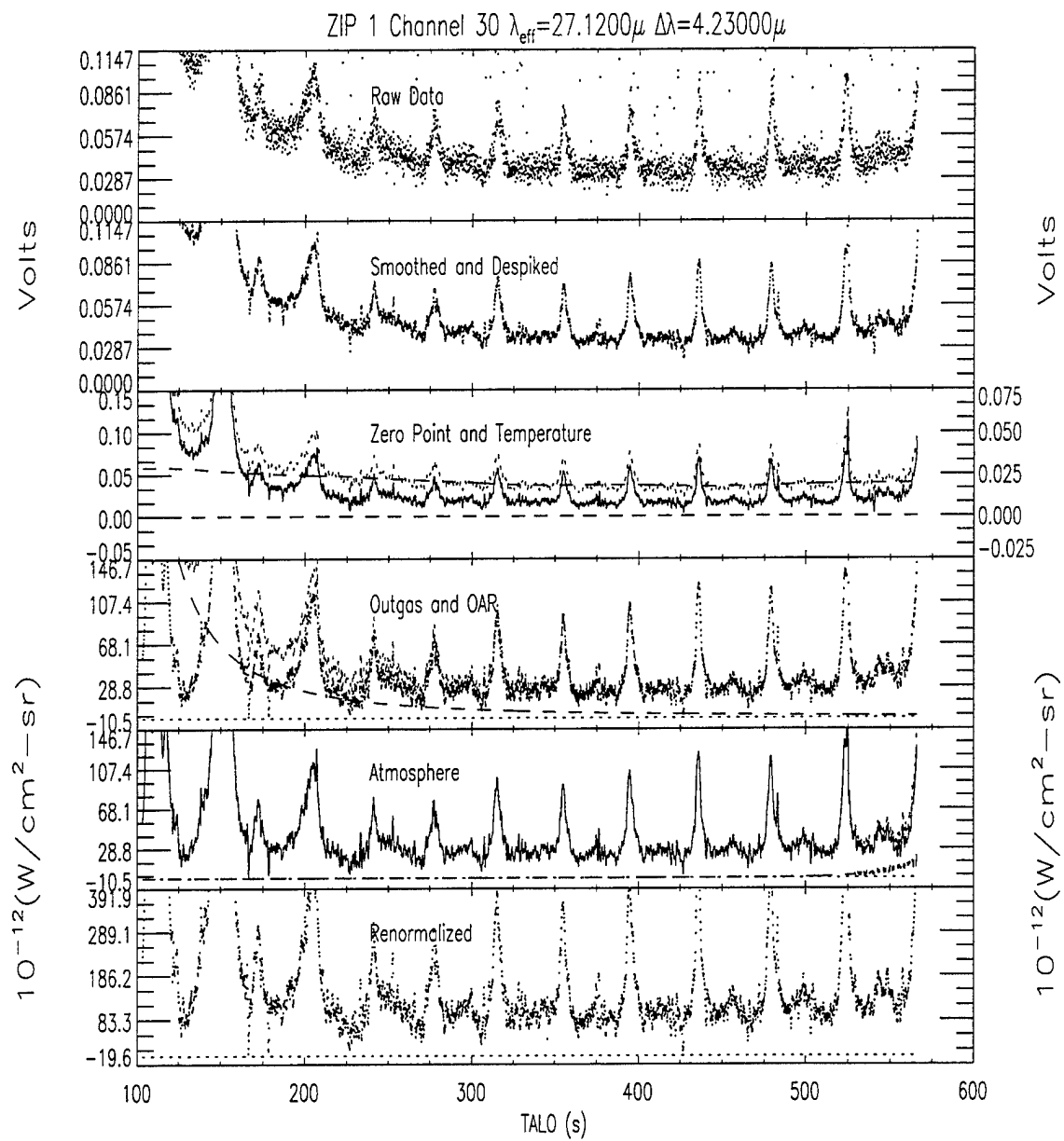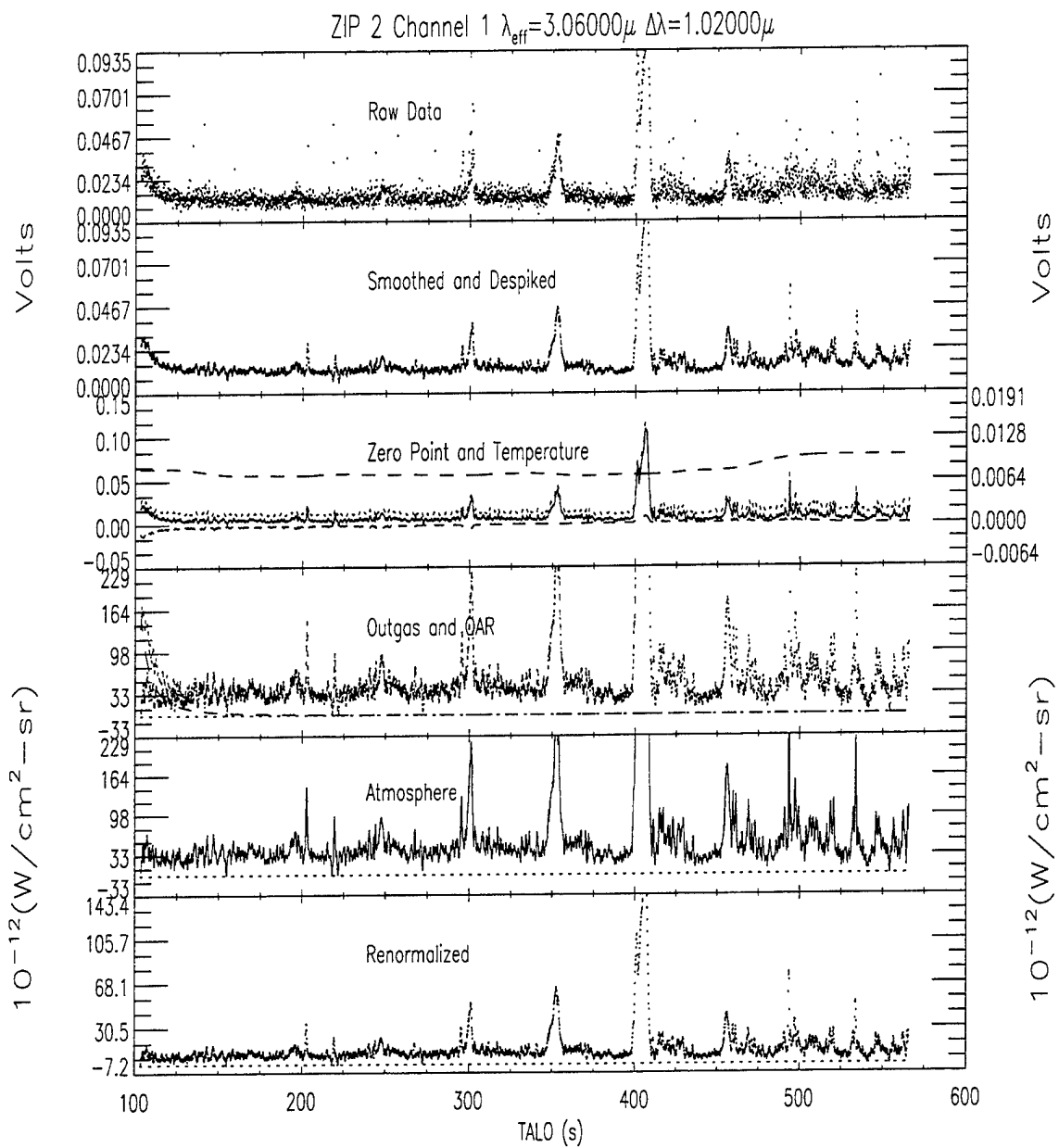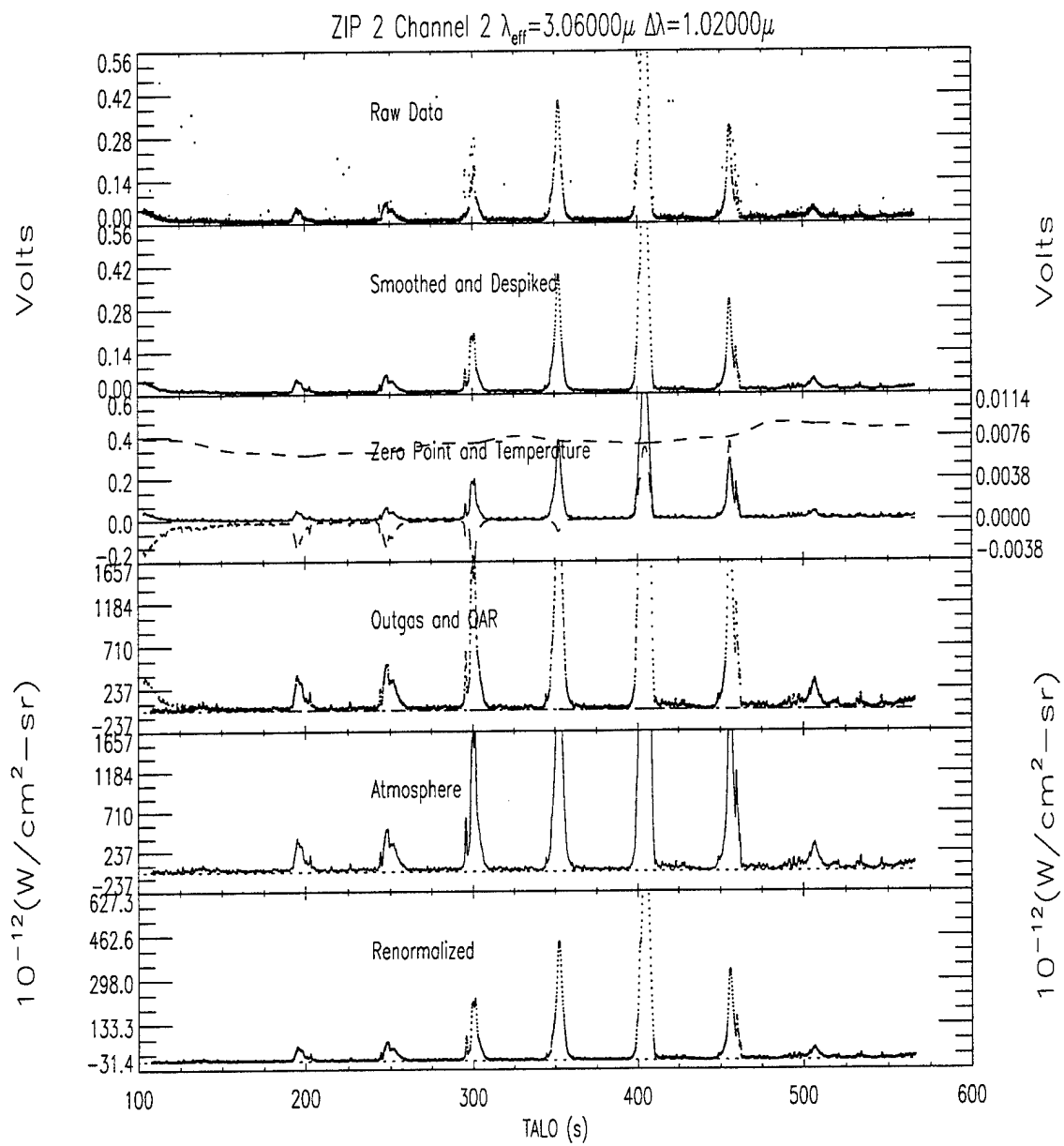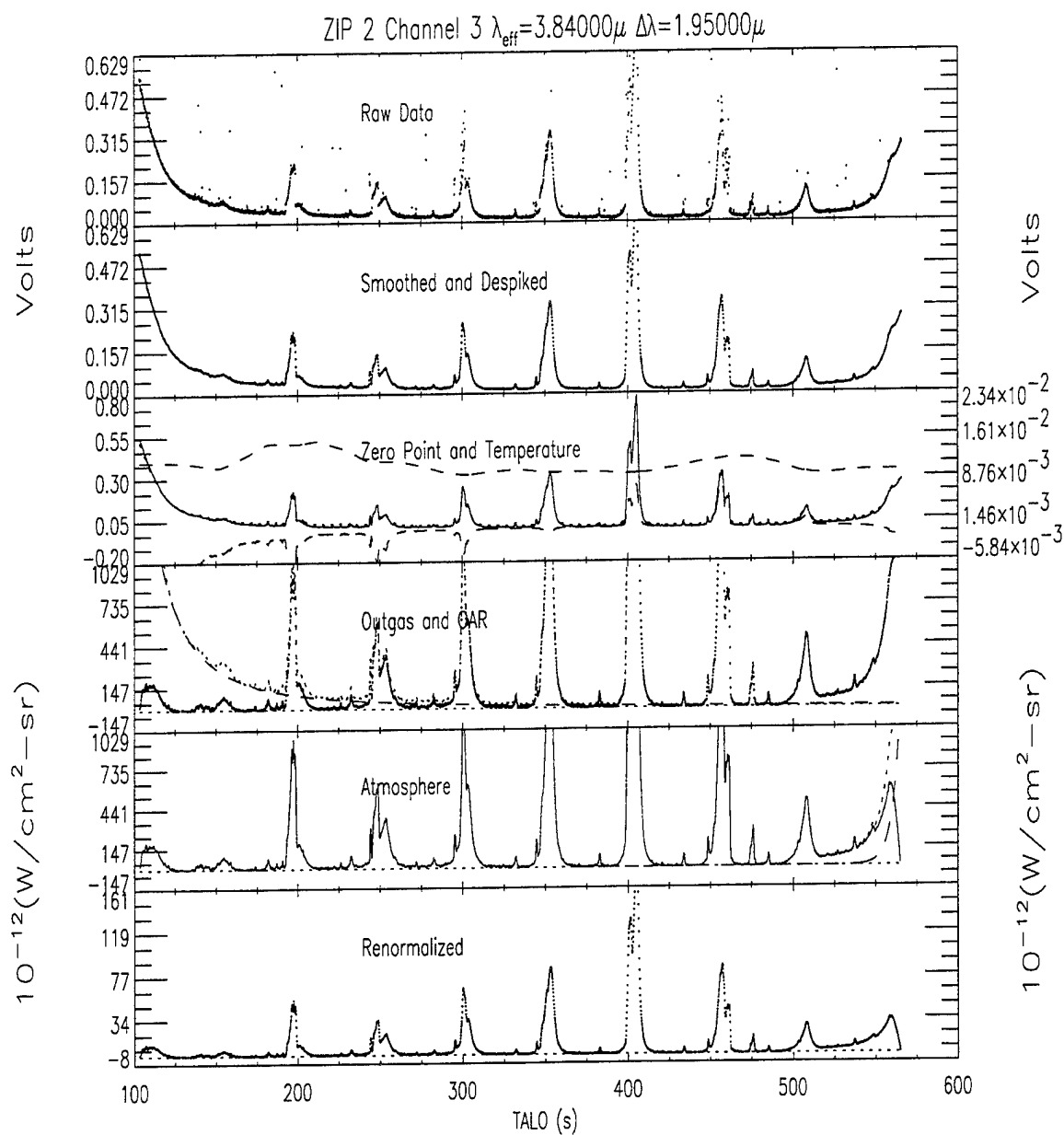
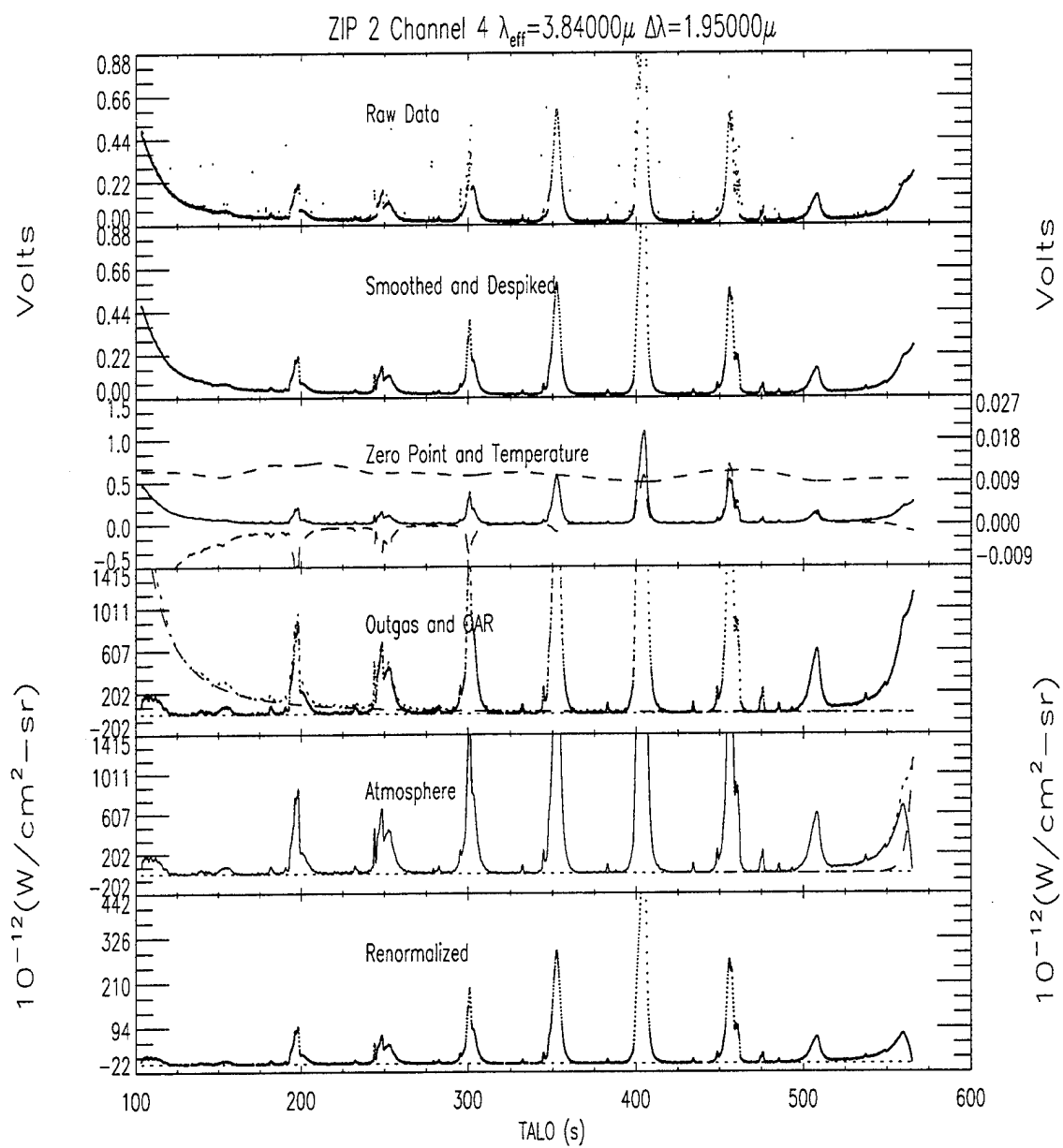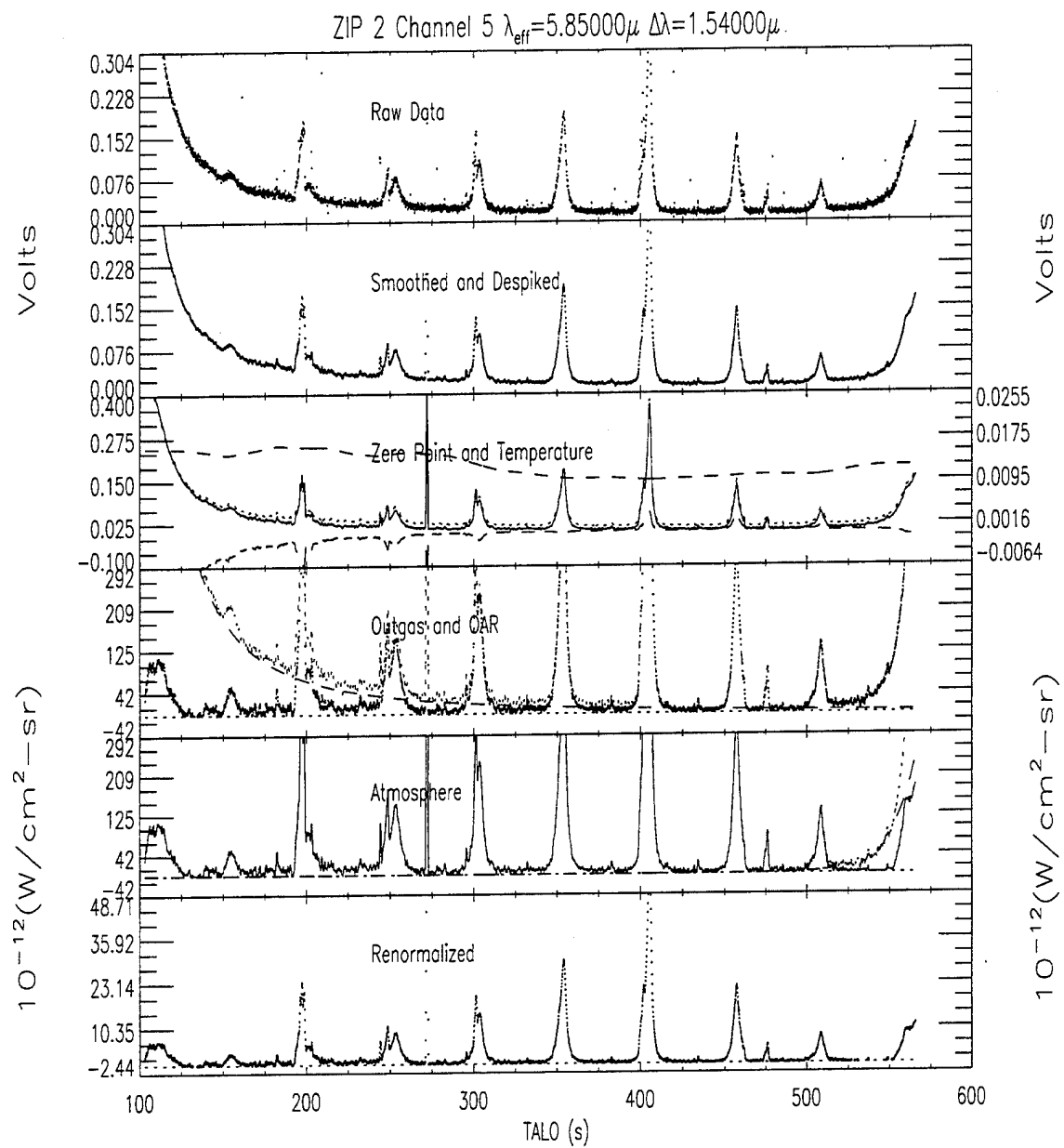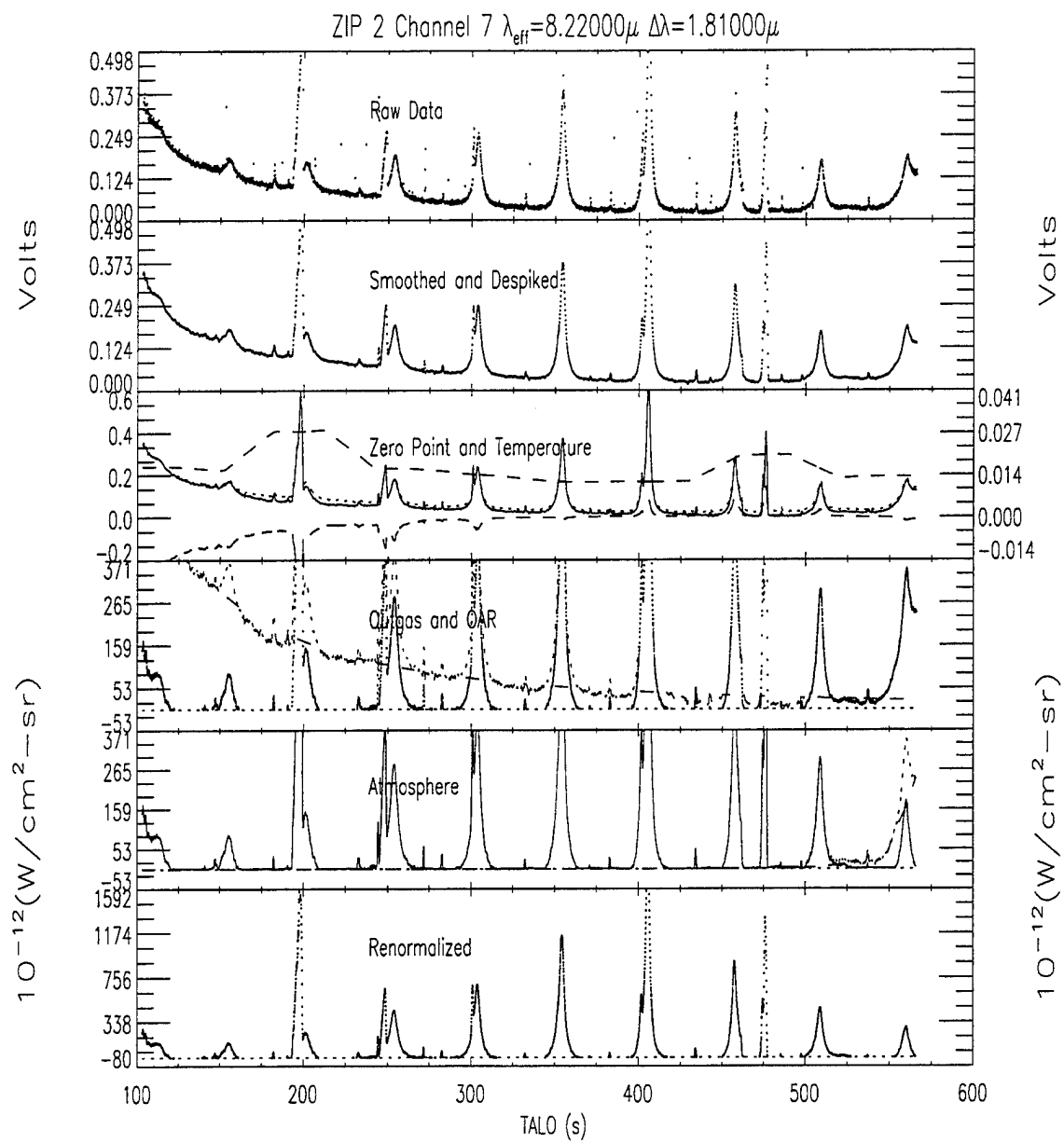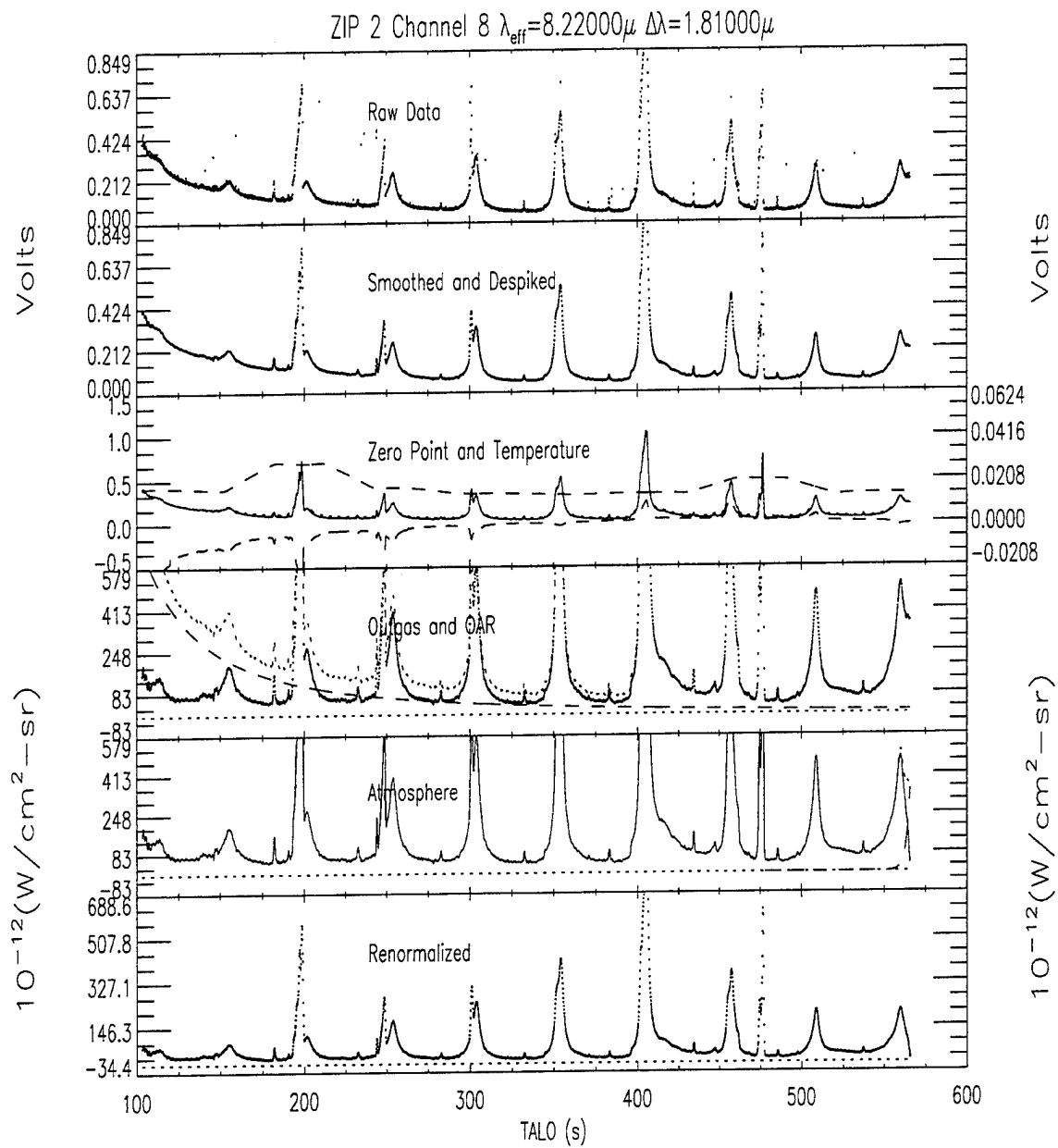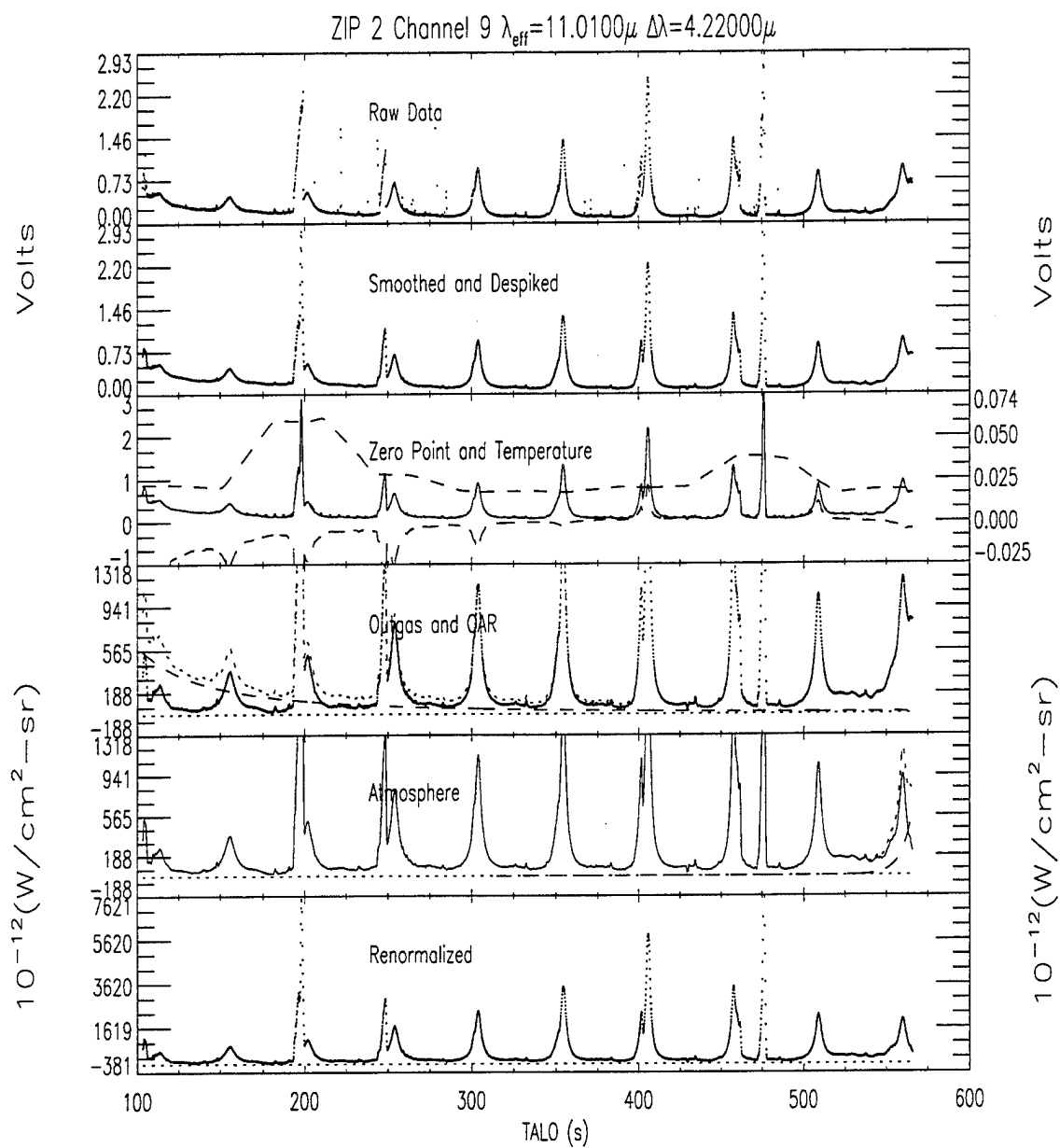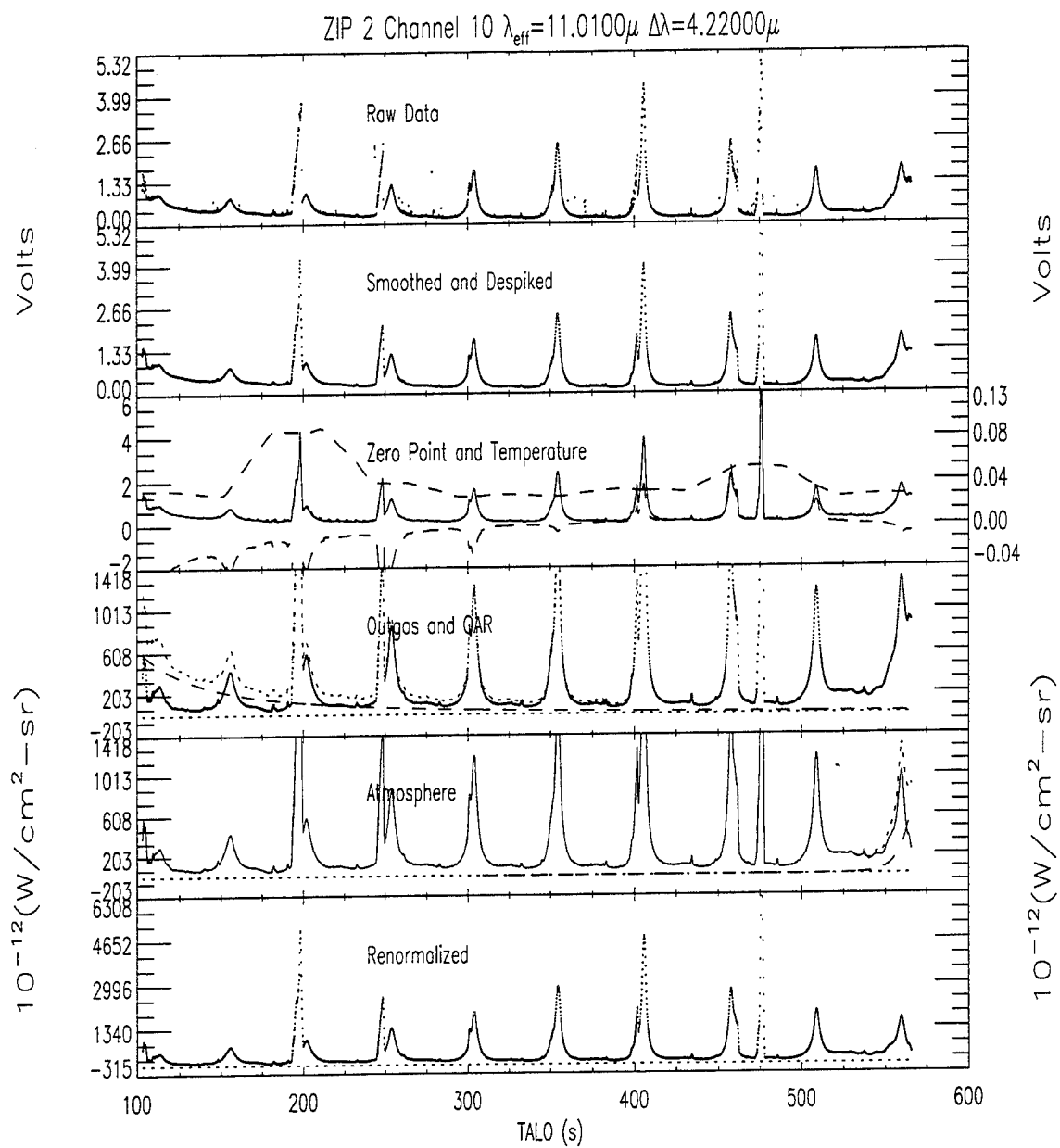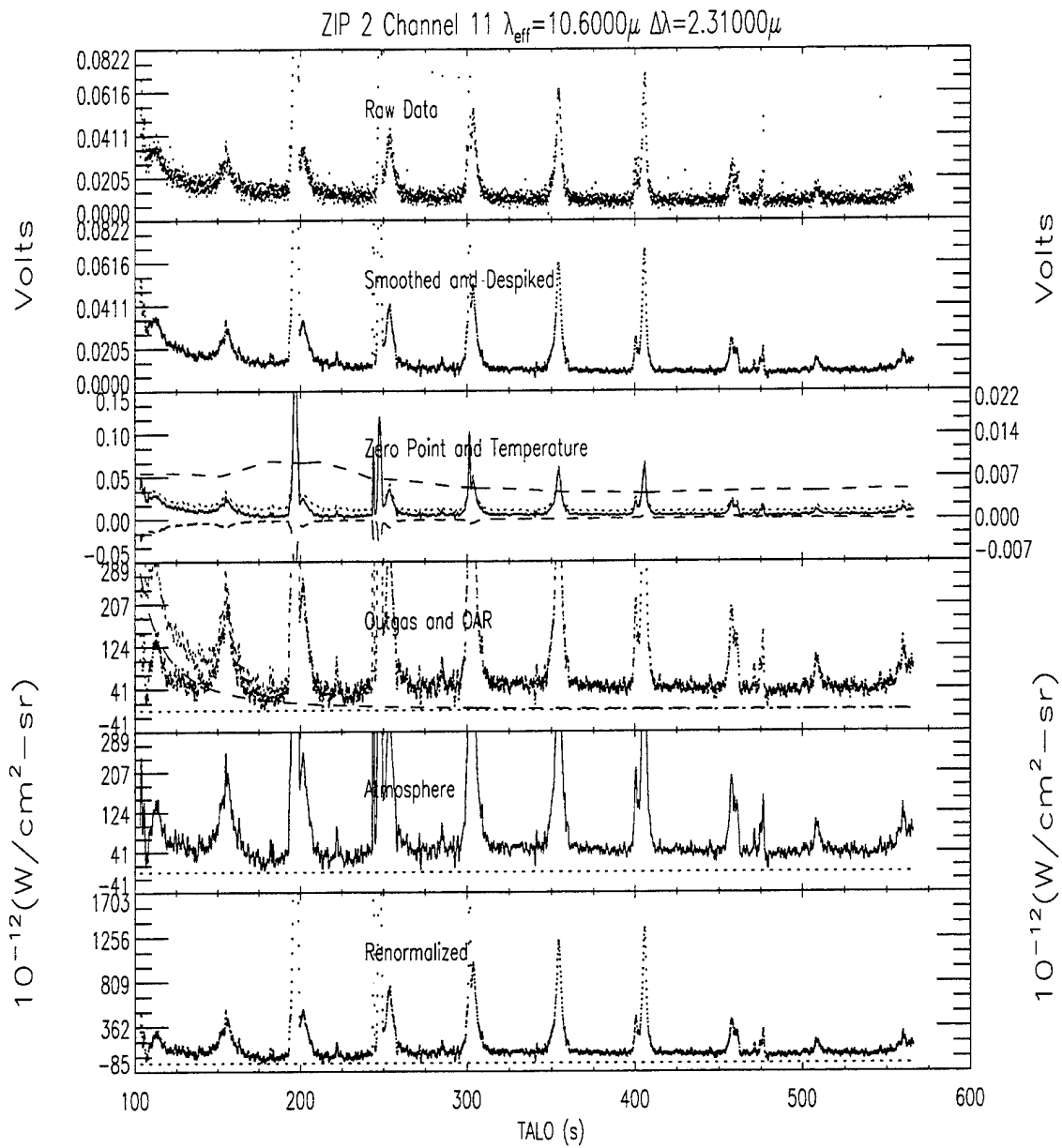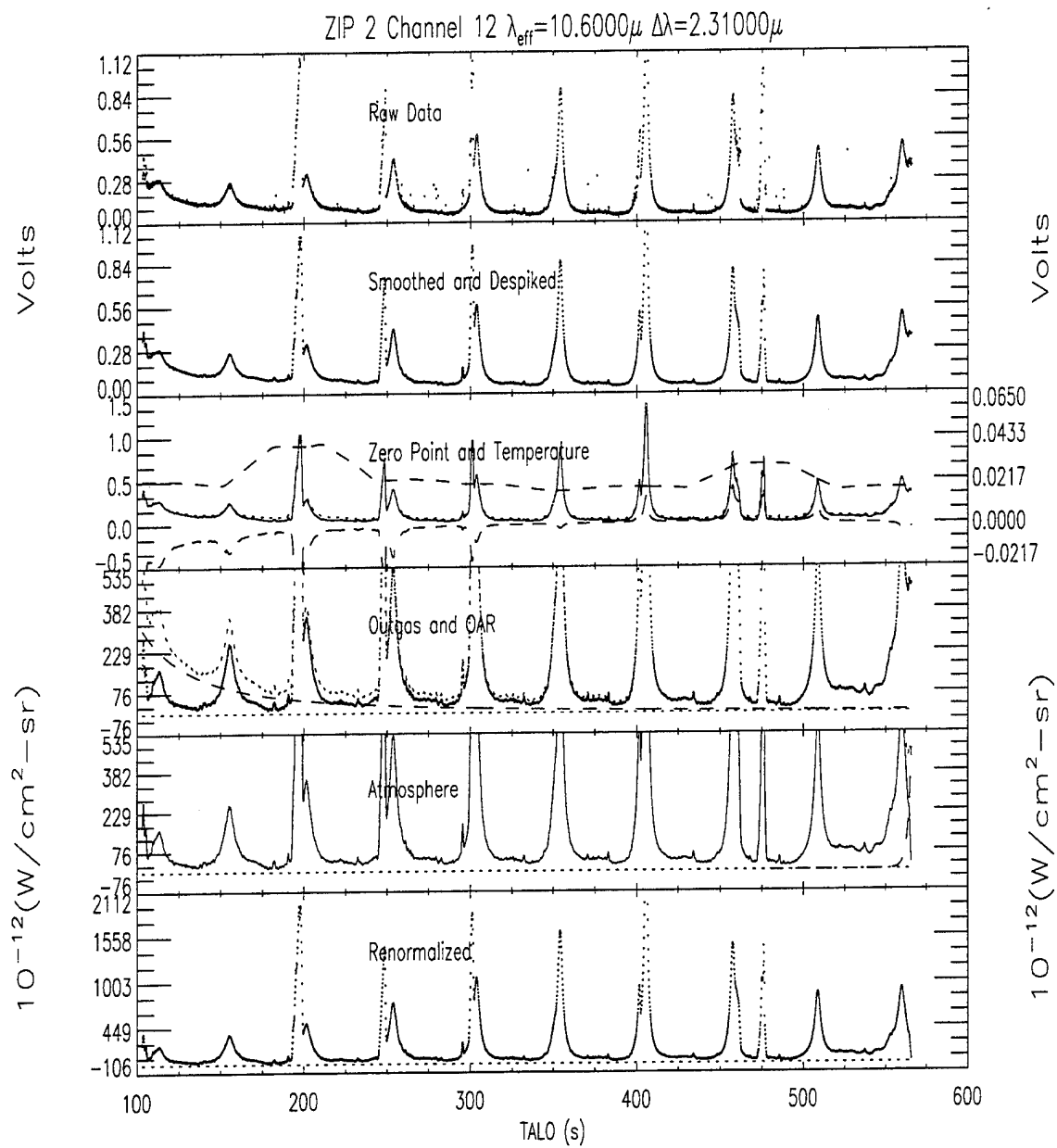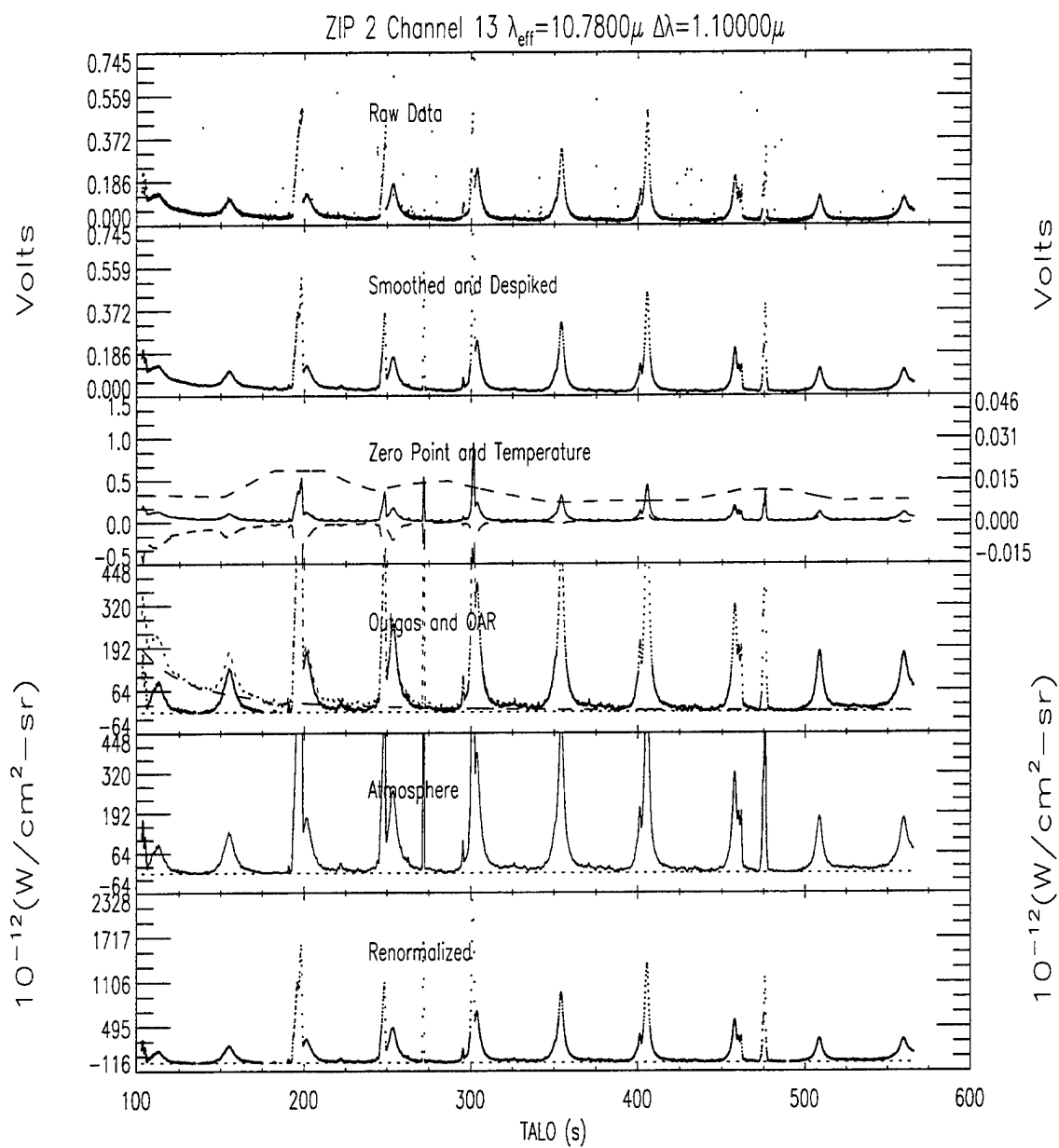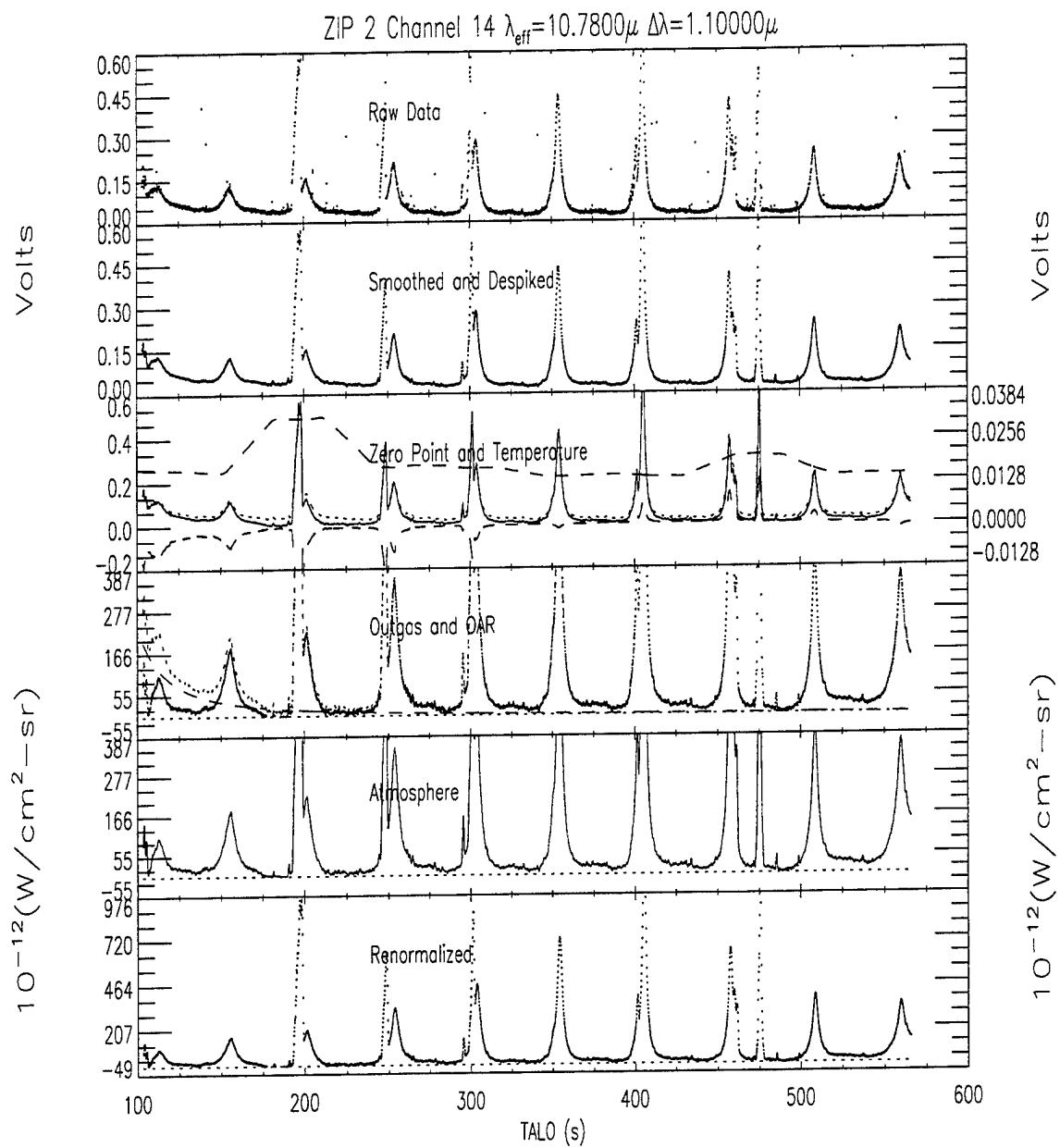**Figure A.3   Pipeline Flow for ZIP1 Channel 3**
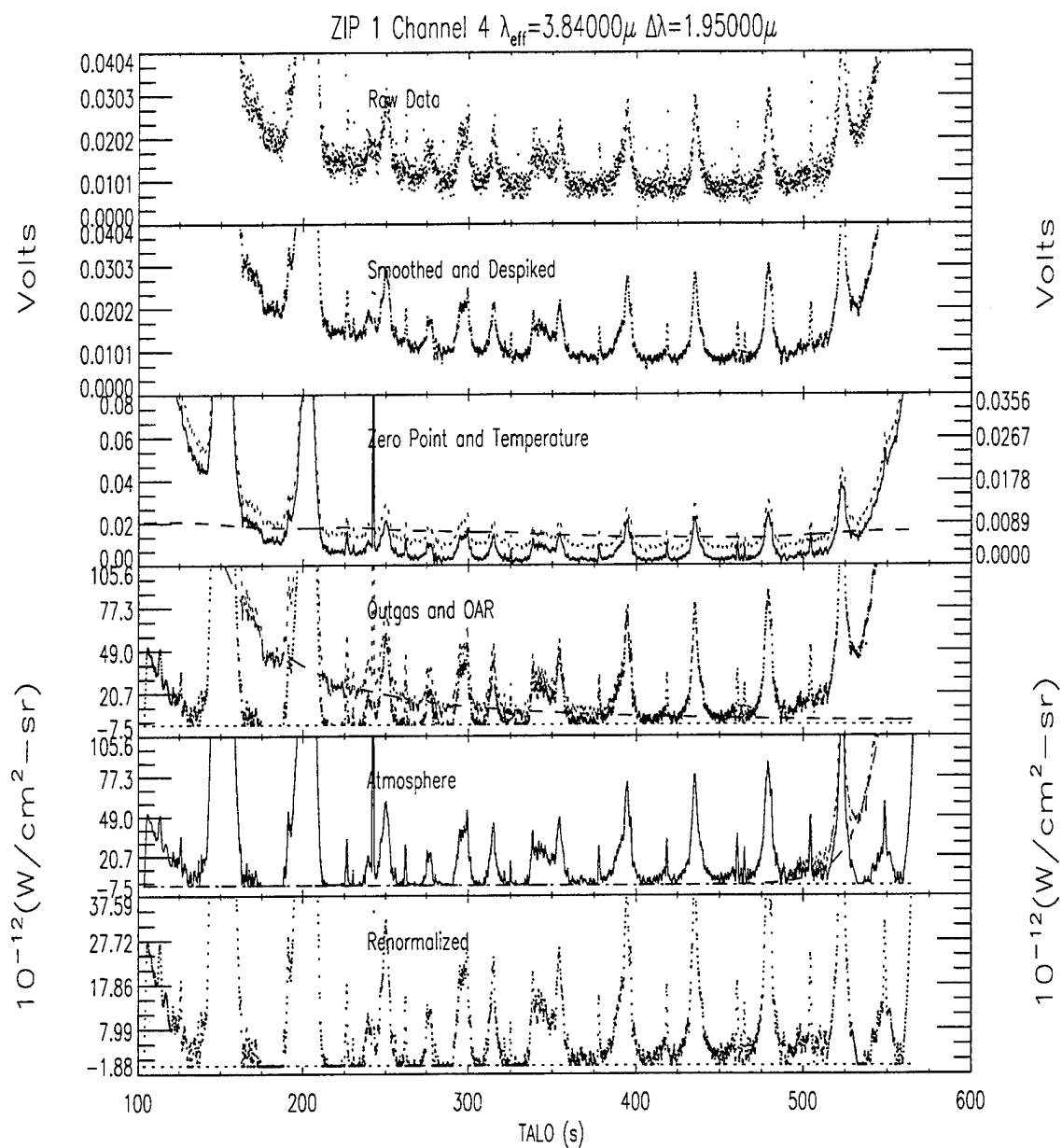
Figure A.4   Pipeline Flow for ZIP1 Channel 4
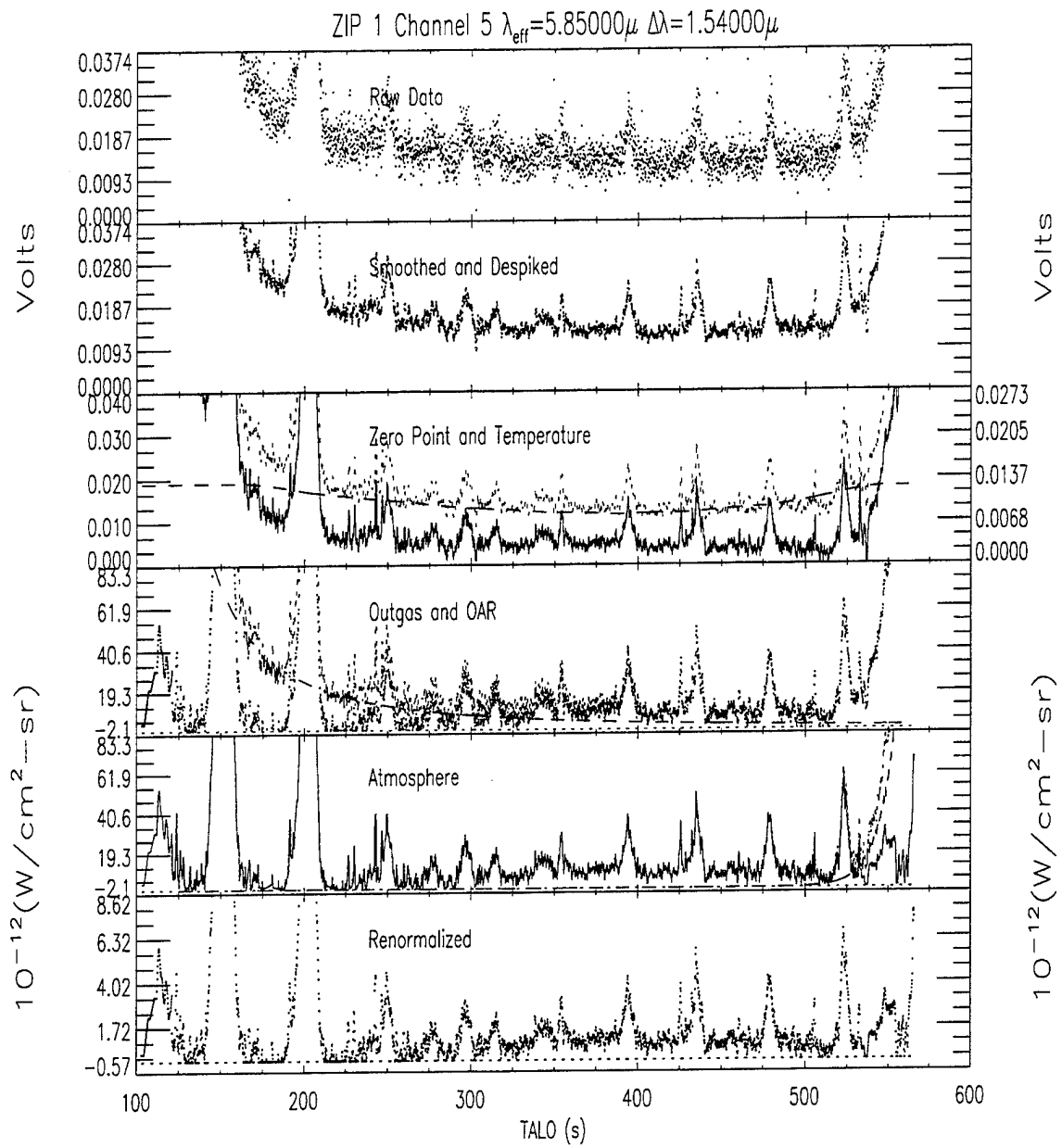
Figure A.5   Pipeline Flow for ZIP1 Channel 5
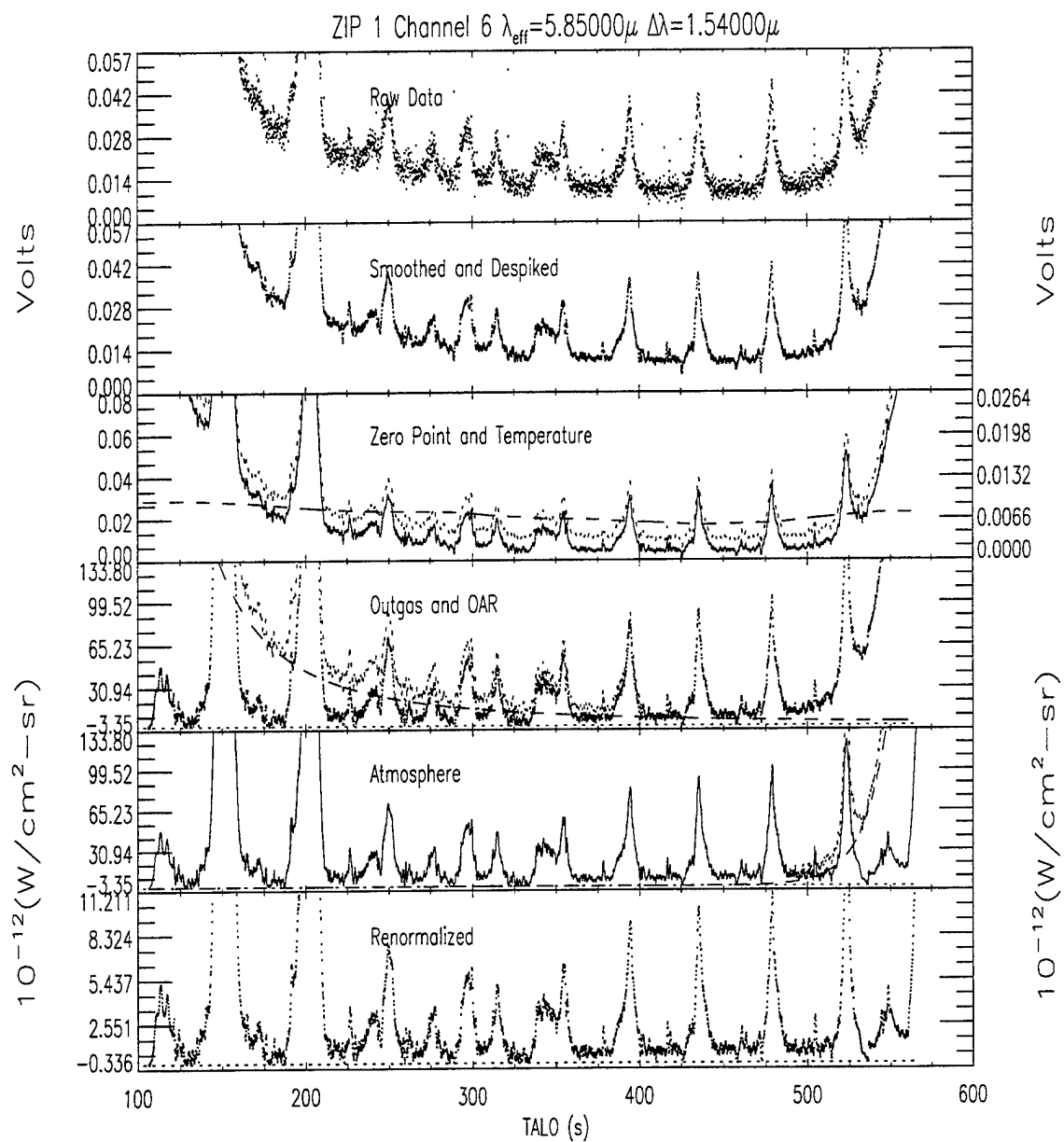
Figure A.6   Pipeline Flow for ZIP1 Channel 6
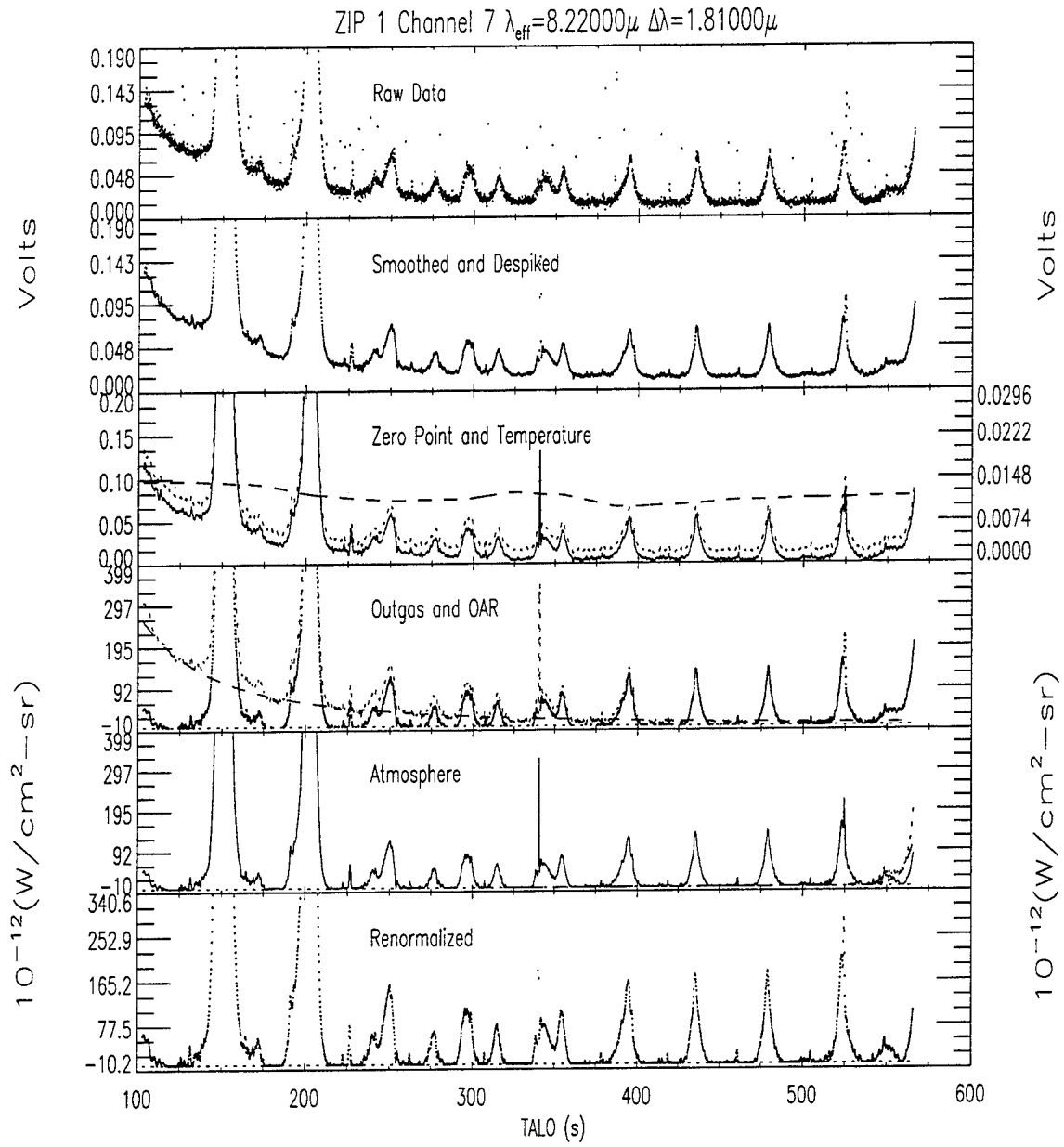
Figure A.7   Pipeline Flow for ZIP1 Channel 7
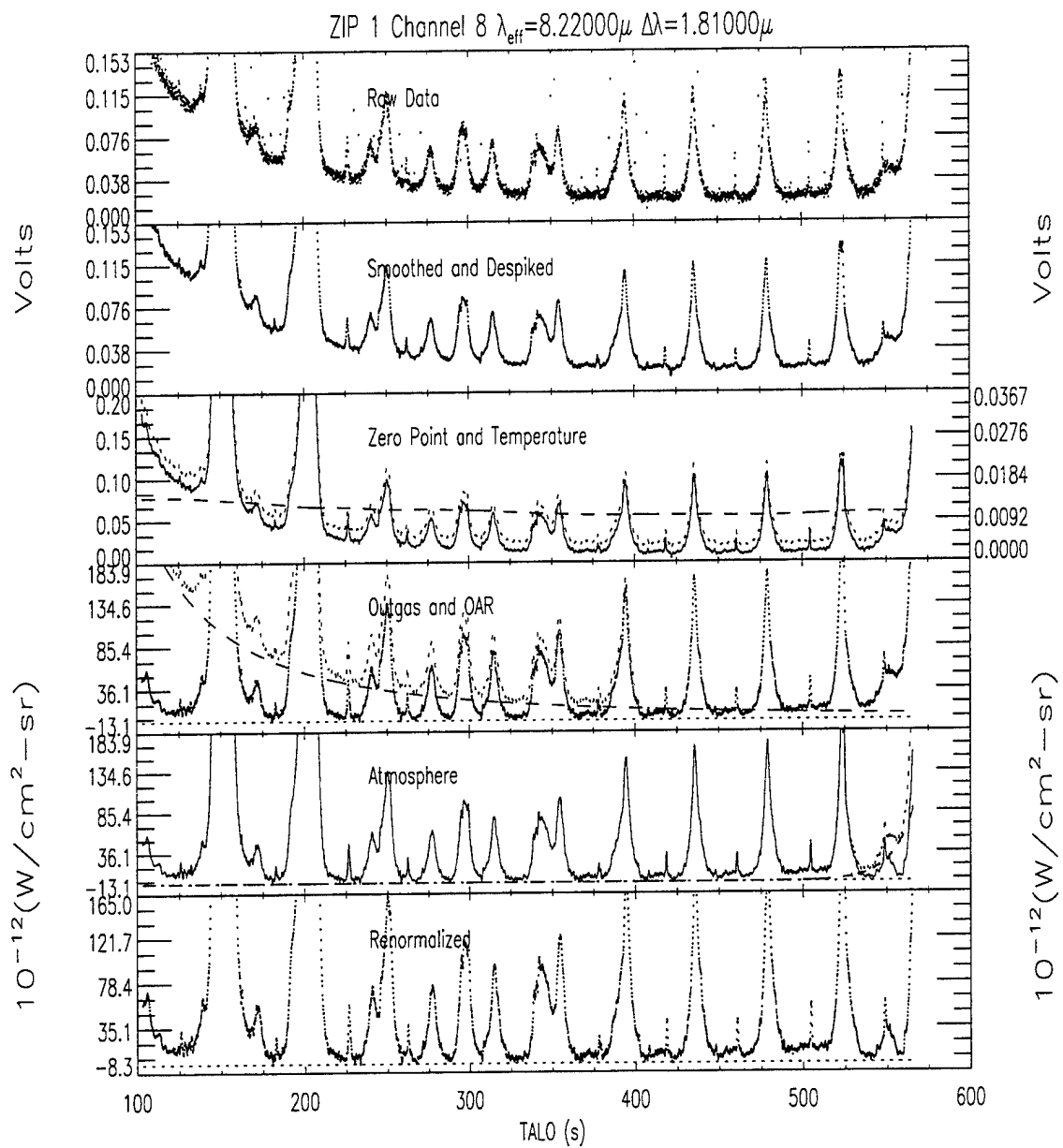
Figure A.8   Pipeline Flow for ZIP1 Channel 8
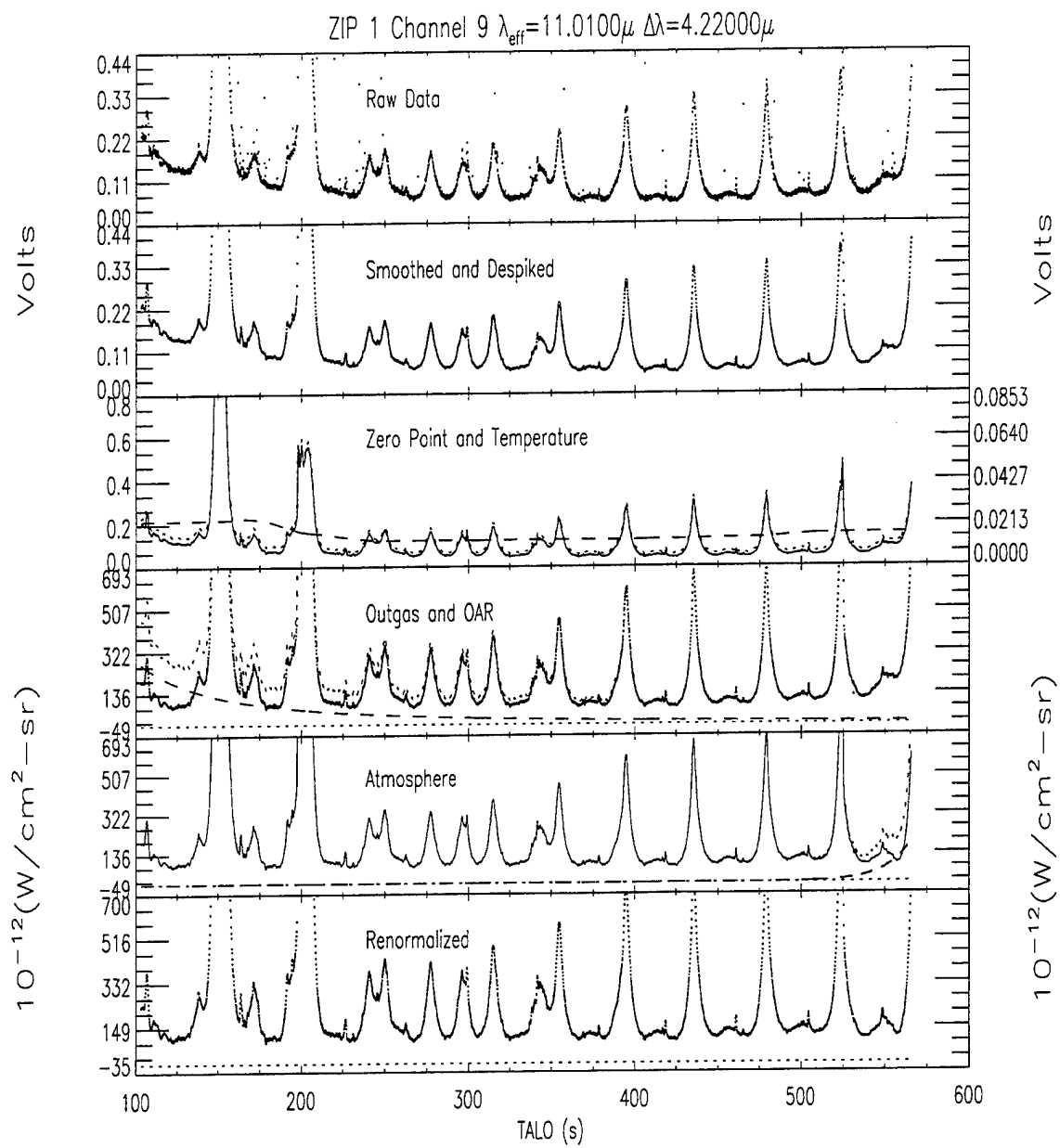
Figure A.9   **Pipeline Flow for ZIP1 Channel 9**
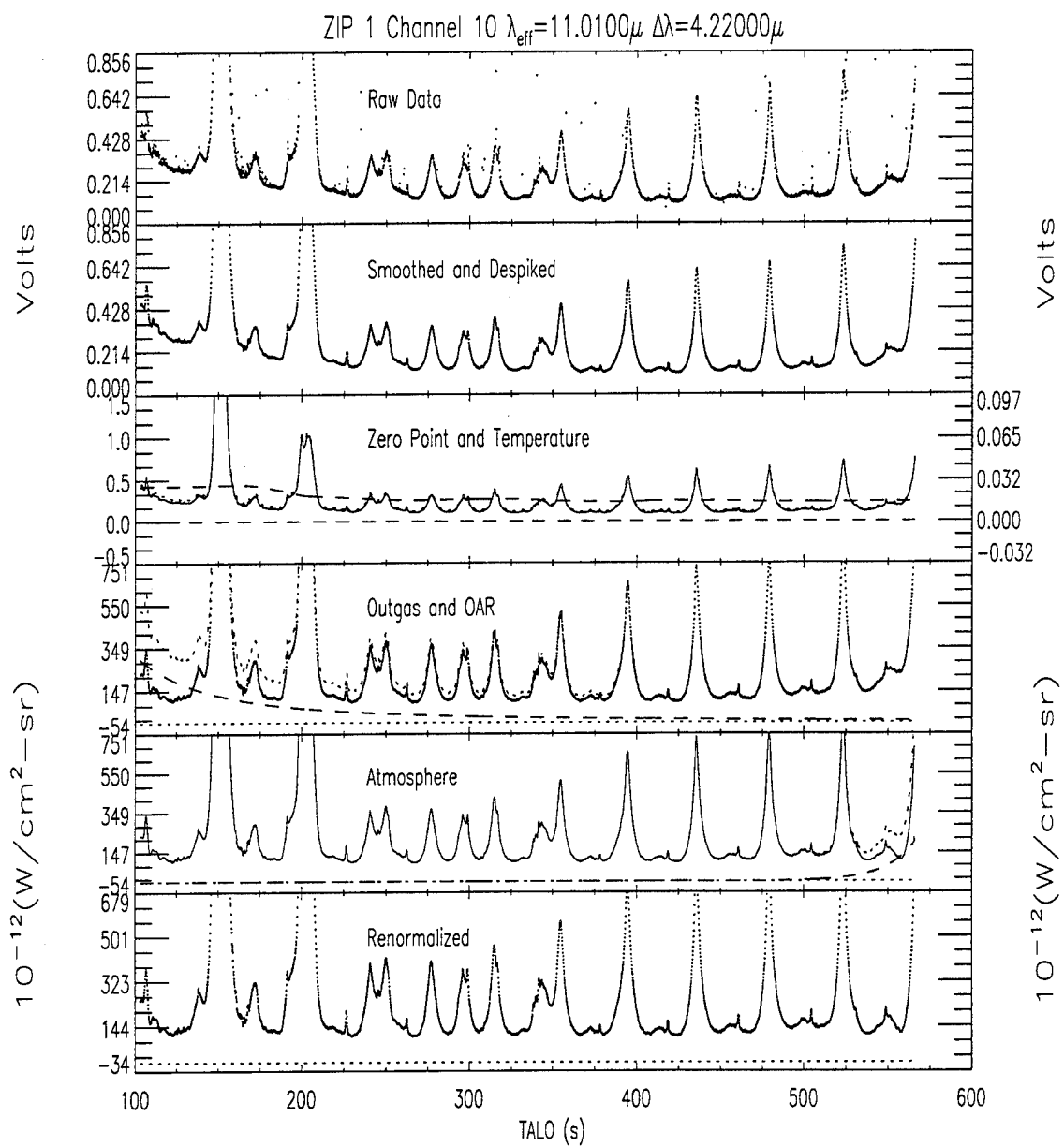
Figure A.10   Pipeline Flow for ZIP1 Channel 10
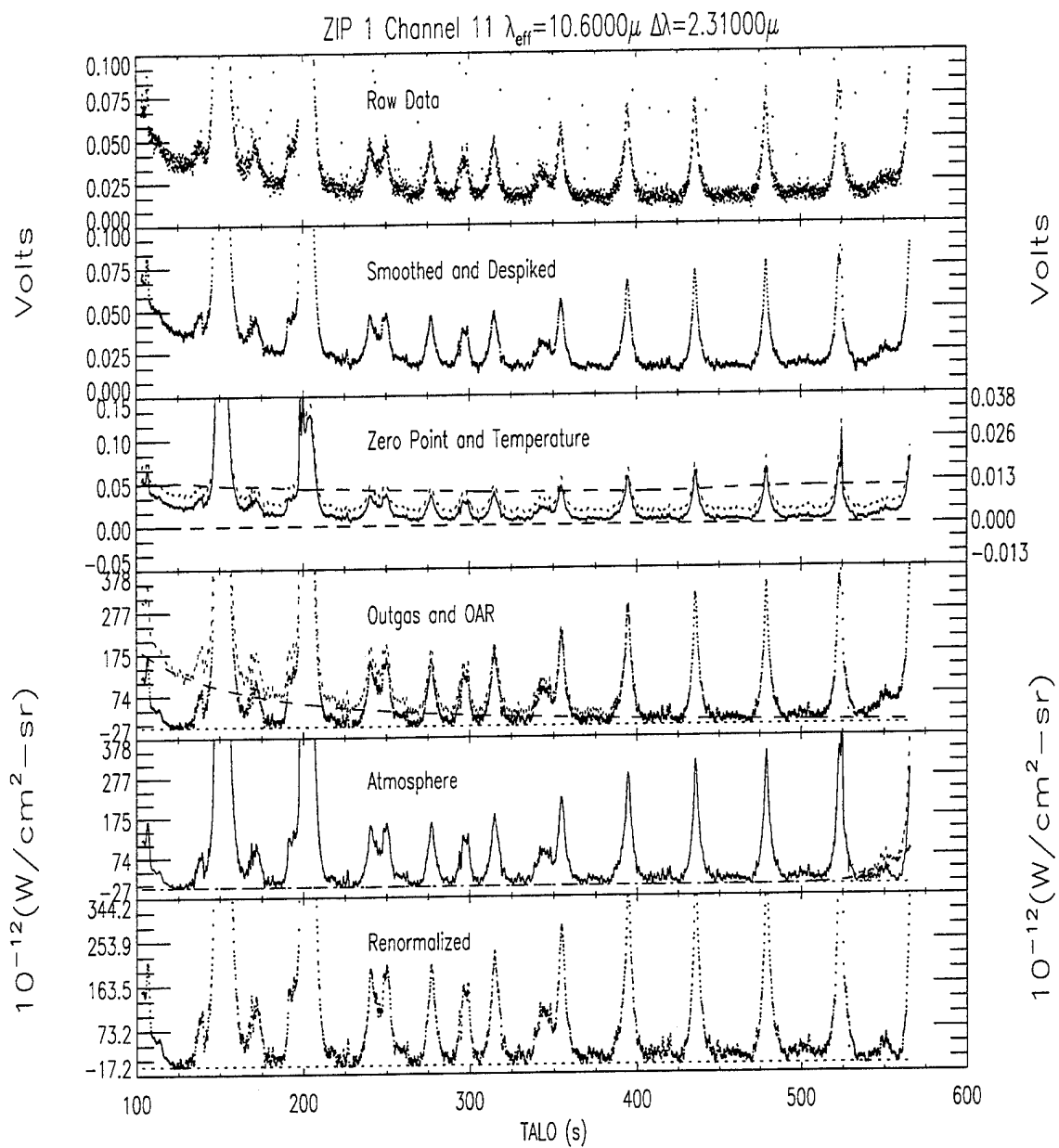
Figure A.11   Pipeline Flow for ZIP1 Channel 11
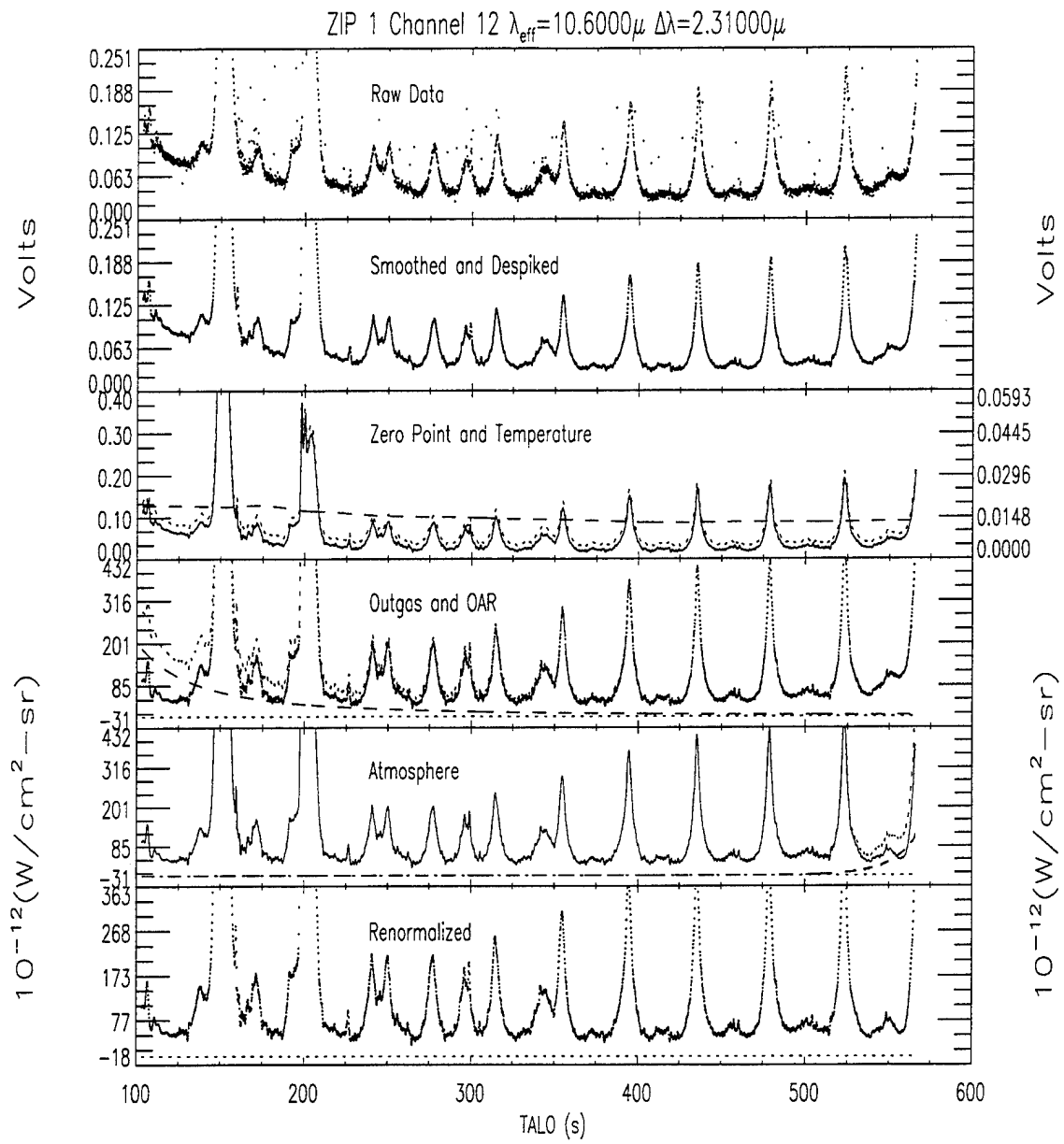
Figure A.12   Pipeline Flow for ZIP1 Channel 12
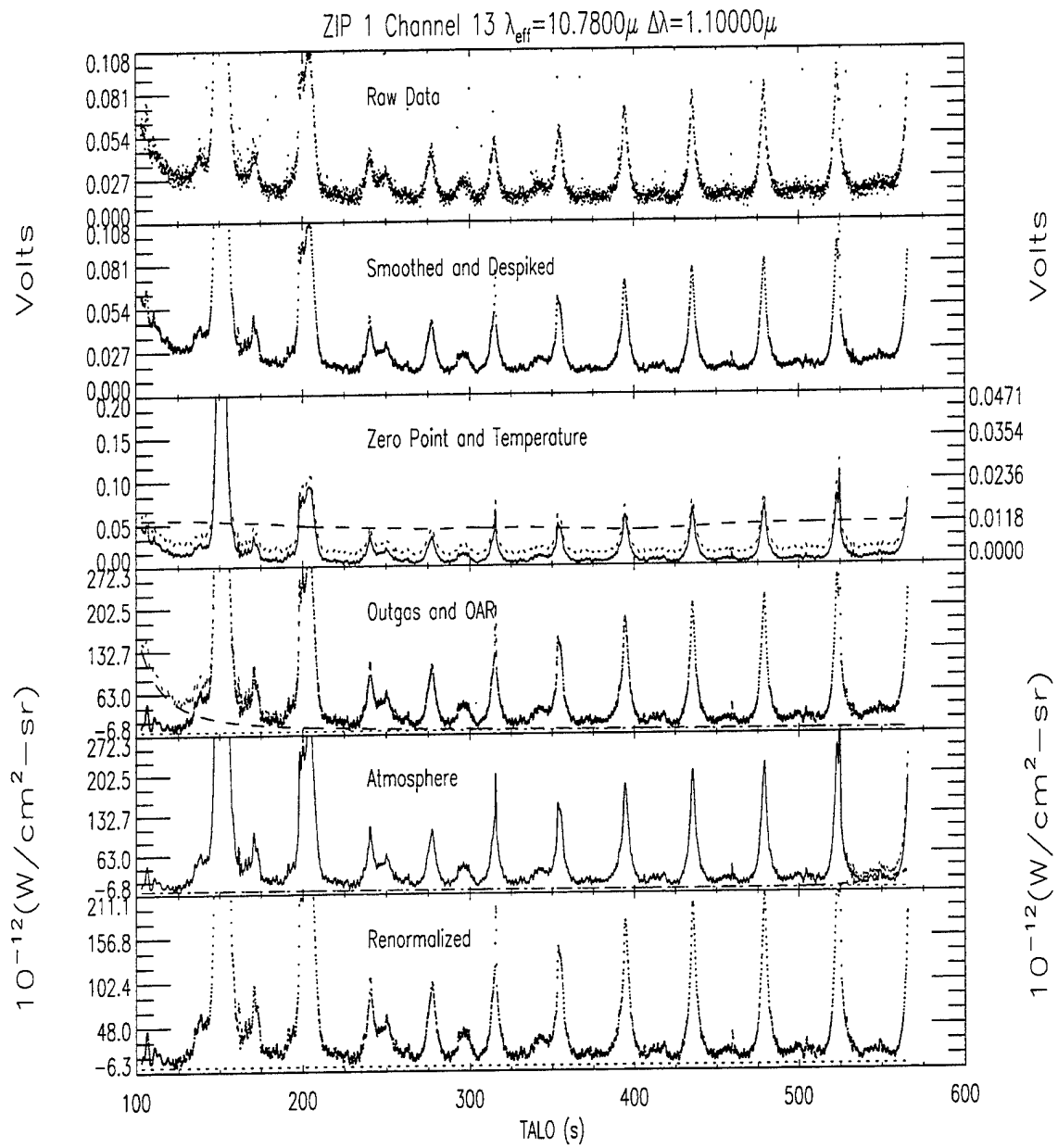
Figure A.13   Pipeline Flow for ZIP1 Channel 13
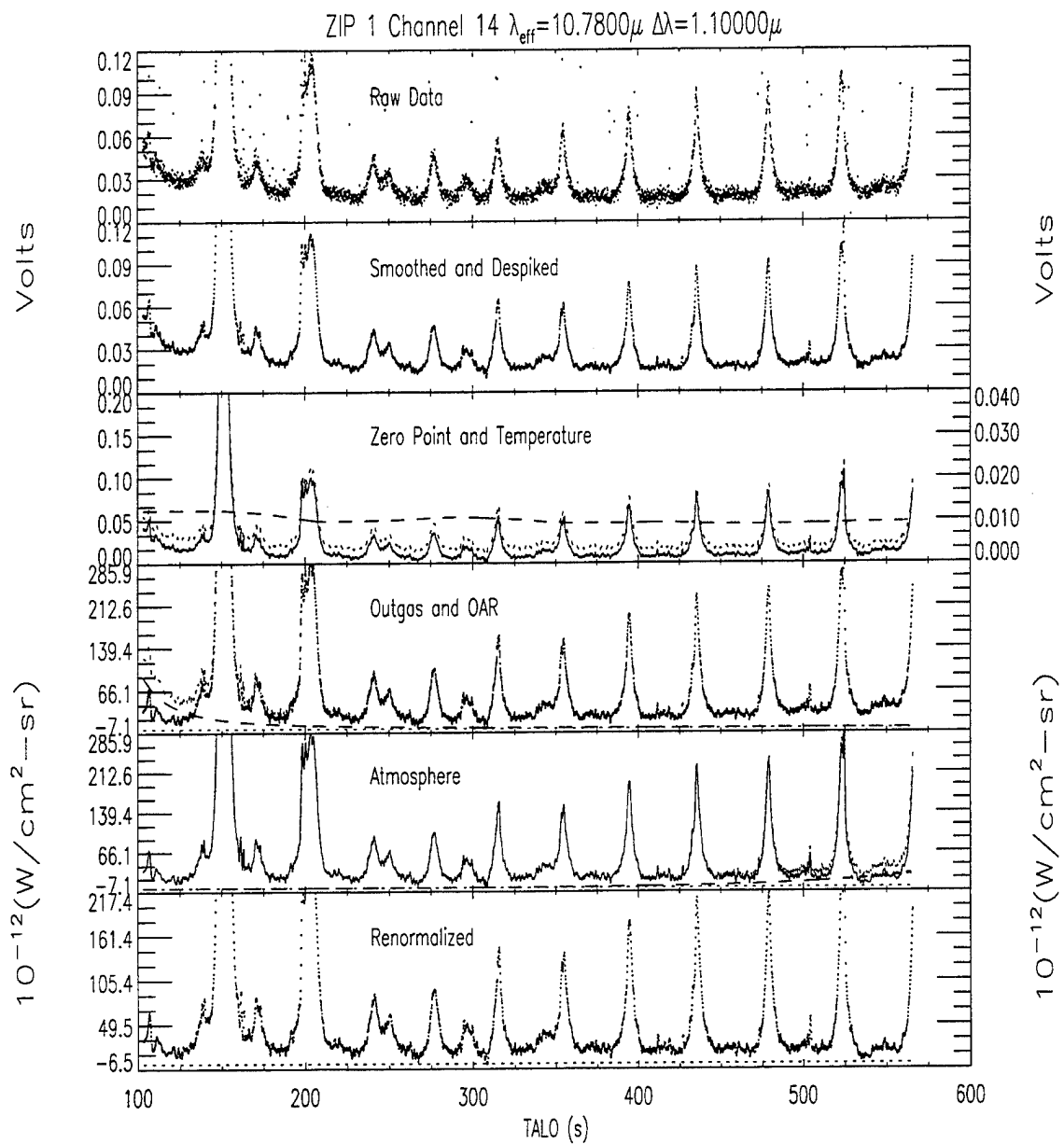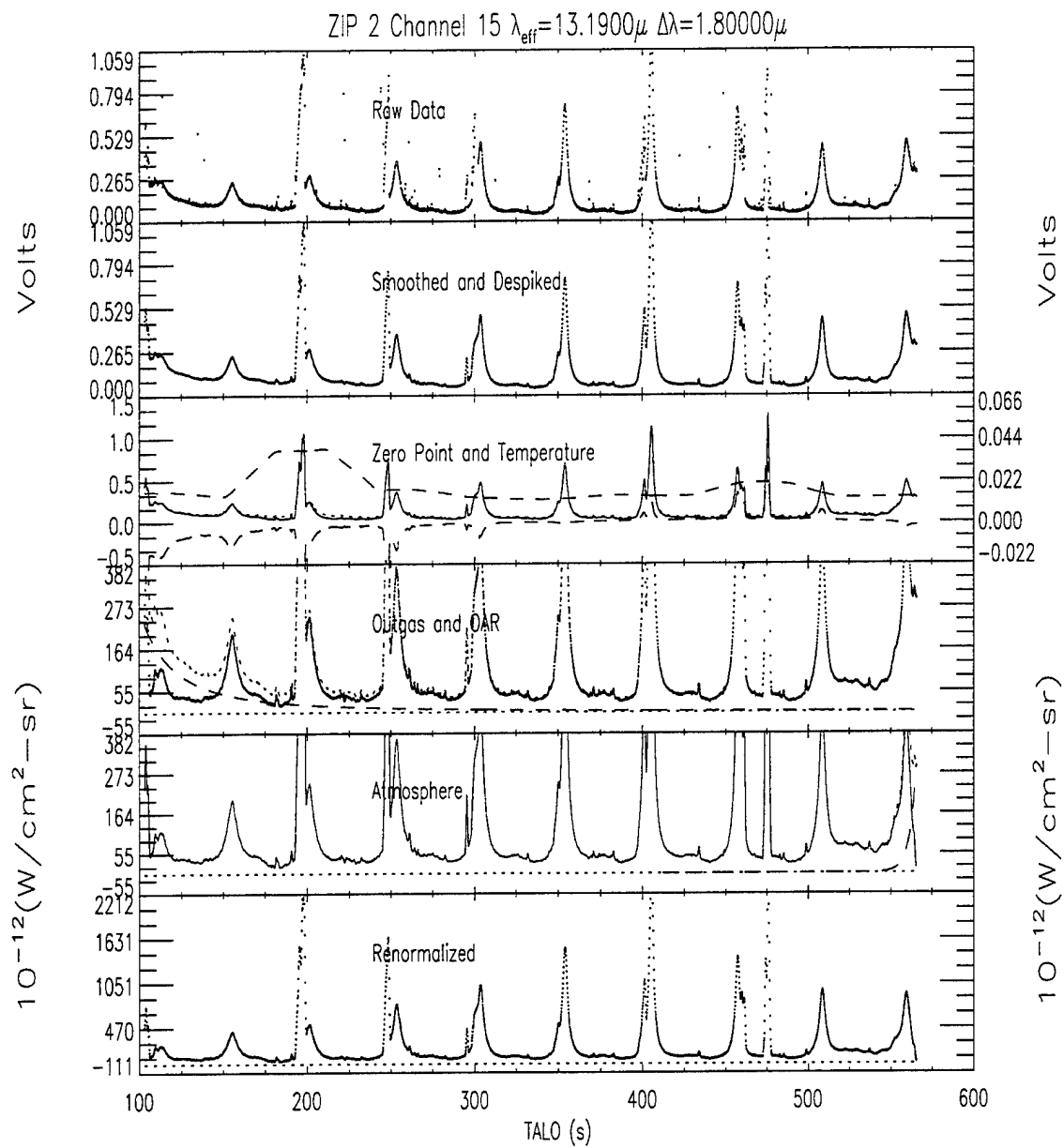
Figure A.14   Pipeline Flow for ZIP1 Channel 14
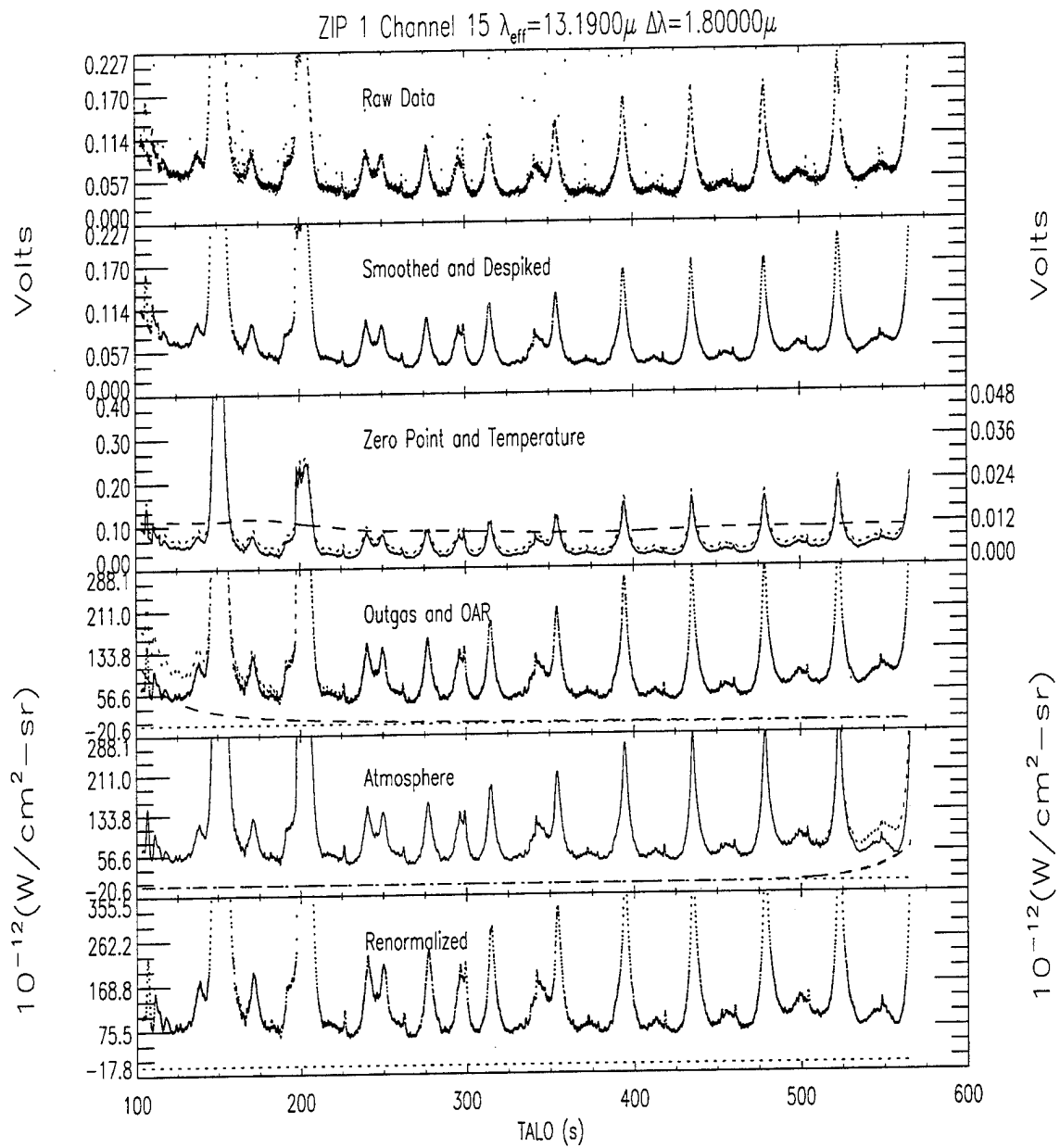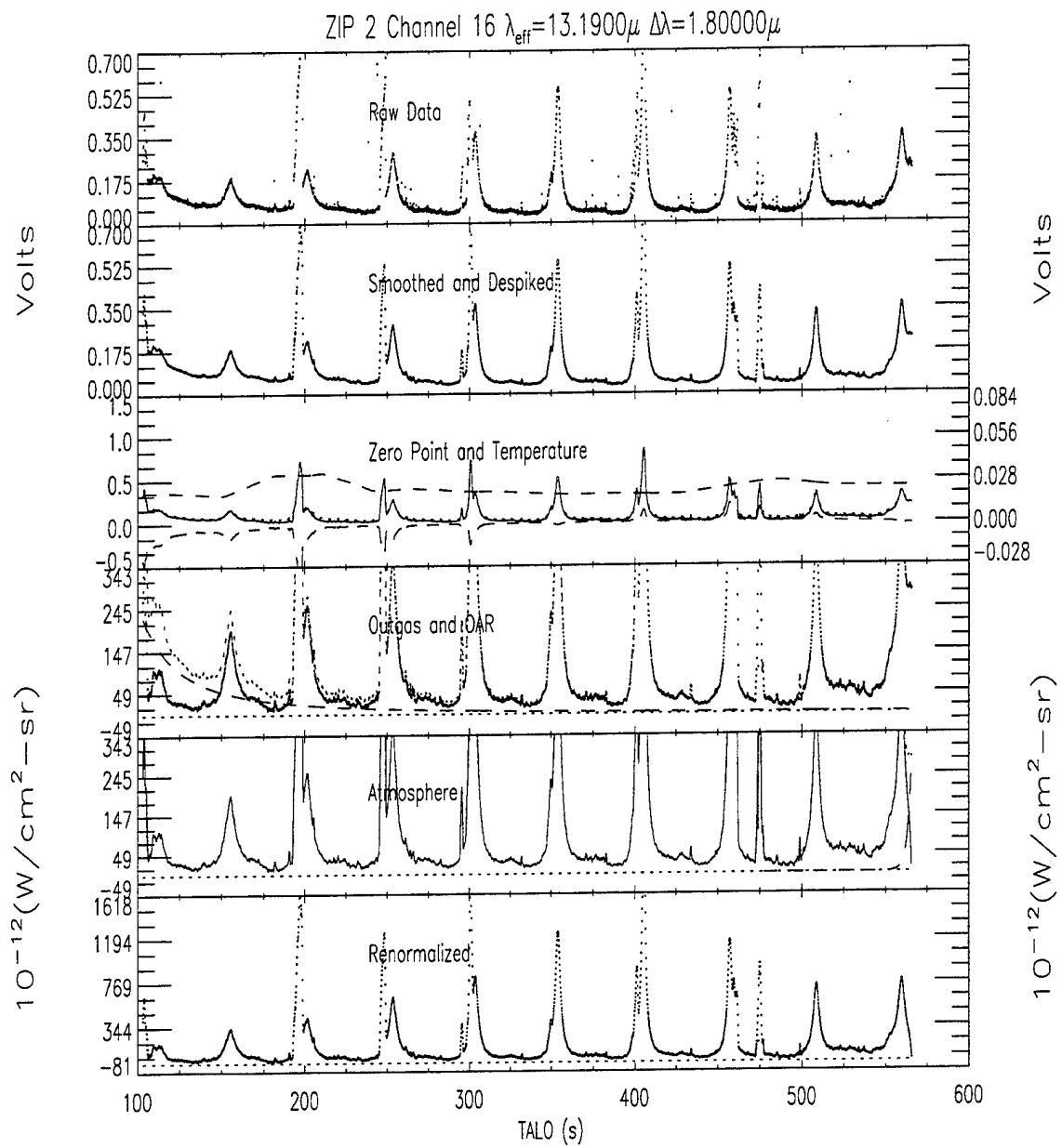
Figure A.15   Pipeline Flow for ZIP1 Channel 15

48
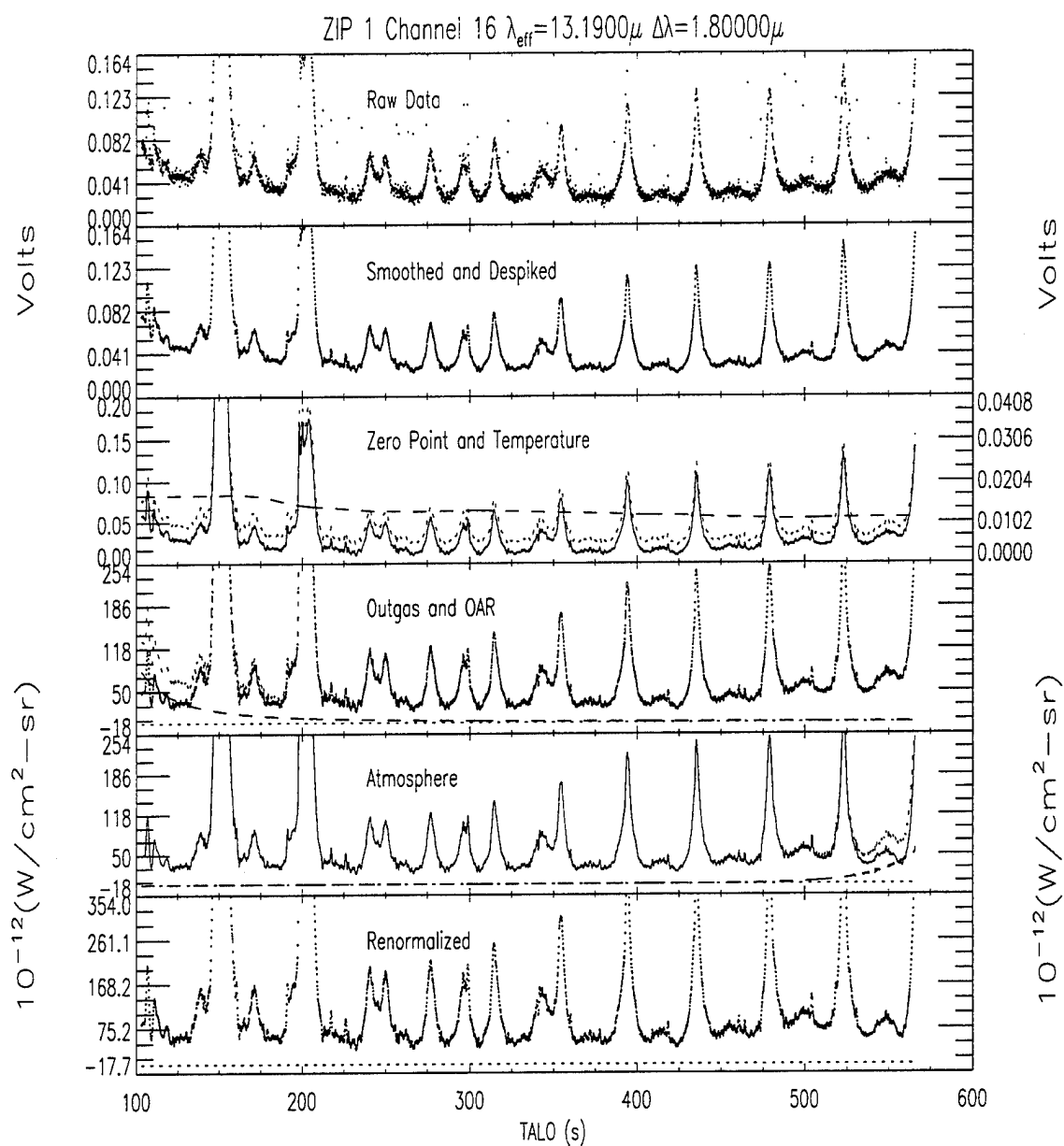
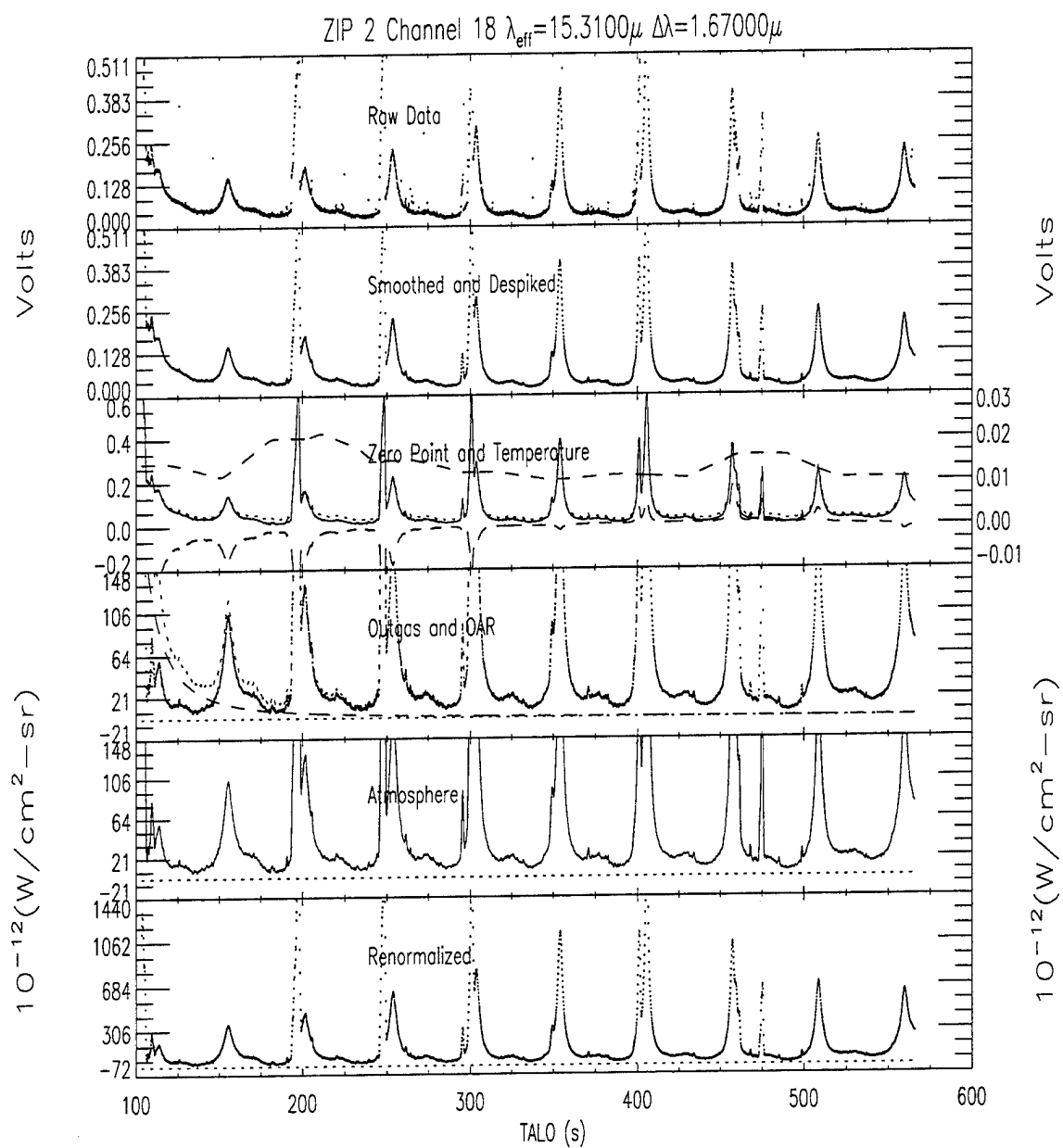**Figure A.16   Pipeline Flow for ZIP1 Channel 16**
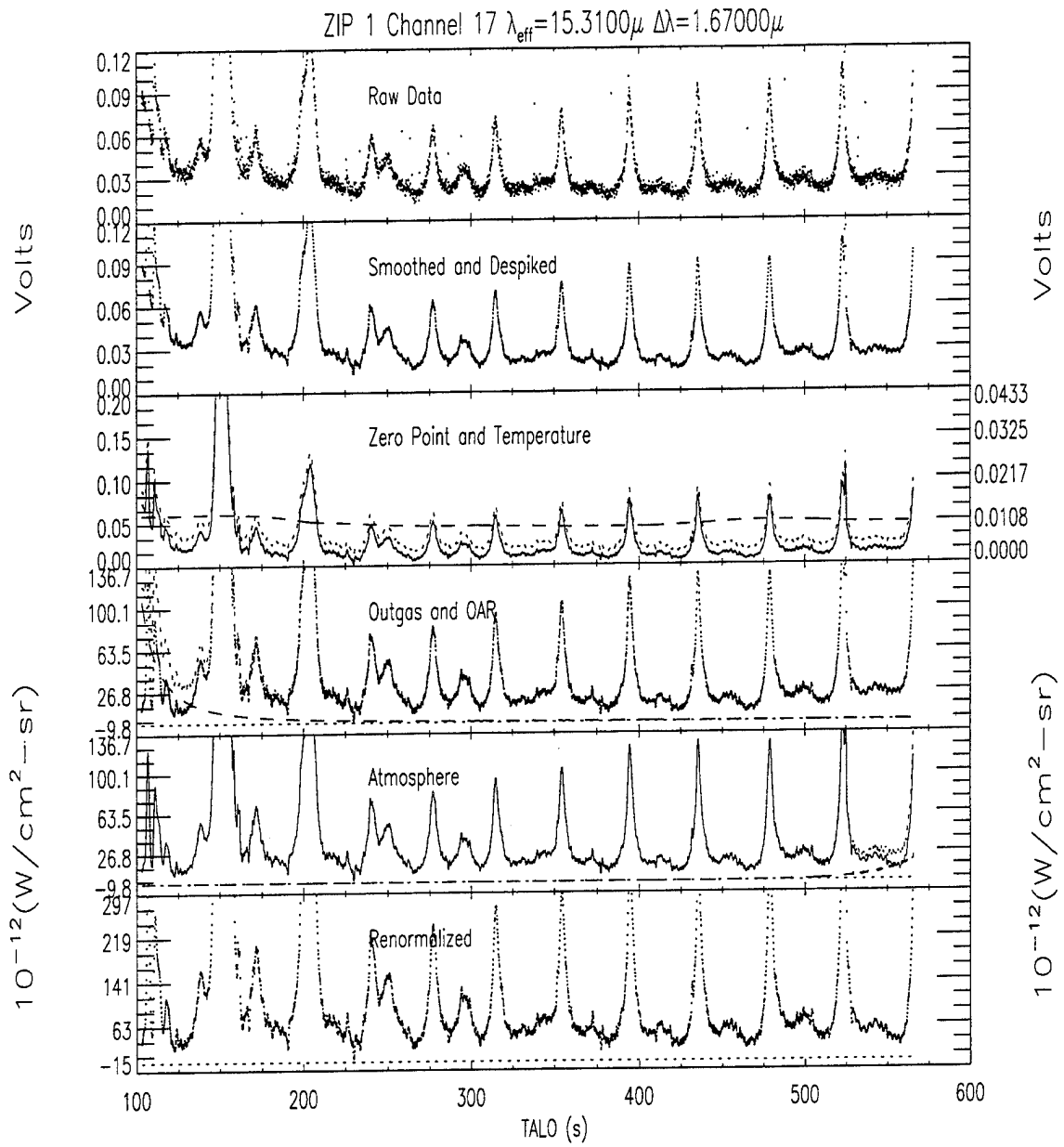
Figure A.17 Pipeline Flow for ZIP1 Channel 17
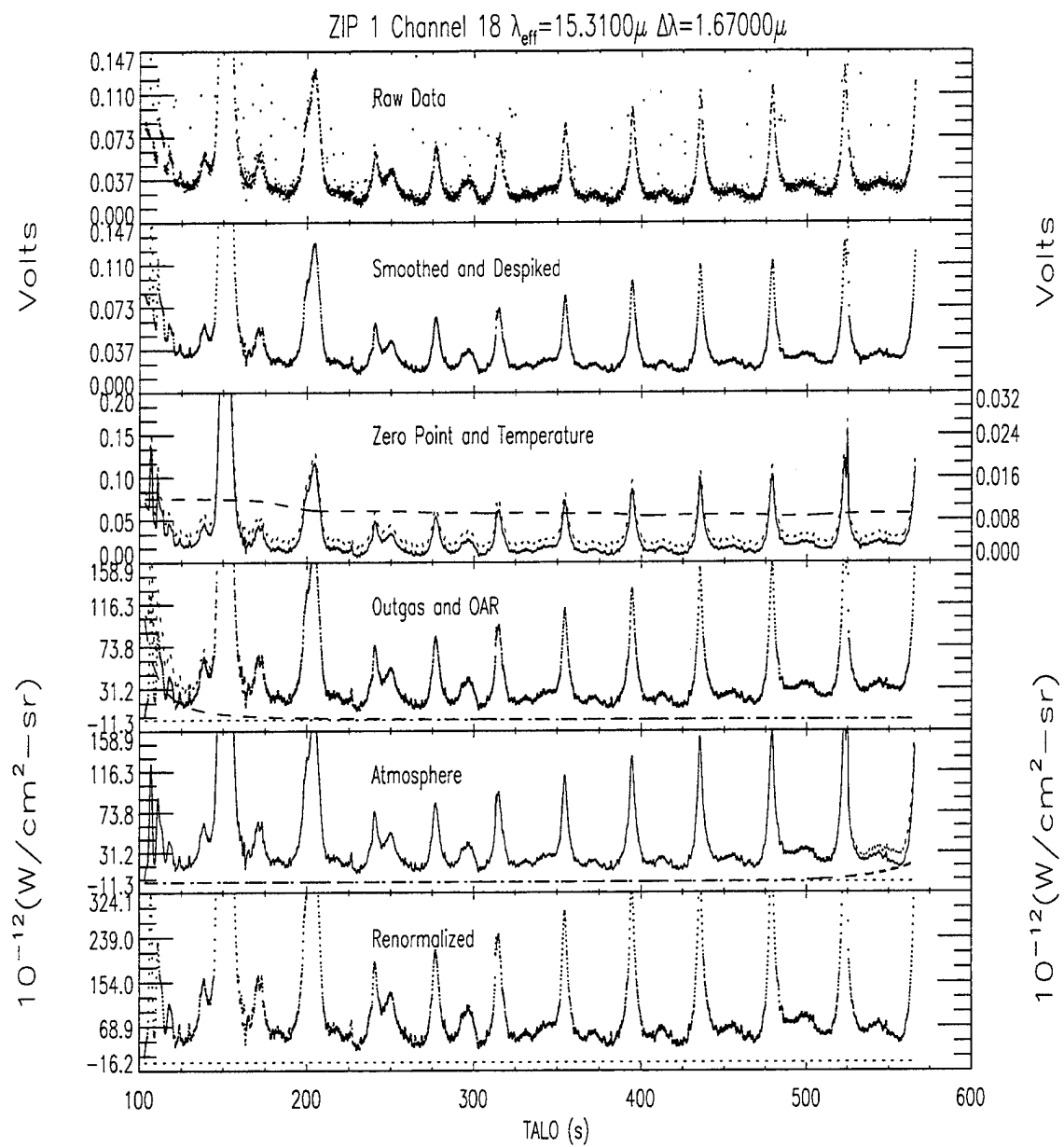
Figure A.18   Pipeline Flow for ZIP1 Channel 18
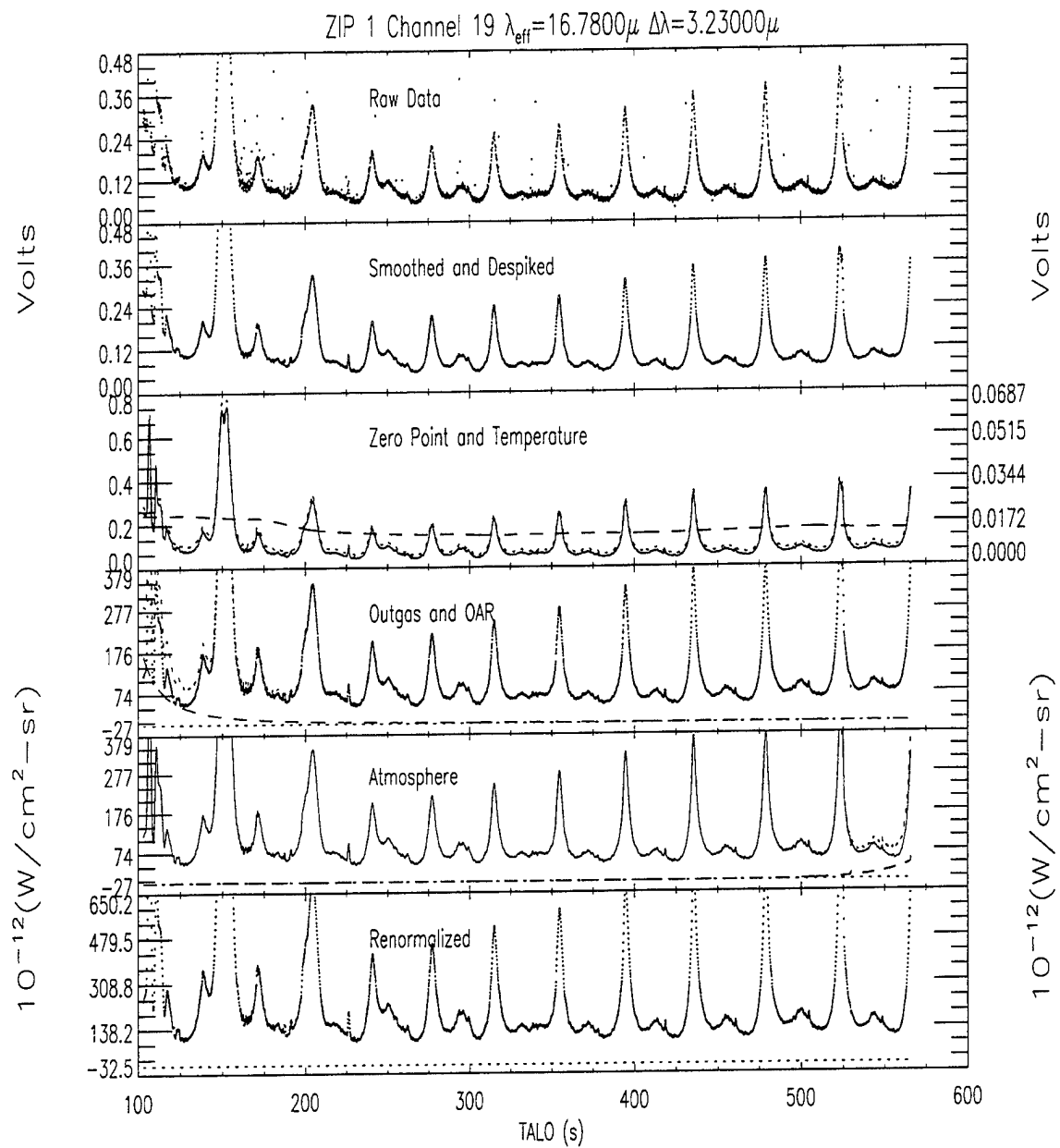
Figure A.19   Pipeline Flow for ZIP1 Channel 19
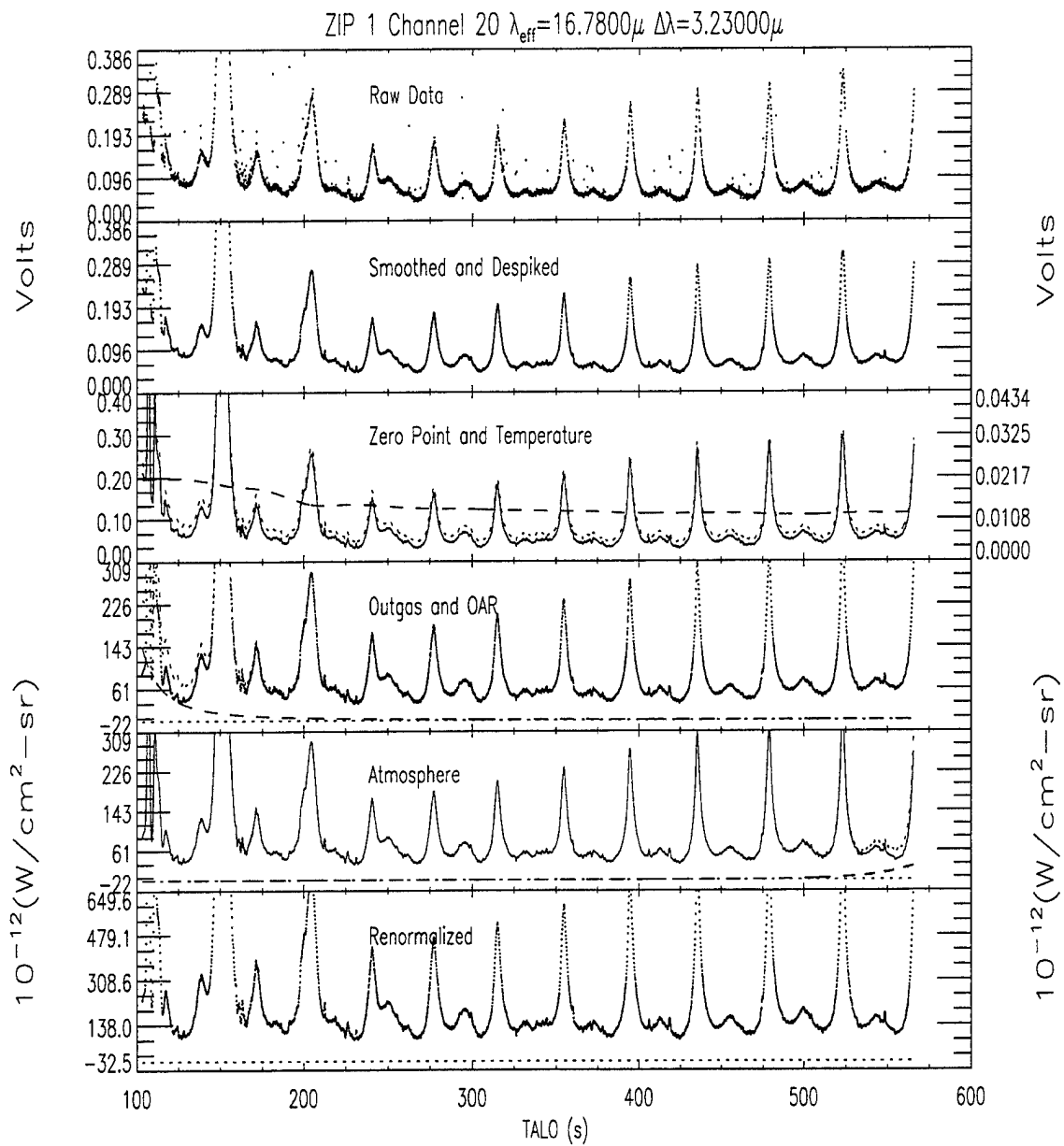
Figure A.20 Pipeline Flow for ZIP1 Channel 20
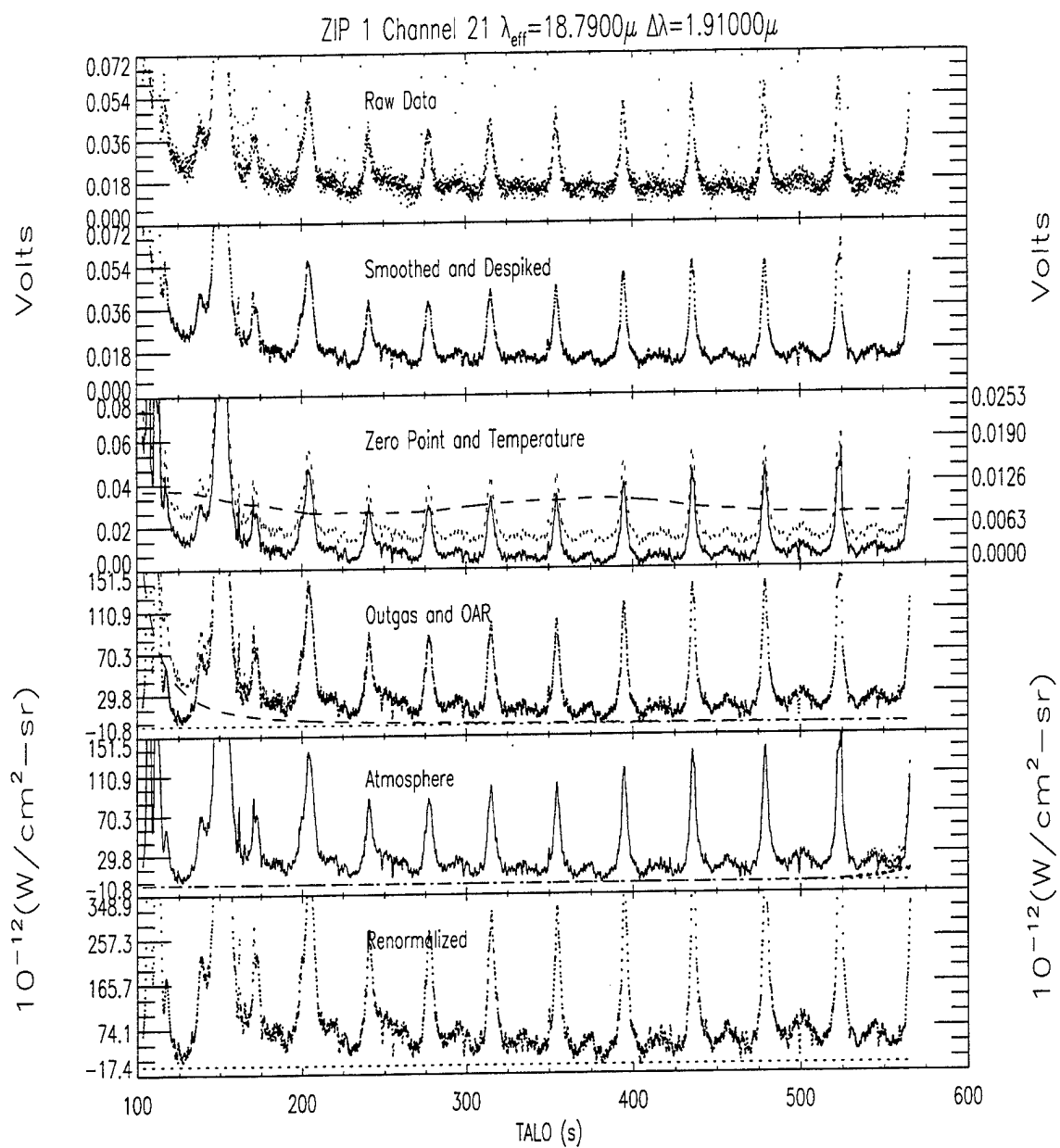
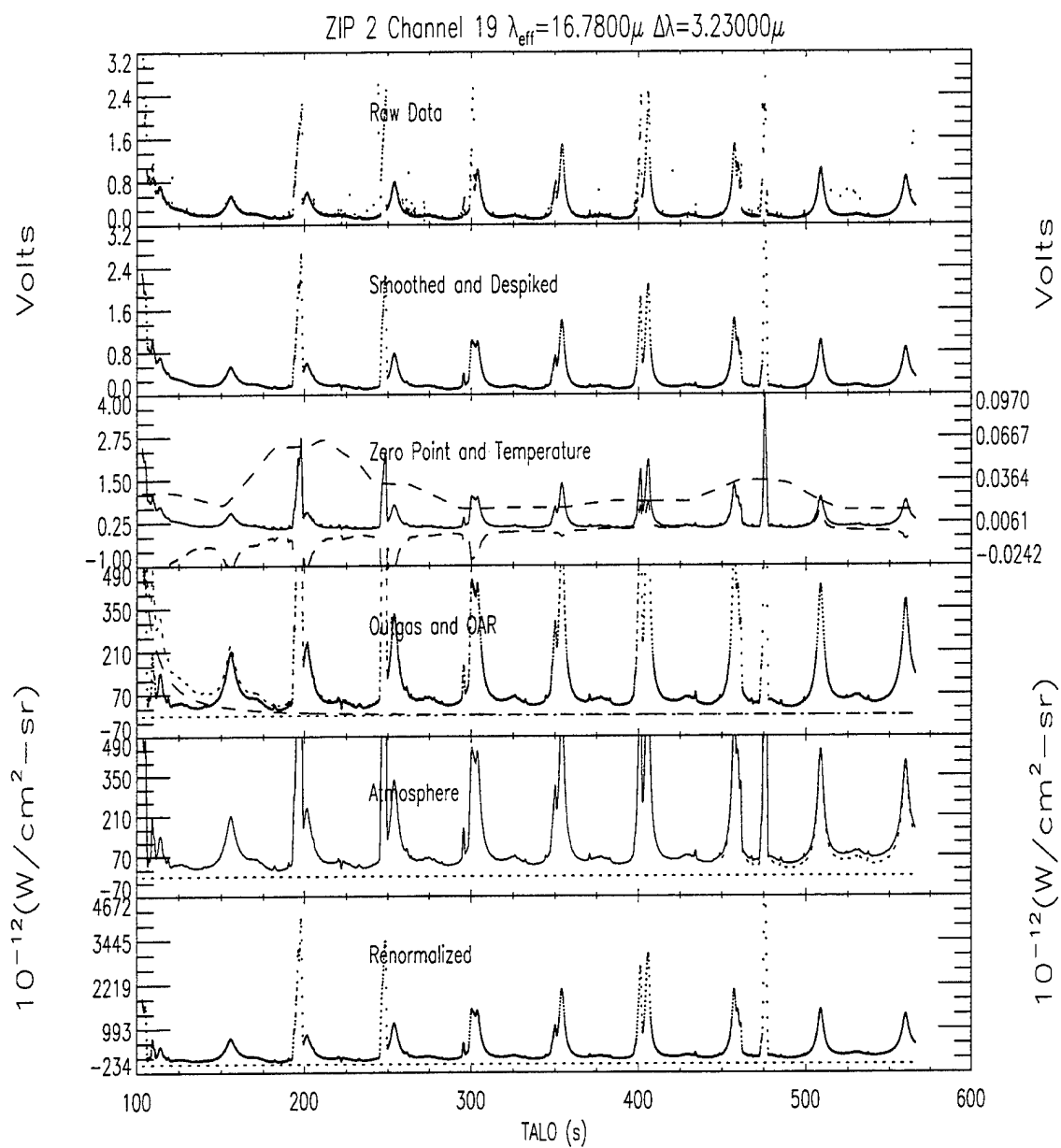**Figure A.21   Pipeline Flow for ZIP1 Channel 21**

54
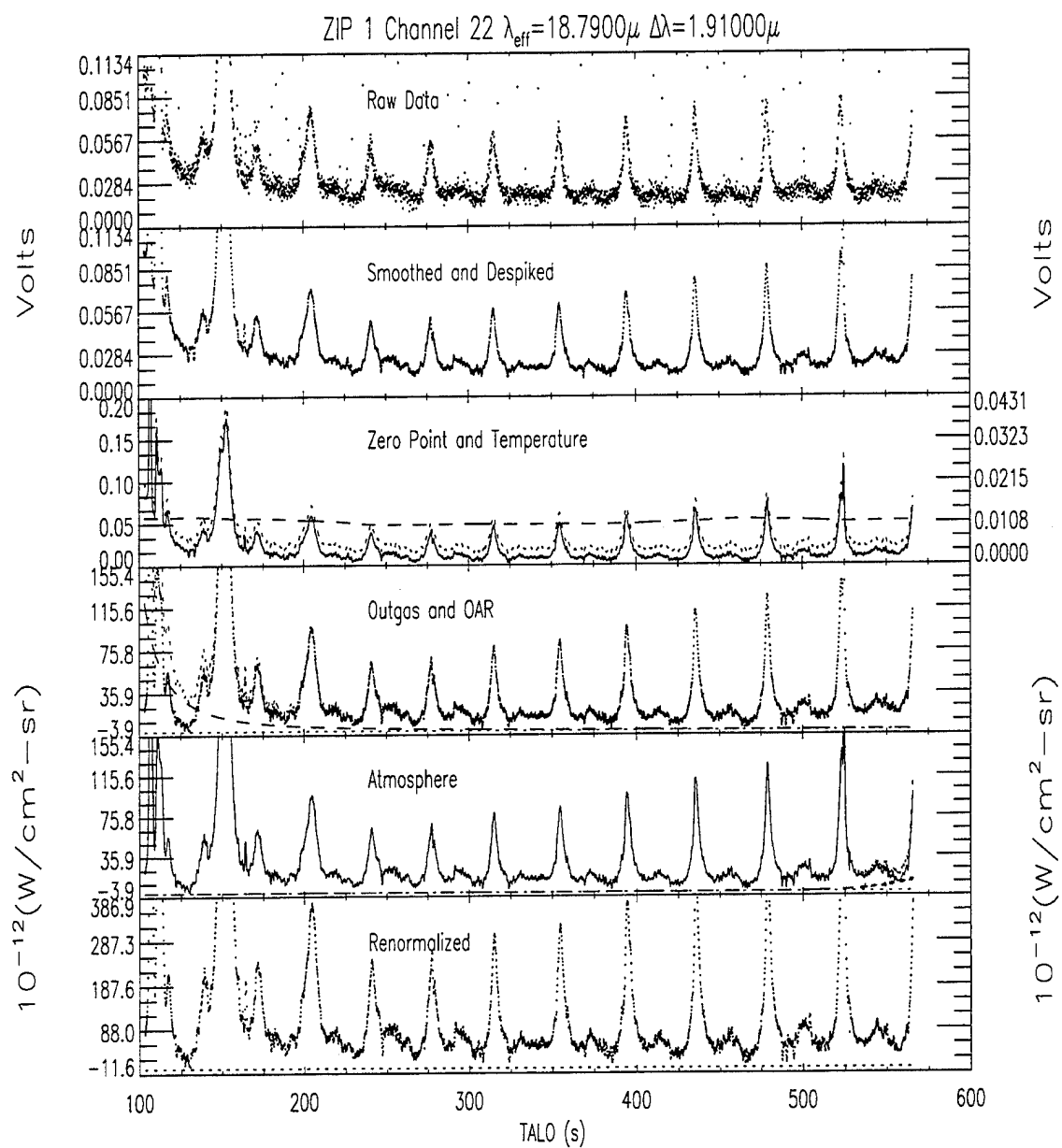
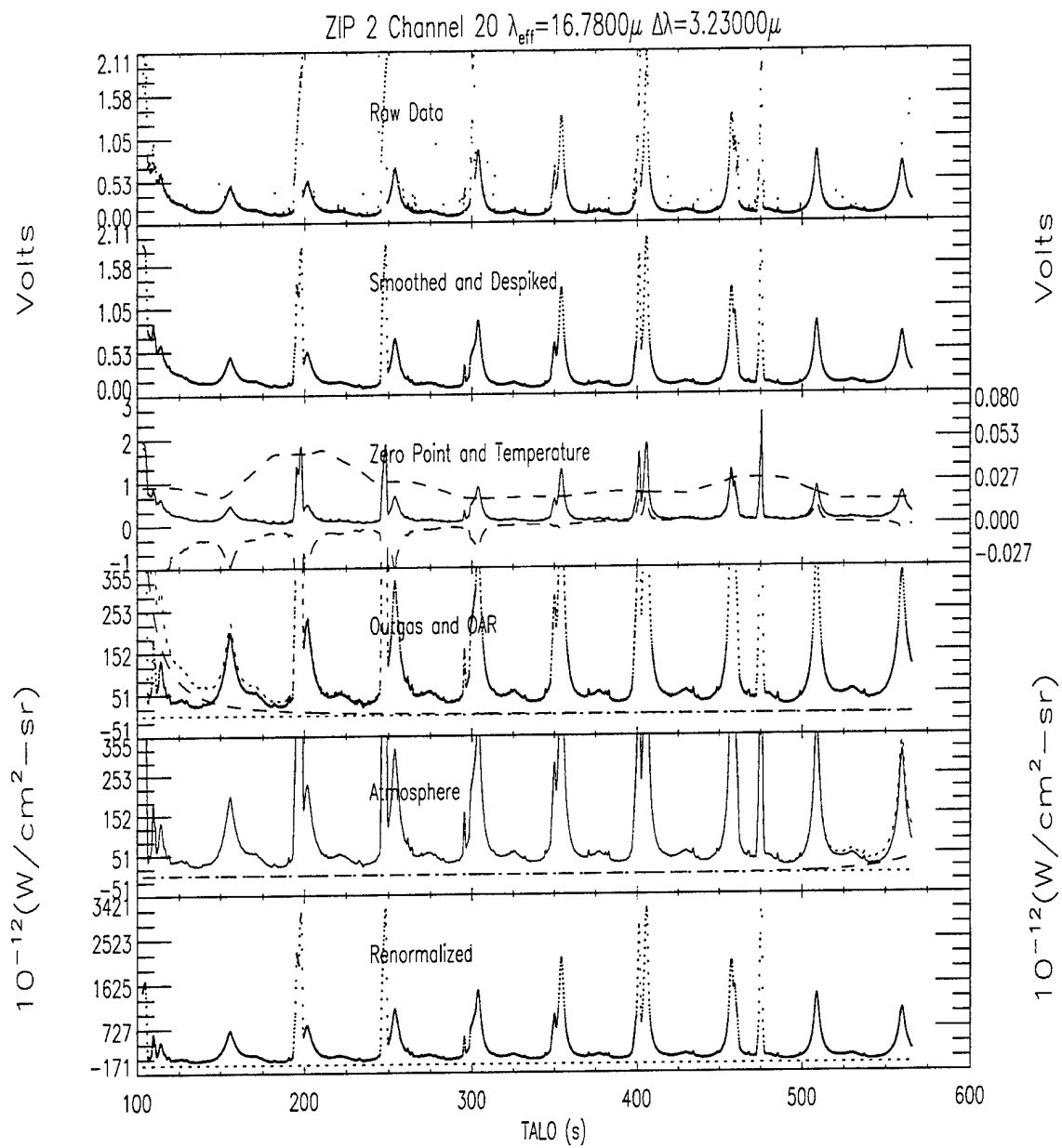**Figure A.22   Pipeline Flow for ZIP1 Channel 22**
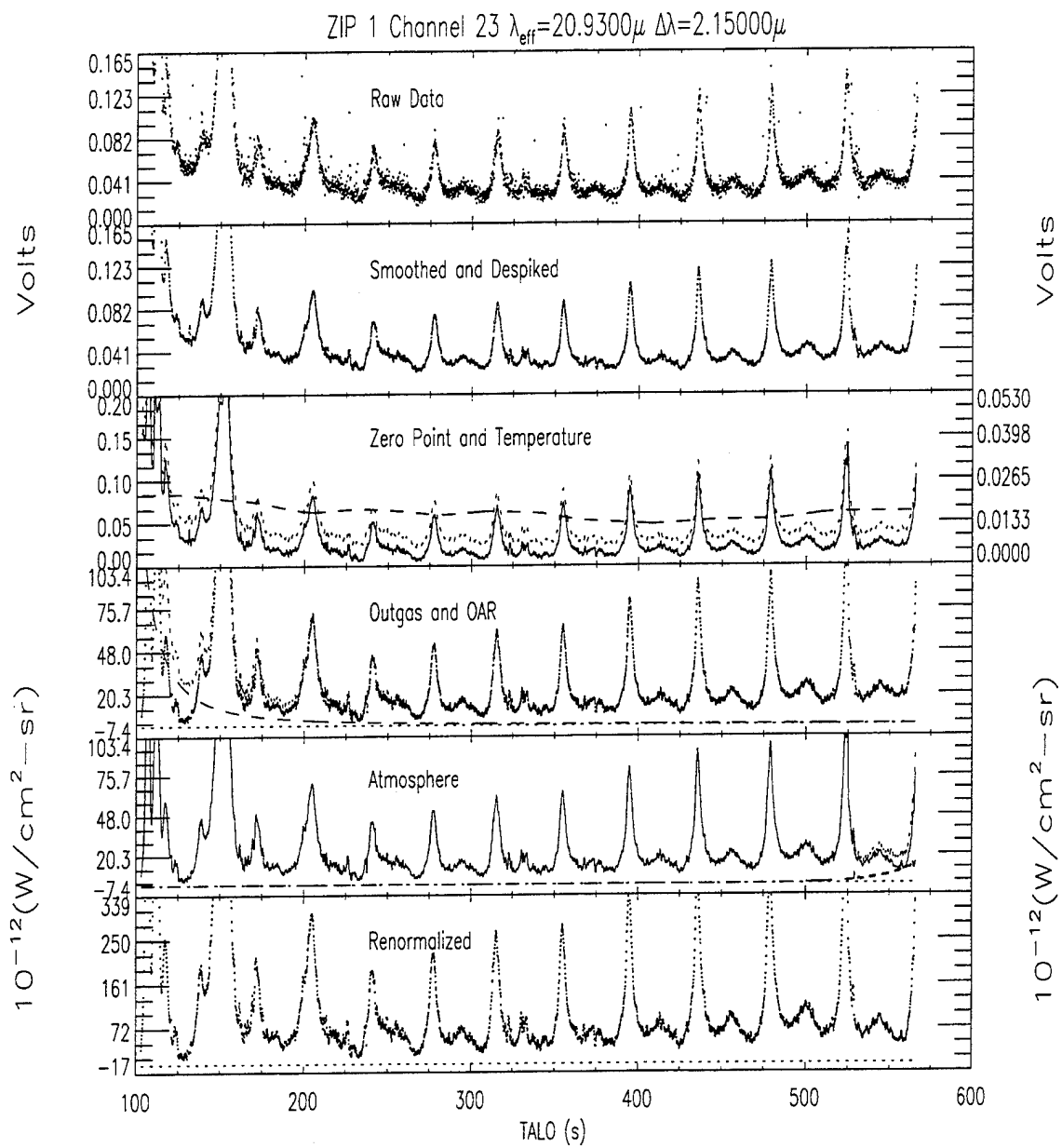
Figure A.23   Pipeline Flow for ZIP1 Channel 23
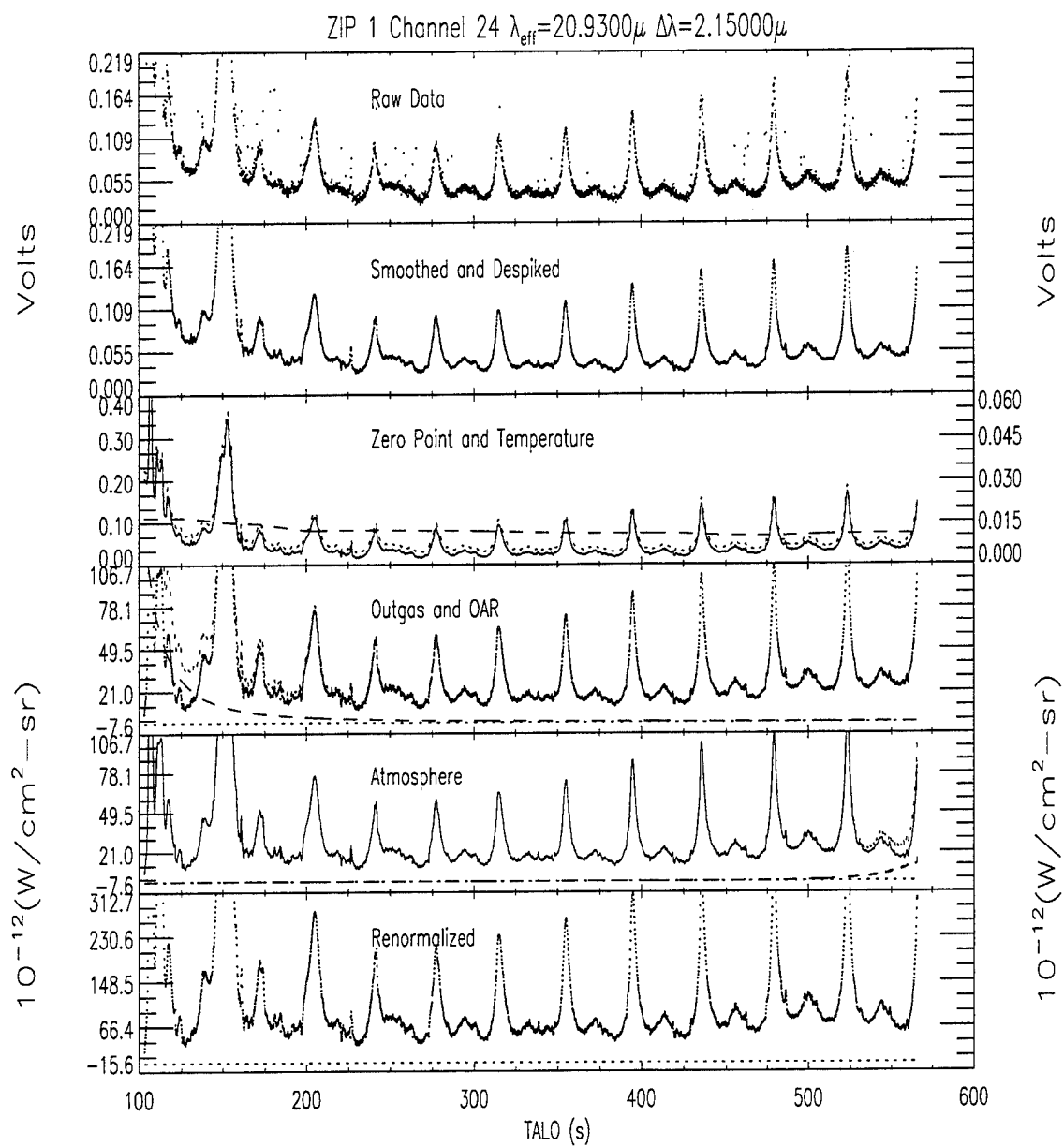
Figure A.24 Pipeline Flow for ZIP1 Channel 24
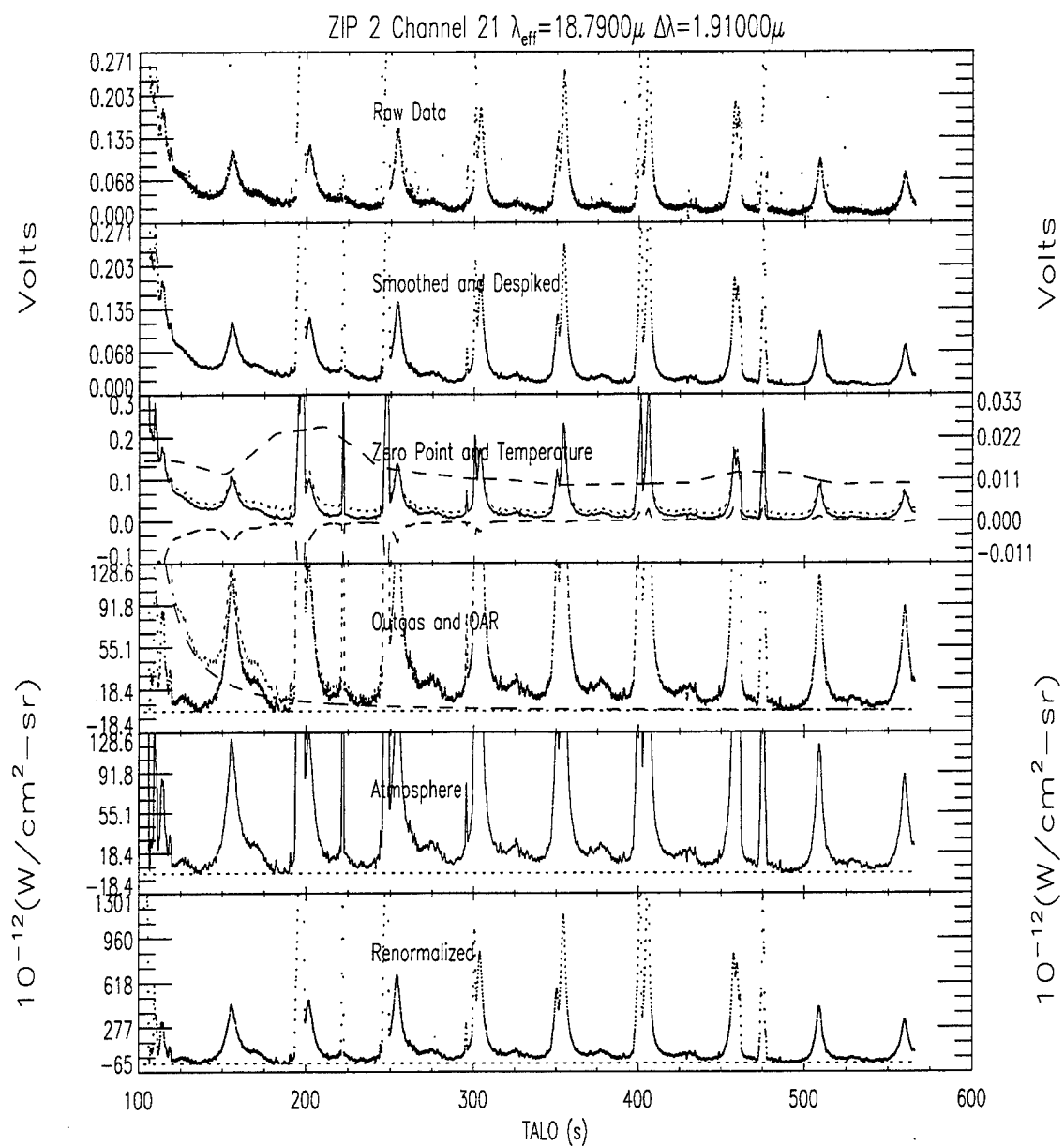
57
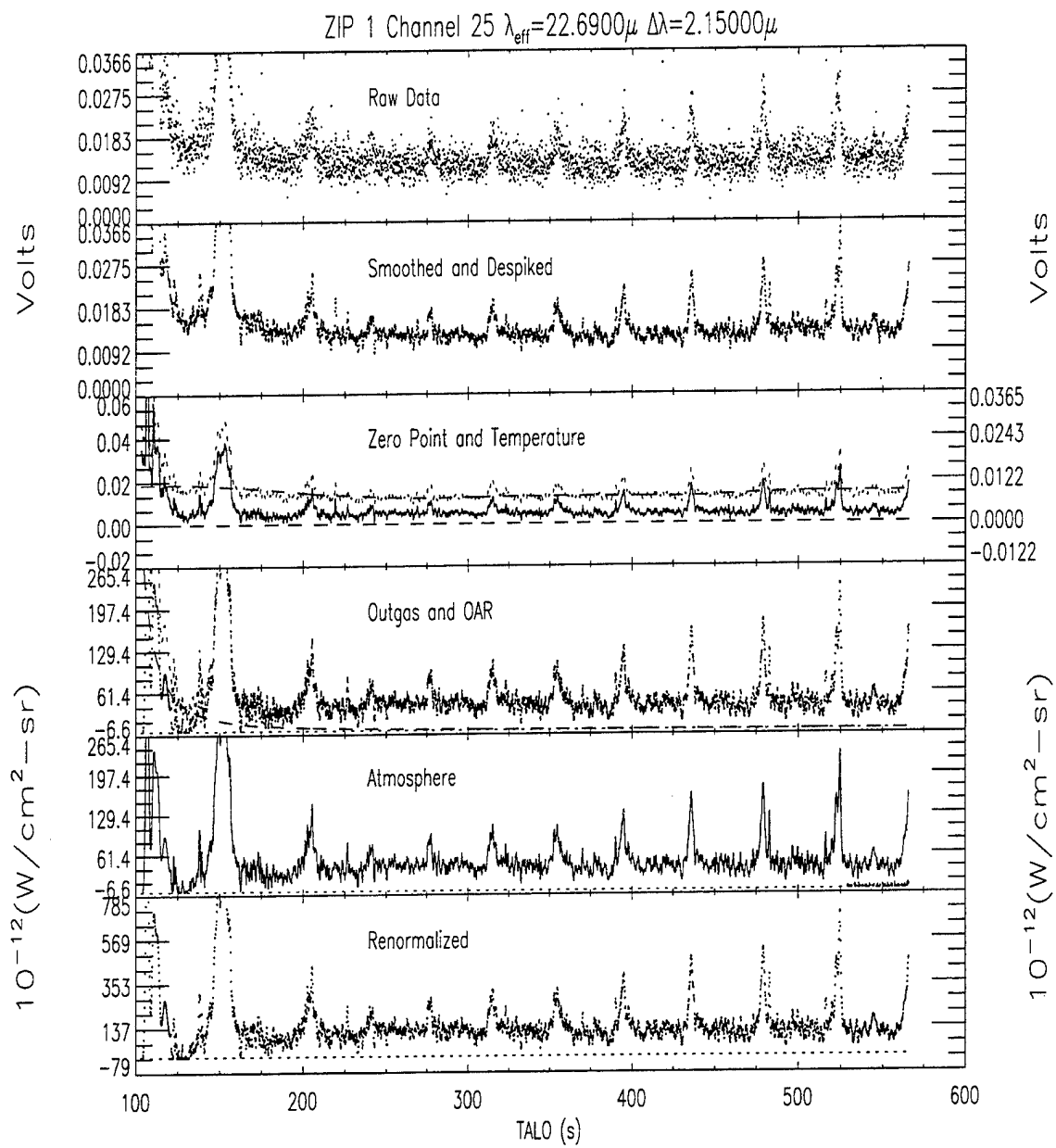
Figure A.25   Pipeline Flow for ZIP1 Channel 25
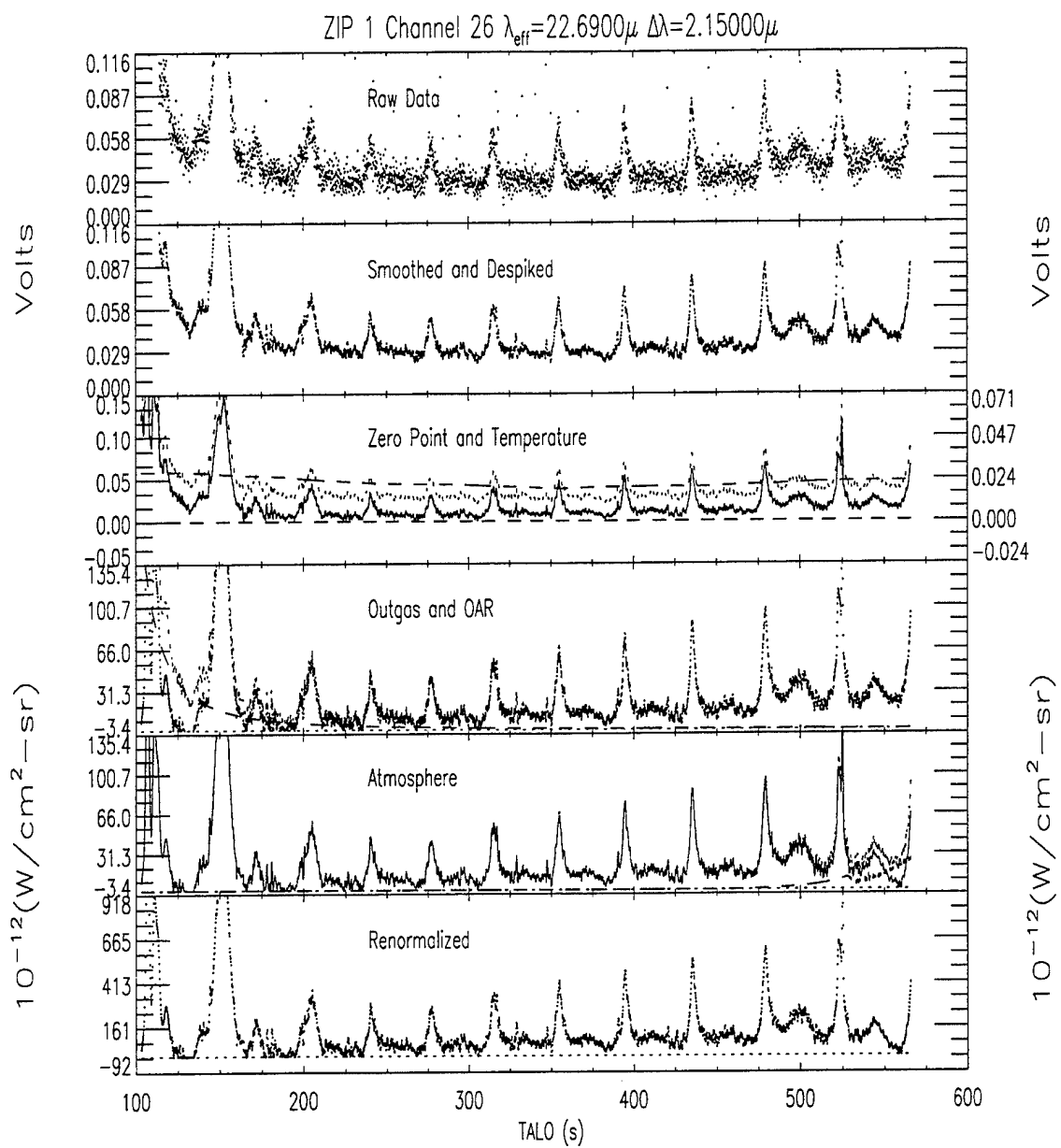
Figure A.26 Pipeline Flow for ZIP1 Channel 26
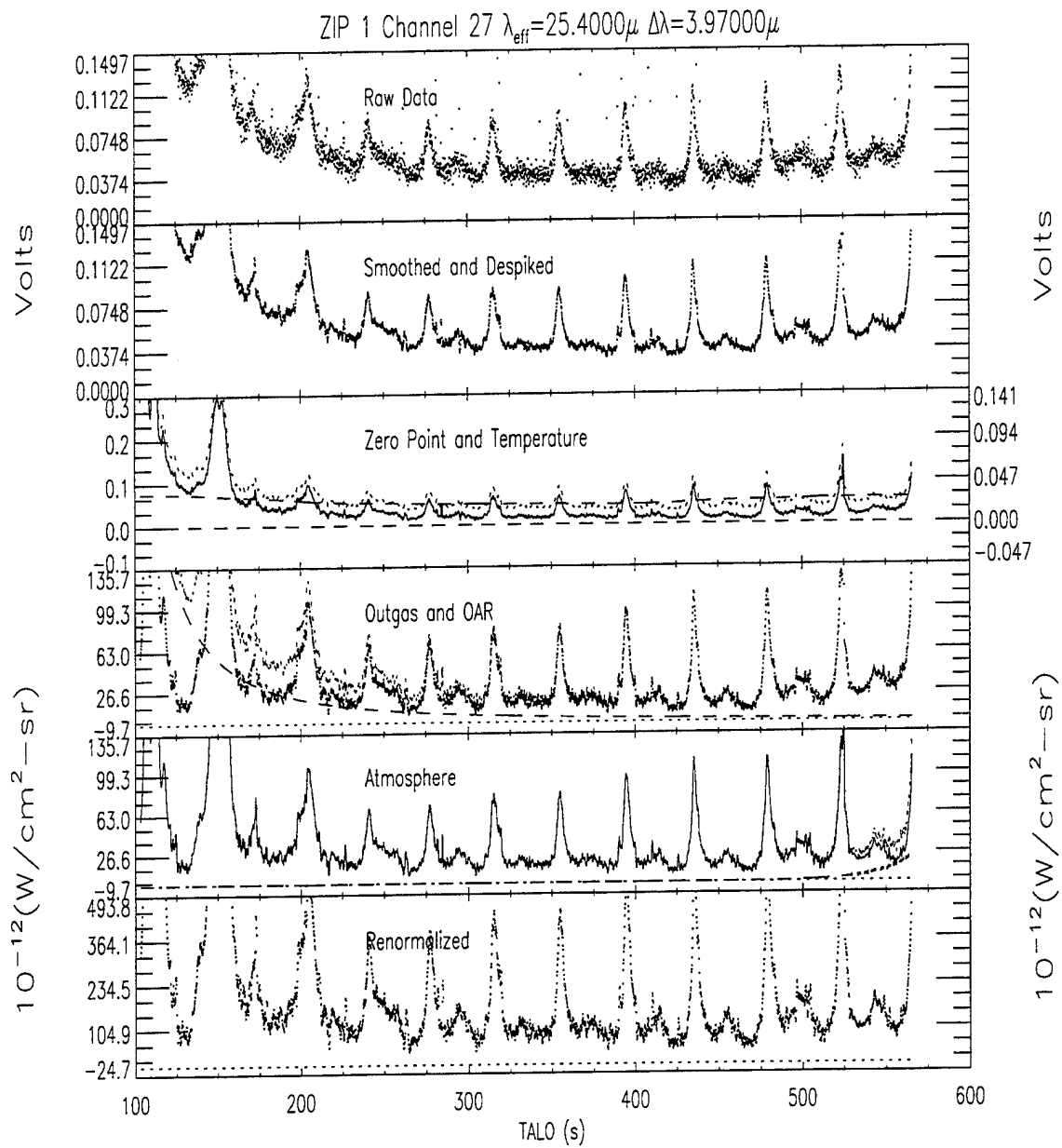
Figure A.27   Pipeline Flow for ZIP1 Channel 27
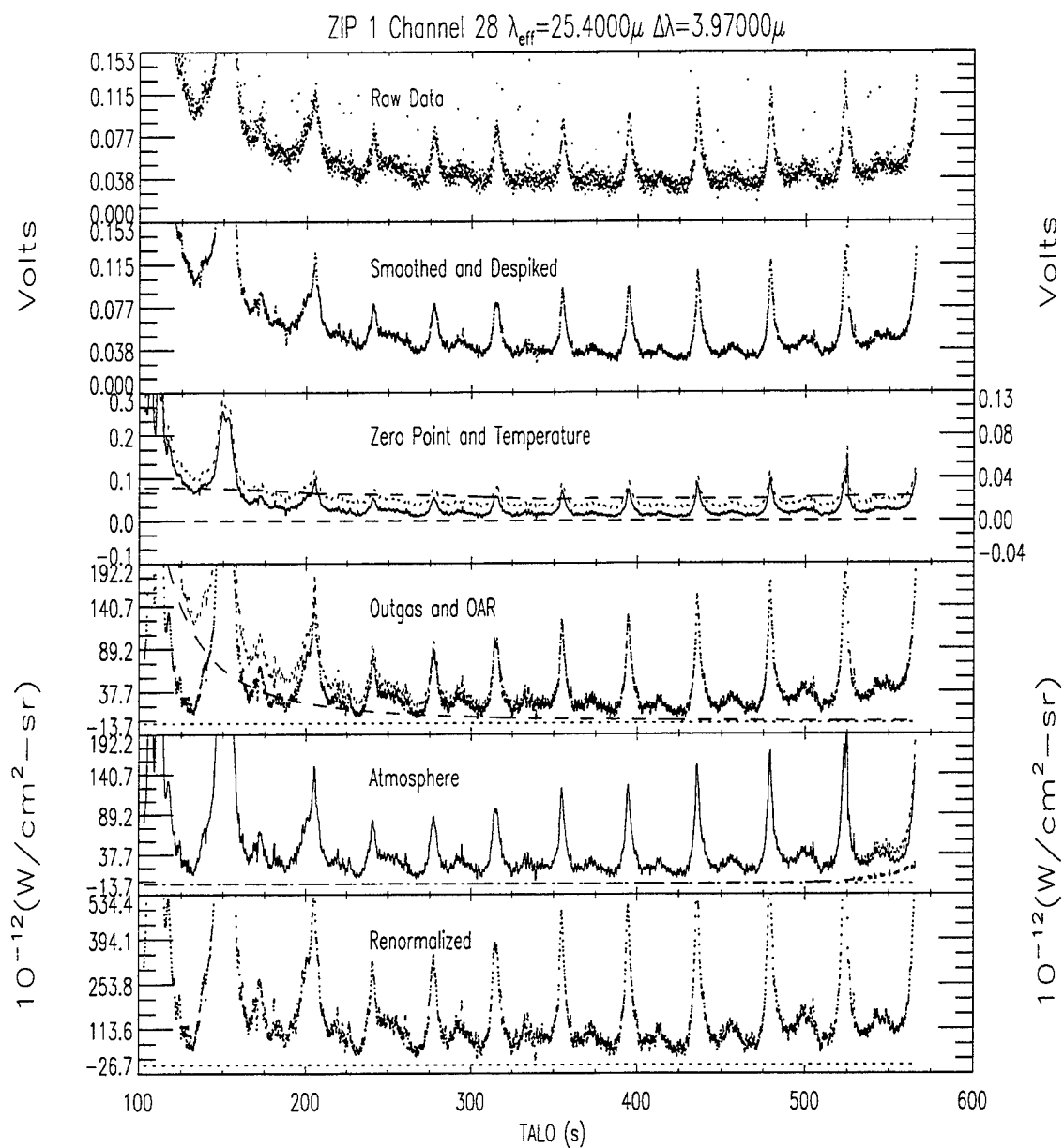
Figure A.28   Pipeline Flow for ZIP1 Channel 28

61
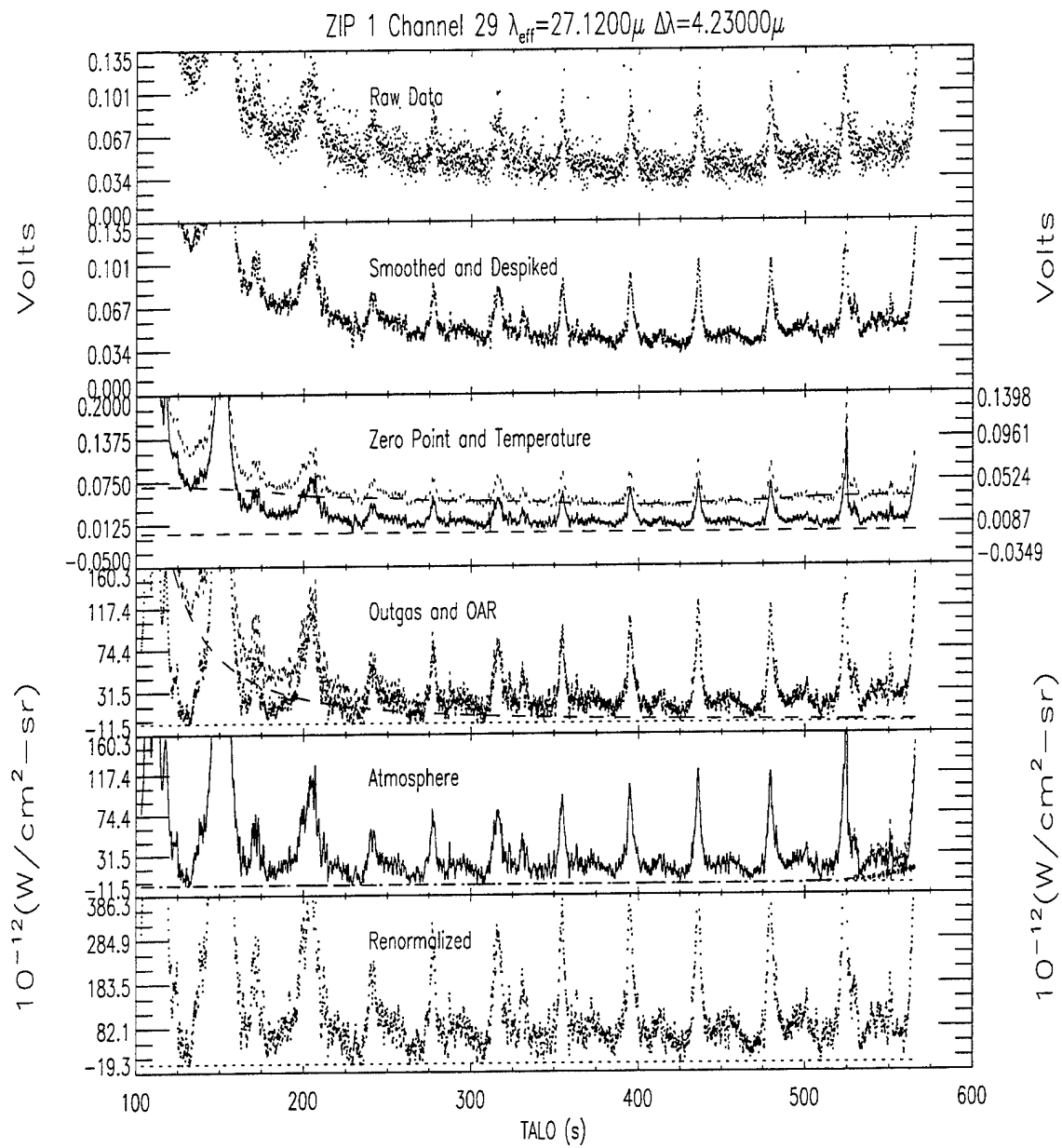
Figure A.29   Pipeline Flow for ZIP1 Channel 29

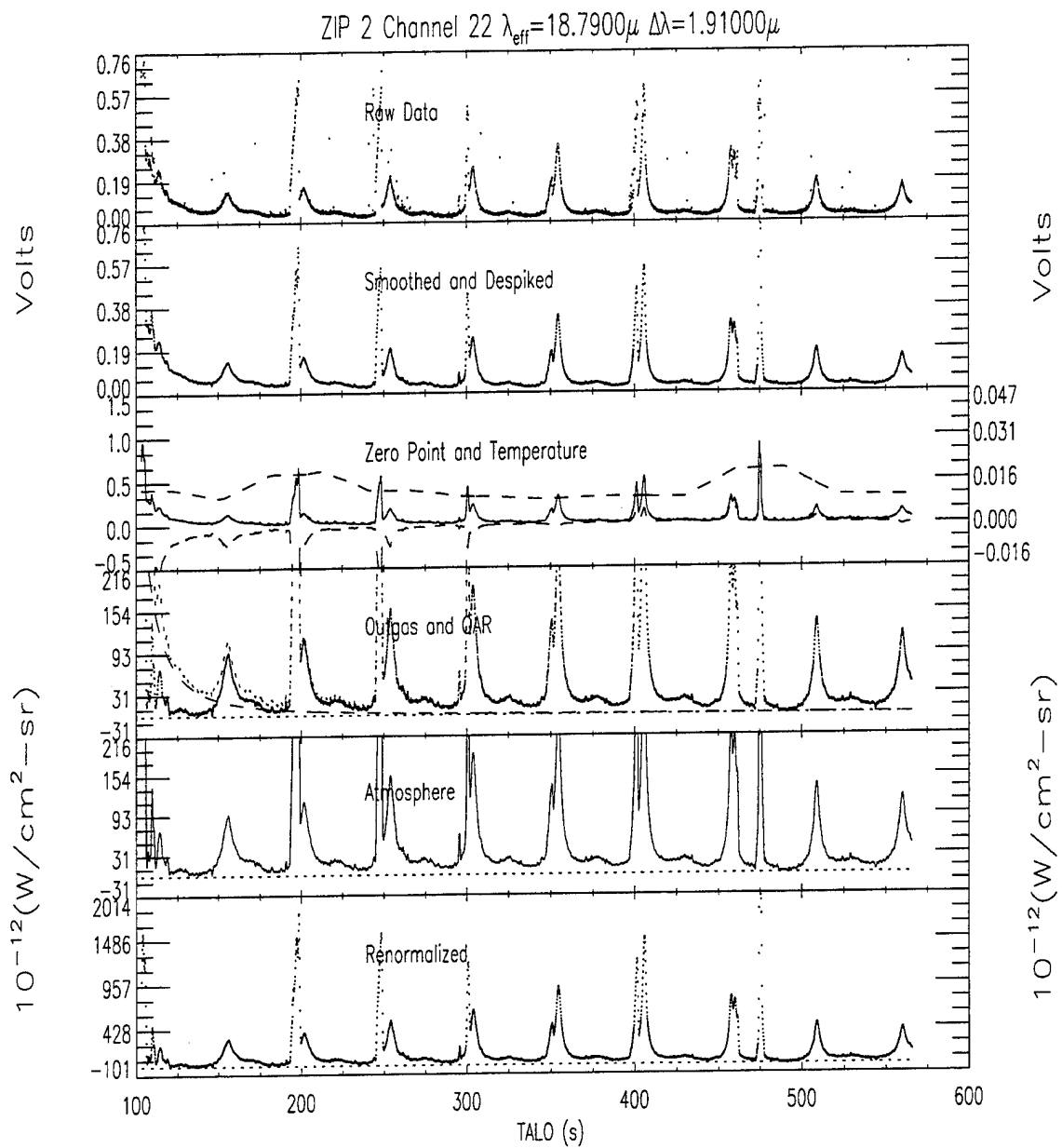**Figure A.30   Pipeline Flow for ZIP1 Channel 30**

Figure A.31   Pipeline Flow for ZIP2 Channel 1

64

Figure A.32   Pipeline Flow for ZIP2 Channel 2

65

Figure A.33 Pipeline Flow for ZIP2 Channel 3

Figure A.34   Pipeline Flow for ZIP2 Channel 4

Figure A.35   Pipeline Flow for ZIP2 Channel 5

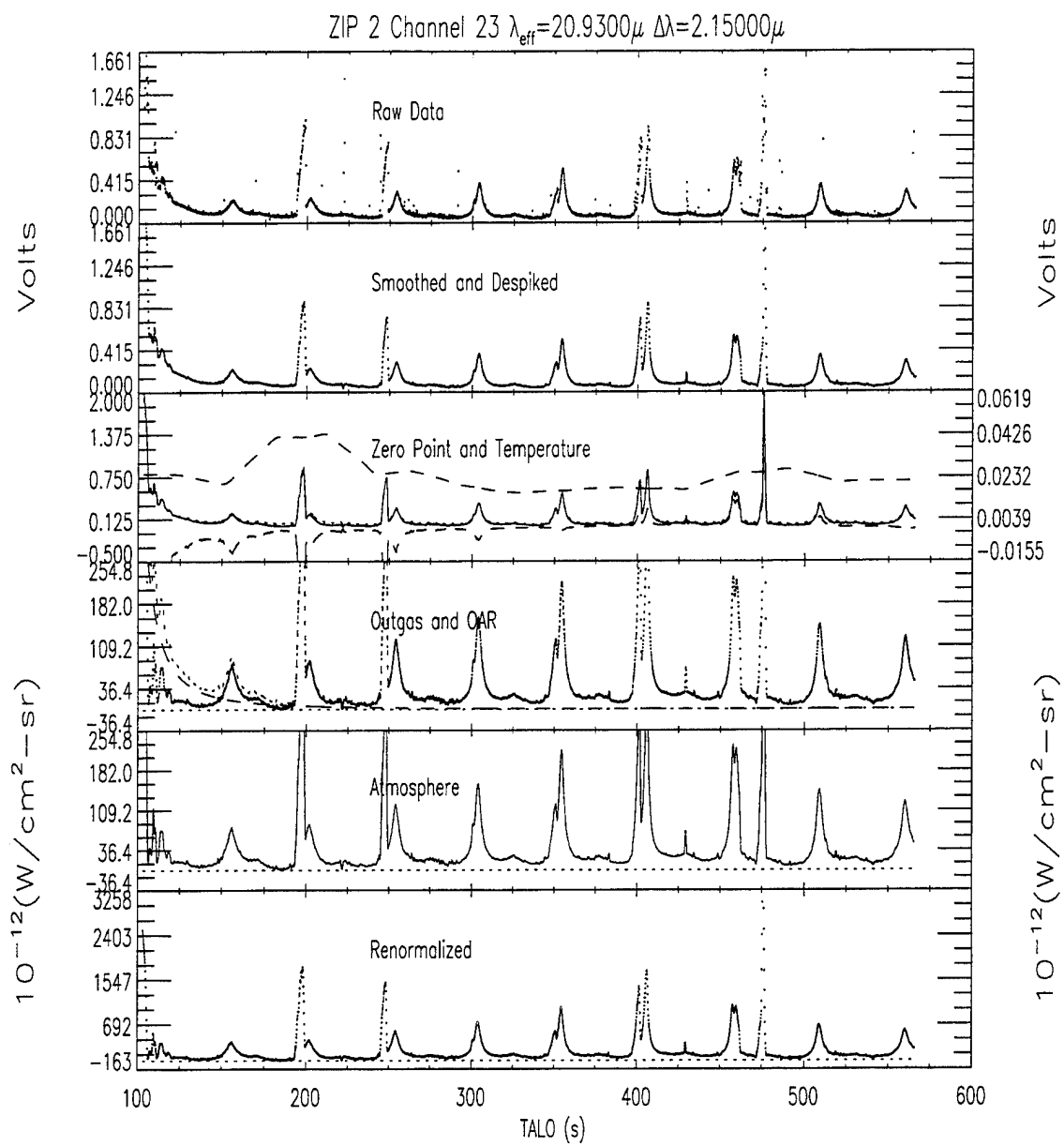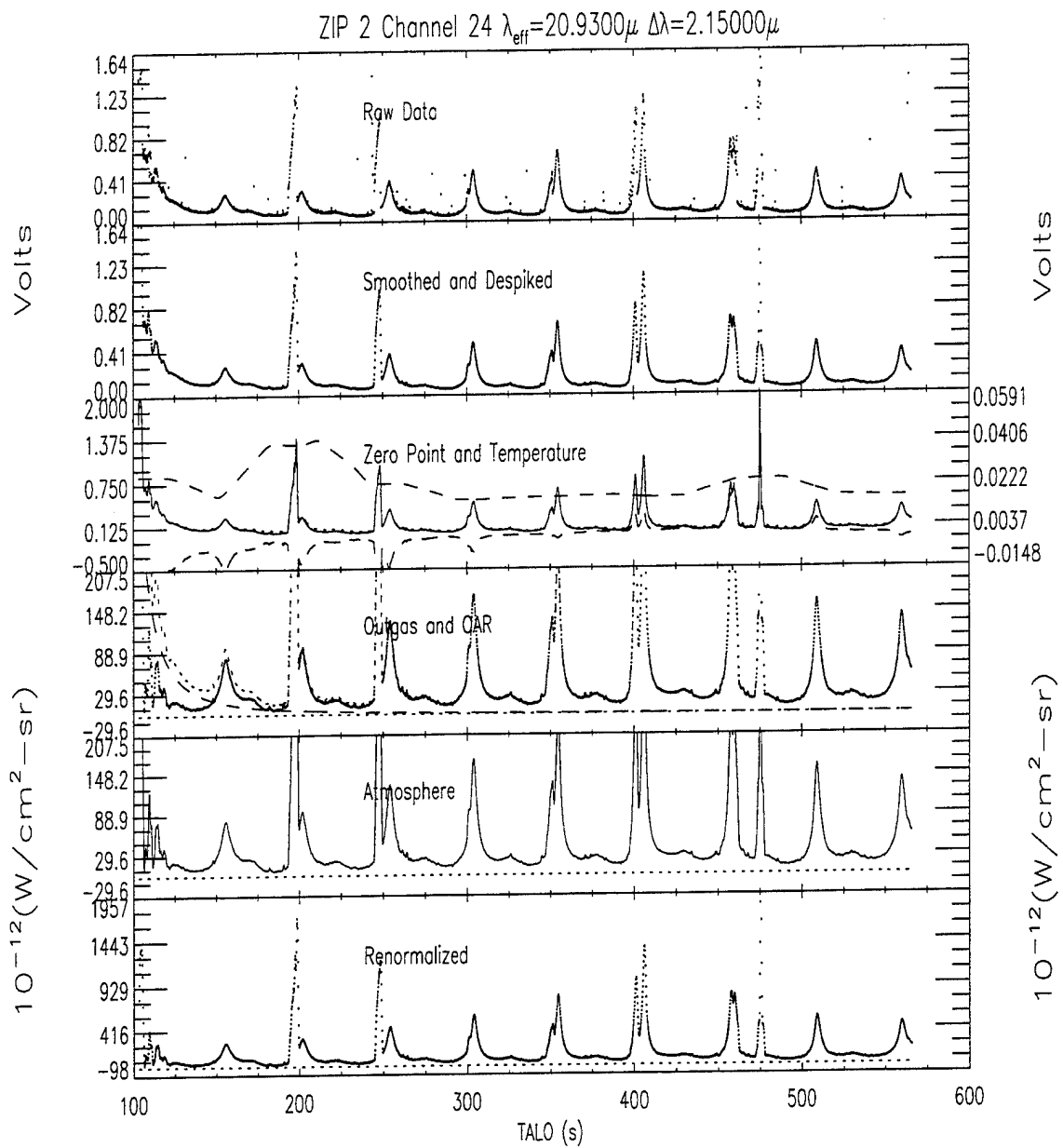**Figure A.36   Pipeline Flow for ZIP2 Channel 7**

Figure A.37 Pipeline Flow for ZIP2 Channel 8

Figure A.38 Pipeline Flow for ZIP2 Channel 9

71

Figure A.39   Pipeline Flow for ZIP2 Channel 10

72

Figure A.40   Pipeline Flow for ZIP2 Channel 11

73

Figure A.41   Pipeline Flow for ZIP2 Channel 12

Figure A.42   Pipeline Flow for ZIP2 Channel 13

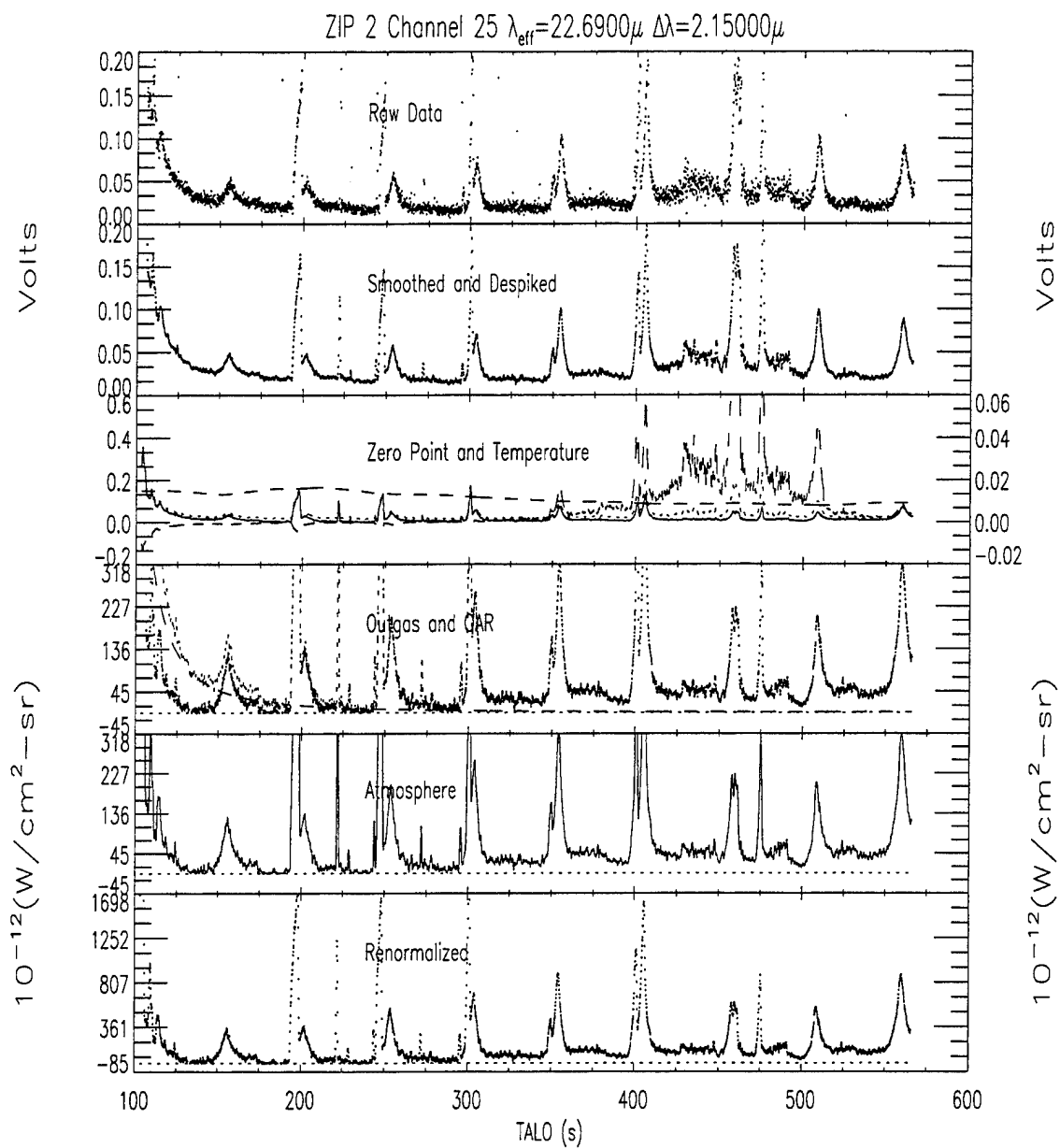**Figure A.43   Pipeline Flow for ZIP2 Channel 14**
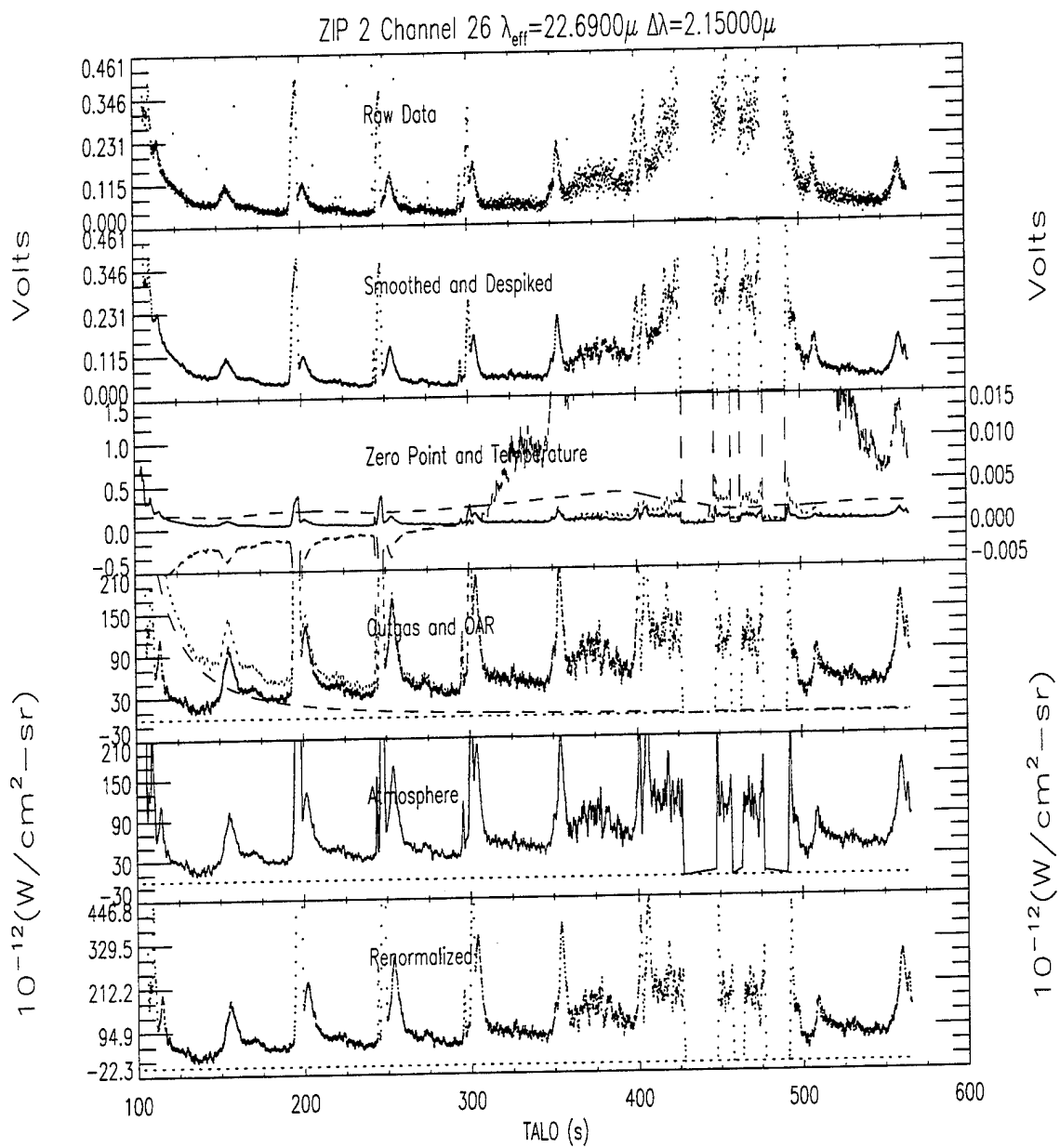
Figure A.44 Pipeline Flow for ZIP2 Channel 15

Figure A.45 Pipeline Flow for ZIP2 Channel 16
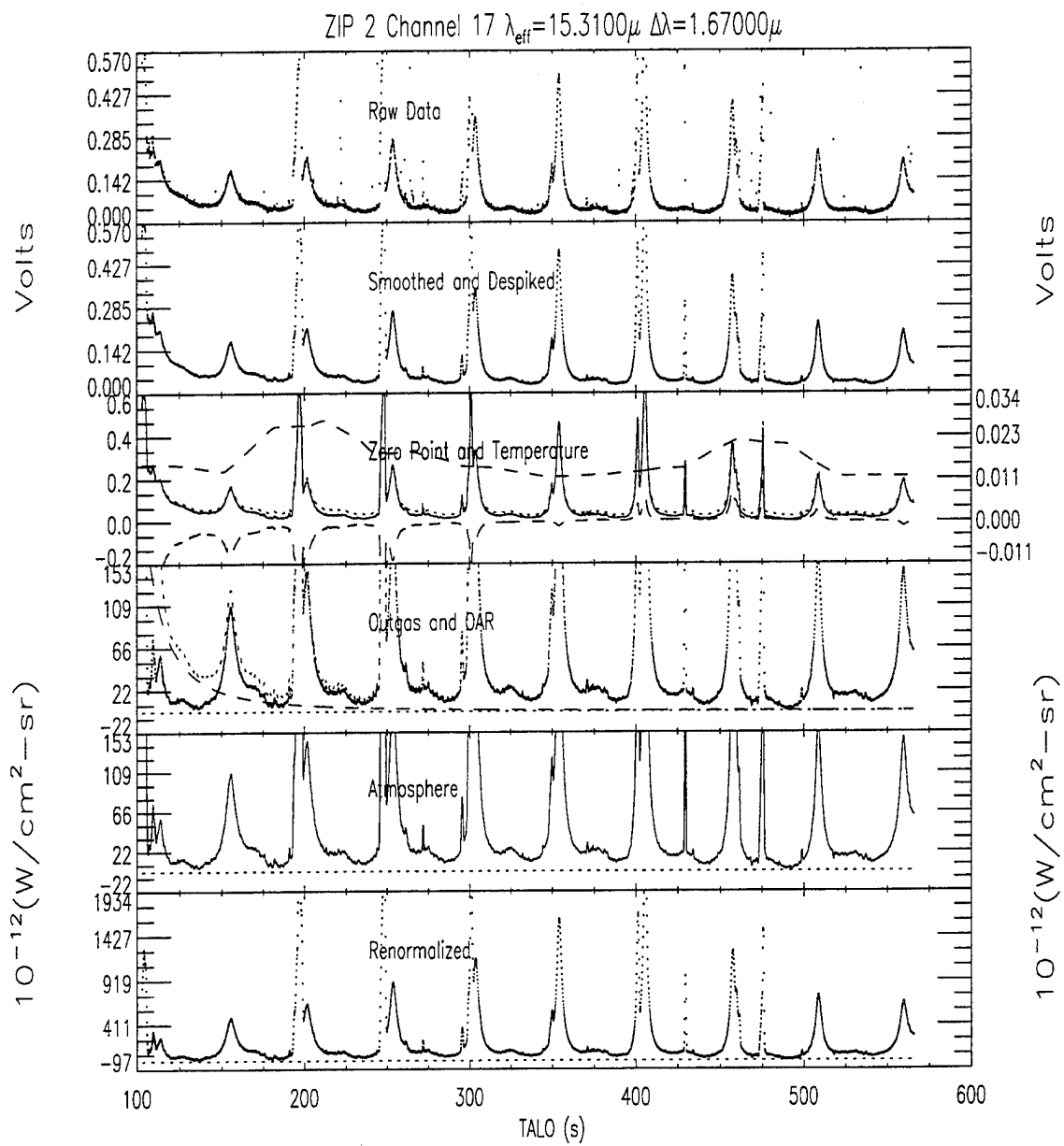
Figure A.46 Pipeline Flow for ZIP2 Channel 17

79

Figure A.47 Pipeline Flow for ZIP2 Channel 18

Figure A.48   Pipeline Flow for ZIP2 Channel 19

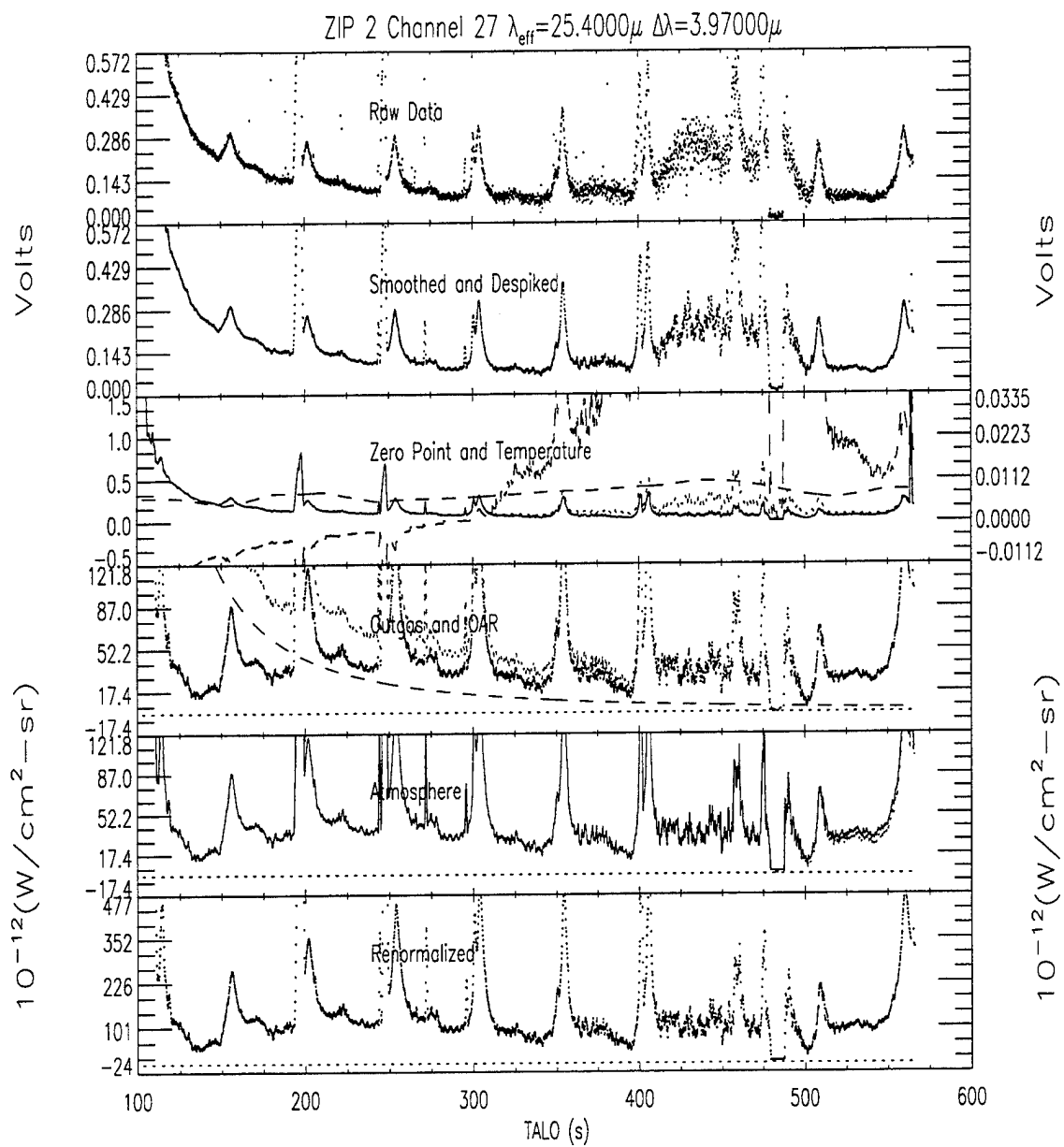**Figure A.49   Pipeline Flow for ZIP2 Channel 20**

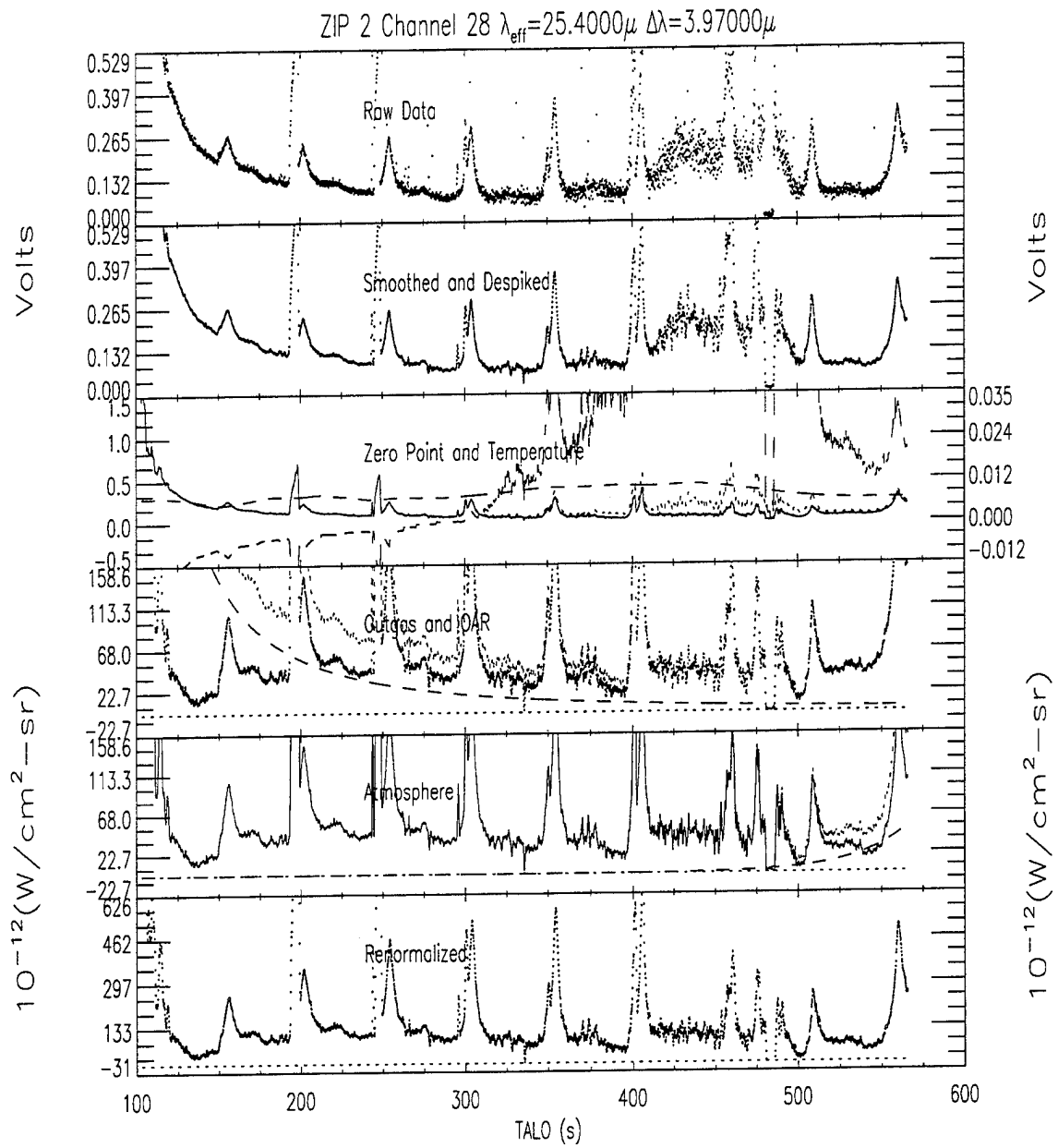**Figure A.50 Pipeline Flow for ZIP2 Channel 21**

Figure A.51 Pipeline Flow for ZIP2 Channel 22

Figure A.52 Pipeline Flow for ZIP2 Channel 23

Figure A.53   Pipeline Flow for ZIP2 Channel 24

Figure A.54   Pipeline Flow for ZIP2 Channel 25

Figure A.55   Pipeline Flow for ZIP2 Channel 26

Figure A.56   Pipeline Flow for ZIP2 Channel 27

Figure A.57   Pipeline Flow for ZIP2 Channel 28
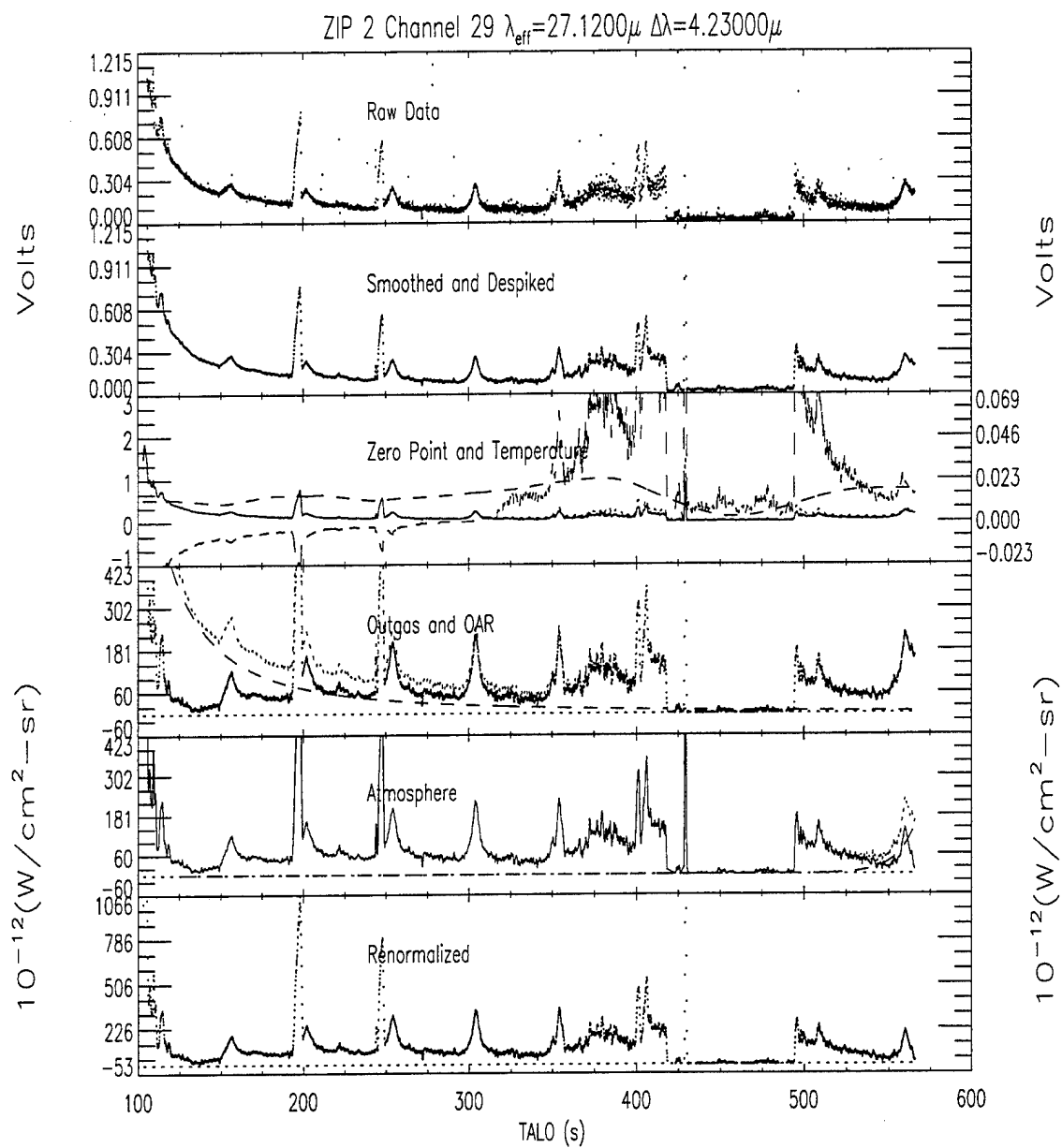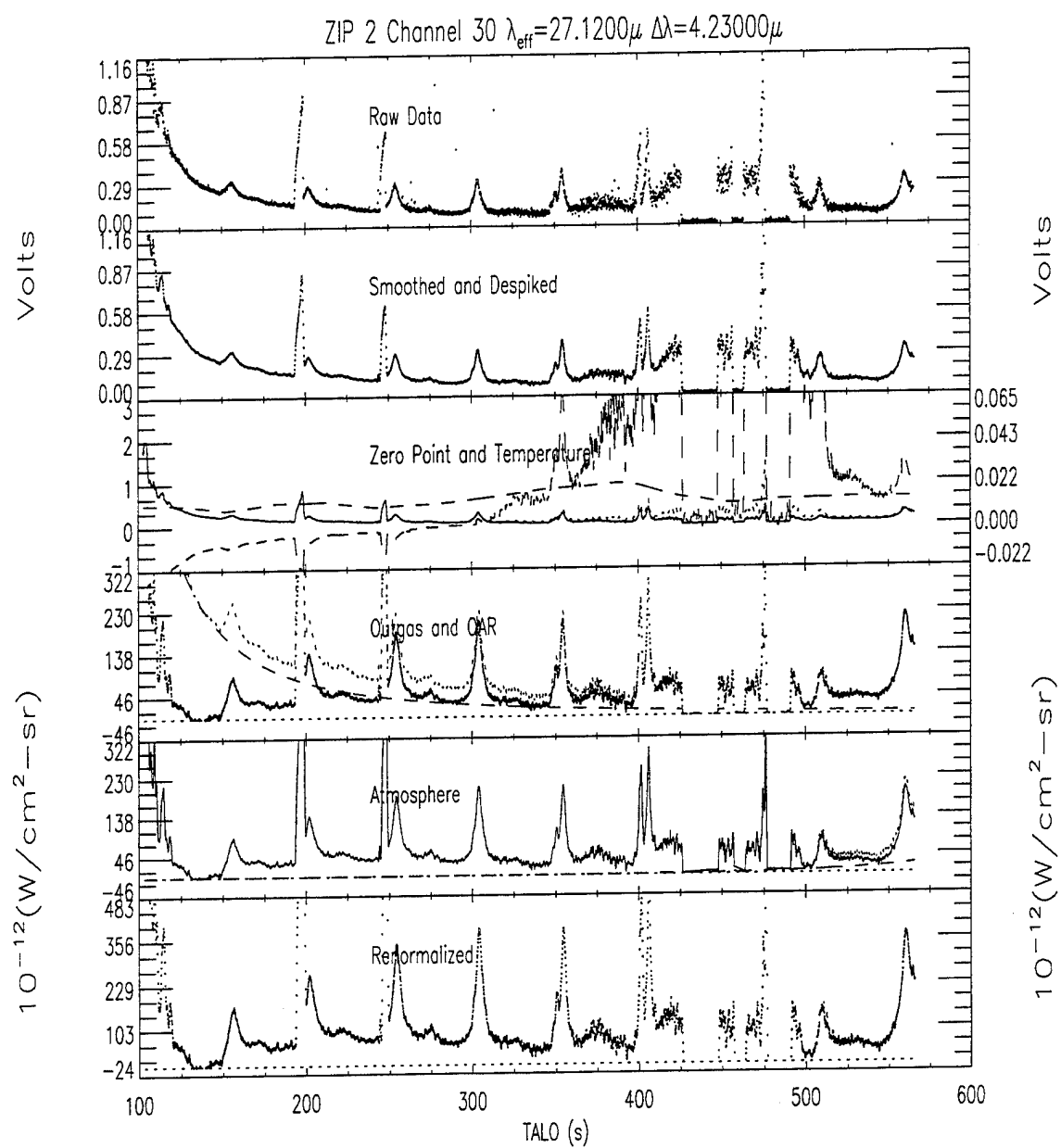
Figure A.58 Pipeline Flow for ZIP2 Channel 29

Figure A.59 Pipeline Flow for ZIP2 Channel 30